Radiation imaging in magnetic confinement fusion

Robin Barnsley, with ITER and EFDA/JET contributors
Queen's University Belfast and EFDA/JET
Seconded to ITER International Team, Garching, Germany

Alan Costley, George Vayakis, *ITER IT, Naka, Japan.*
Chris Walker, *ITER IT, Garching Germany.*

1)	Overview of fusion research and diagnostics	
2)	ITER diagnostics	
3)	Infra-red	Thermography of walls and targets.
4)	Bolometry	Radiated power IR –> hard x-ray.
5)	Visible	Imaging for protection and control. Many techniques simpler in visble.
6)	VUV	Characteristic of cooler edge plasma.
7)	X-ray	Hot core plasma. Direct imaging and crystal spectroscopy.
8)	Gamma-ray	Spectroscopy of nuclear reactions.

EFDA EUROPEAN FUSION DEVELOPMENT AGREEMENT

The European Fusion Development Agreement (EFDA) was established in 1999 as a framework contract between EURATOM and its partners in the field of controlled fusion (the Associates).

EFDA incorporates the following three interrelated activities:

- Technology activities carried out by the Associations and by European industry.
- The collective use of the JET facilities for the period beyond 1999
- The European contributions to international collaborations such as ITER

The Agreement is part of a Long-Term Programme of co-operation covering all the activities in the field of fusion research by magnetic confinement in the European Union and in the Swiss Confederation. Recently, some Eastern European countries (i.e. the Czech Republic, Hungary, Latvia and Romania), which aspire to European Union membership, have also joined the programme.

EFDA EUROPEAN FUSION DEVELOPMENT AGREEMENT

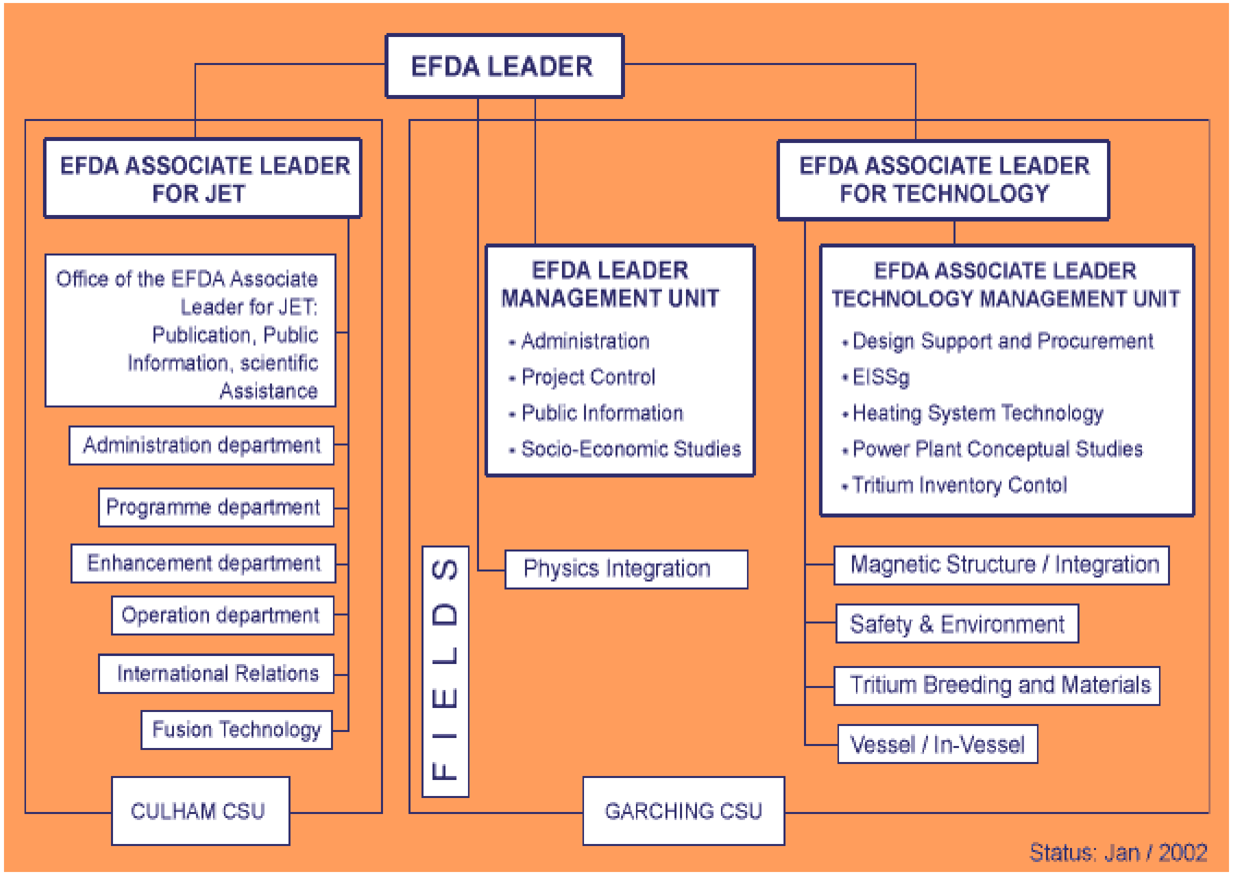

ITER

The Way to Fusion Energy

On 28th June the ITER Parties announced in Moscow their agreement to site ITER in Cadarache, France.

Europe: 50% (of which France 10%).

Japan: 10% of costs. 20% of contracts. EU support for Director General.

China, Korea (south), Russia, USA: 10%.

Thermonuclear fusion reactions

- D + D -> ^{3}He + n or T + p
- D + ^{3}He -> ^{4}He + p

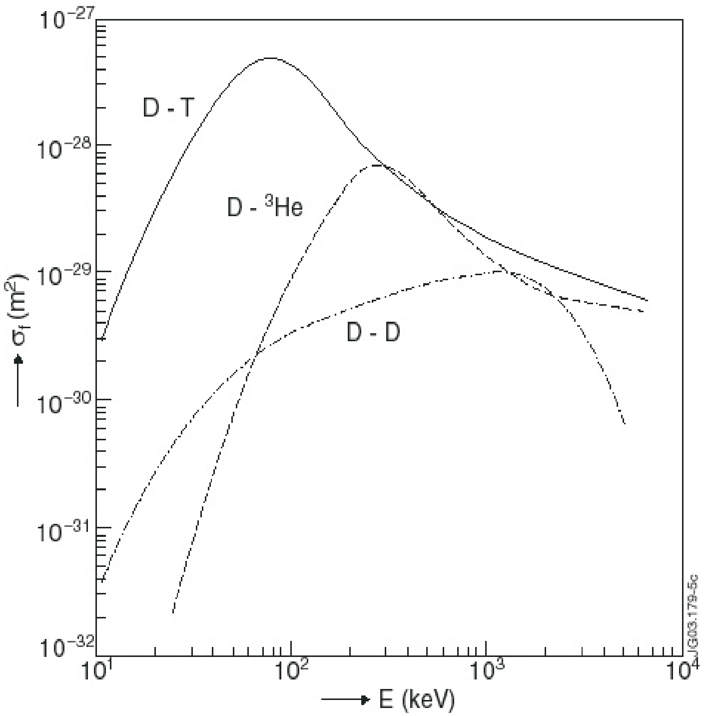

- D + T -> (^{4}He + 3.5 MeV) + (n + 14.1 MeV)

n_{slow} + ^{6}Li -> ^{4}He + T

n_{fast} + ^{7}Li -> ^{4}He + T + n_{slow}

D + Li -> ^{4}He + 100 x 10^6 kWh/ kg

The Tokamak principle

- Closed magnetic field minimizes particle losses
- Combined toroidal and poloidal fields produce helical field, that stabilizes +ve/-ve charged particle drifts.
- Plasma current induced by inner poloidal coils.

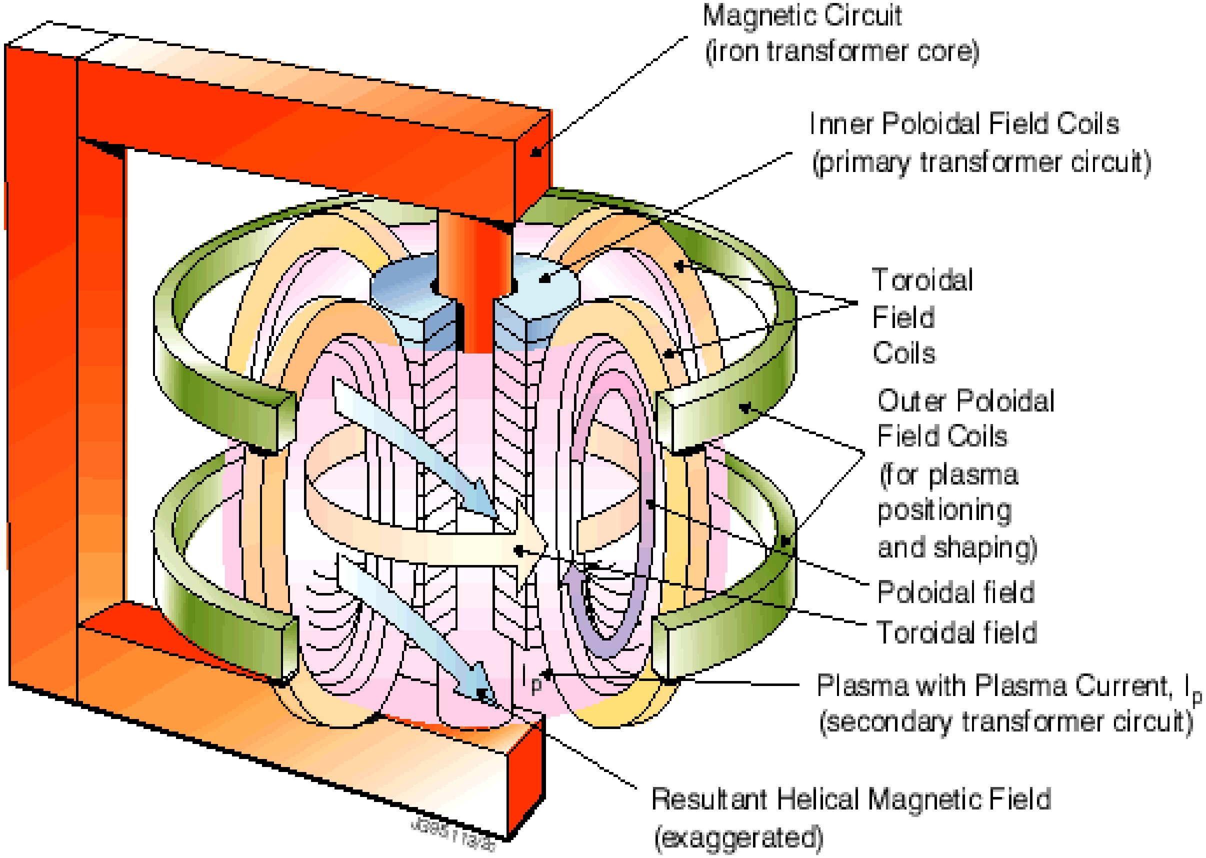

The JET Torus Hall (www.jet.efda.org)

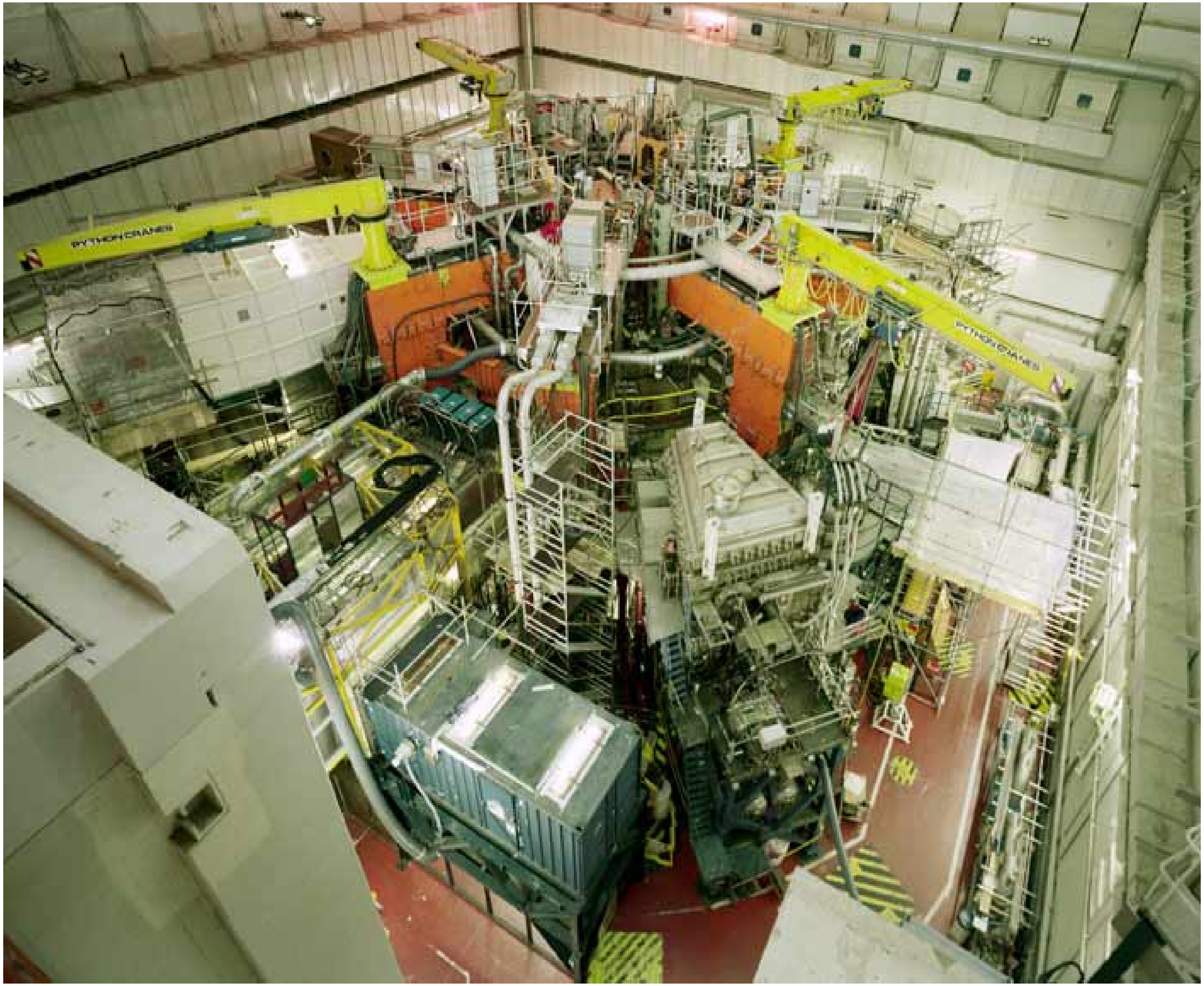

Inside JET without and with plasma

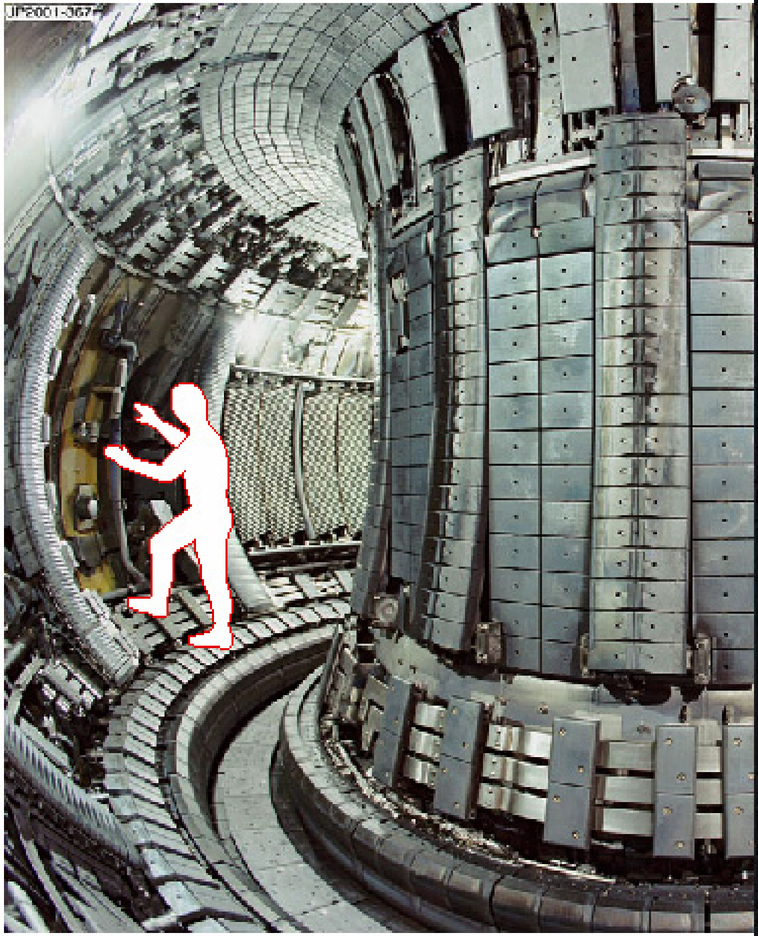

Remote-handling in-vessel since 1997

Visible radiation dominated by D_α near edge
Core radiation mostly x-rays
On JET $0.5 < P_{rad} < 5$ MW

Plasma heating

Ohmic	Inductive	~ 1MW	Ineffective at high Te
Neutral beam			Most effective to date
+ve ion	~ 100 keV	~ 25 MW JET	
-ve ion	~ 1 MeV	~ 50 MW ITER	Greater penetration
Ion cyclotron	~ 40 MHz	~ 10 MW JET	
Lower hybrid	~ 1 GHz	~ 6 MW JET	
Electron cyclotron	~ 100 GHz	~ 5 MW	
Alpha particles	**2.5 MeV**	~ 4 MW JET	Fusion product
		~ 100 MW ITER	

The Lawson criterion for particle and energy confinement

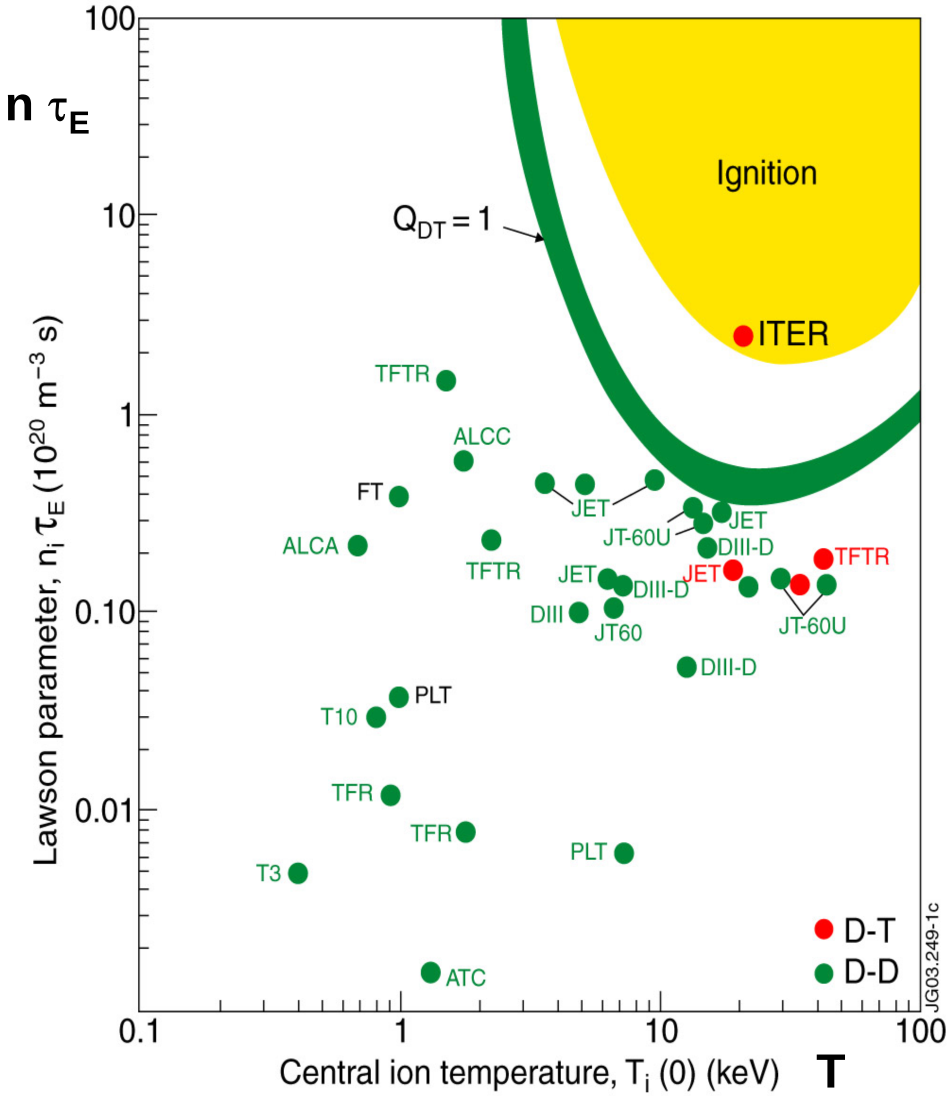

$$n \text{ x } \tau_E > f\,(T)$$

(external power = 0)

$$n \text{ x } \tau_E > f\,(T, Q = P_{fus}/P_{ext})$$

(external power $\neq$ 0)

$$n \text{ x } \tau_E > f\,(T)$$

Sometimes also transformed into:

$n \text{ x } \tau_E \text{ x } T > 10^{21}$ (m^{-3} s keV)

(taking into account temperature dependence near minimum)

D-T fusion achievements to date

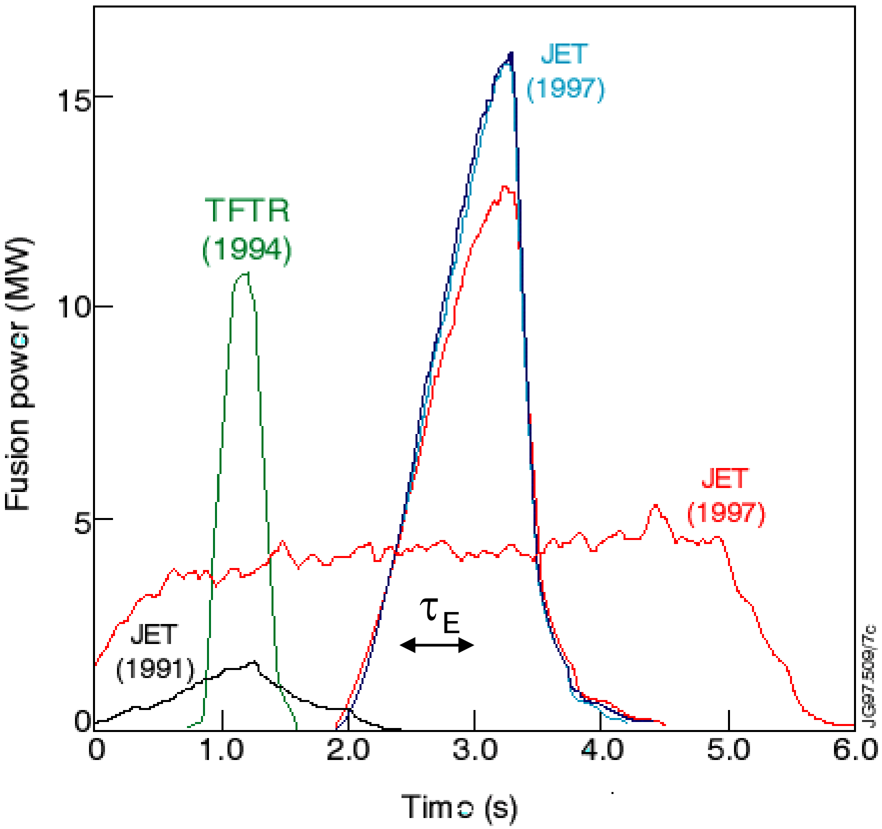

JET has unique D-T capability

- Tritium handling plant
- Remote handling
- Shielded torus hall
- DT compatible diagnostics
- Neutral beam upgrade to ~ 40 MW
- Proposed to run until ITER operational

For a JET D-T plasma,

with 20 MW input into the plasma

total output : max 16 MW

Record:	Q = 0.8 (JET)
Steady state:	Q = 0.3 (JET)
Breakeven:	Q = 1
Ignition:	Q ~ 5

Scaling to ITER from previous experiments

Physics performance can be extrapolated better than factor 2.

Technological developments ongoing for:

- First wall: blanket and divertor modules, diagnostic mirrors.
- Material properties under heavy neutron irradiation.

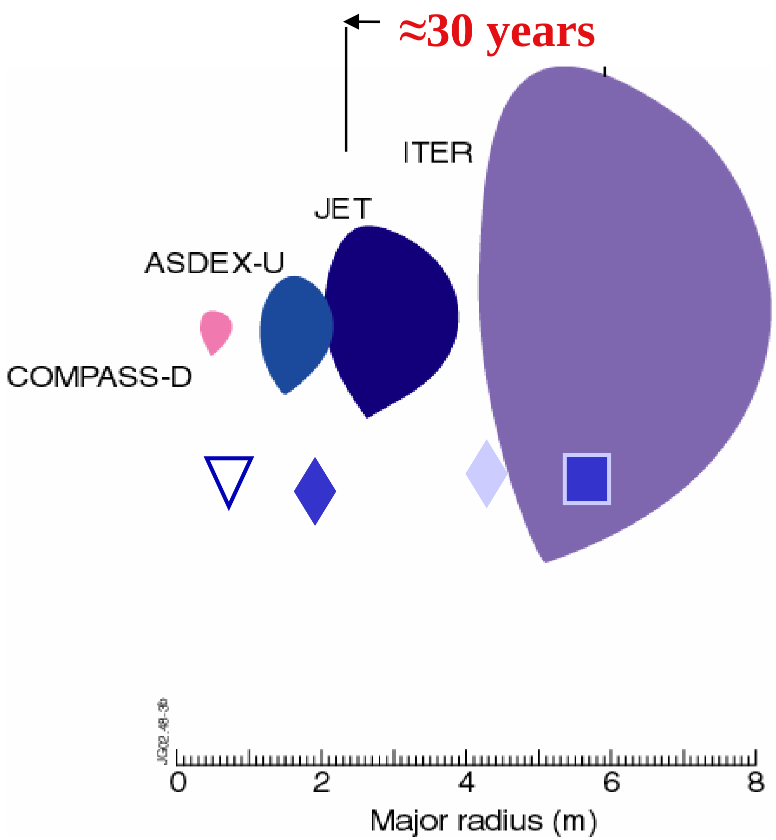

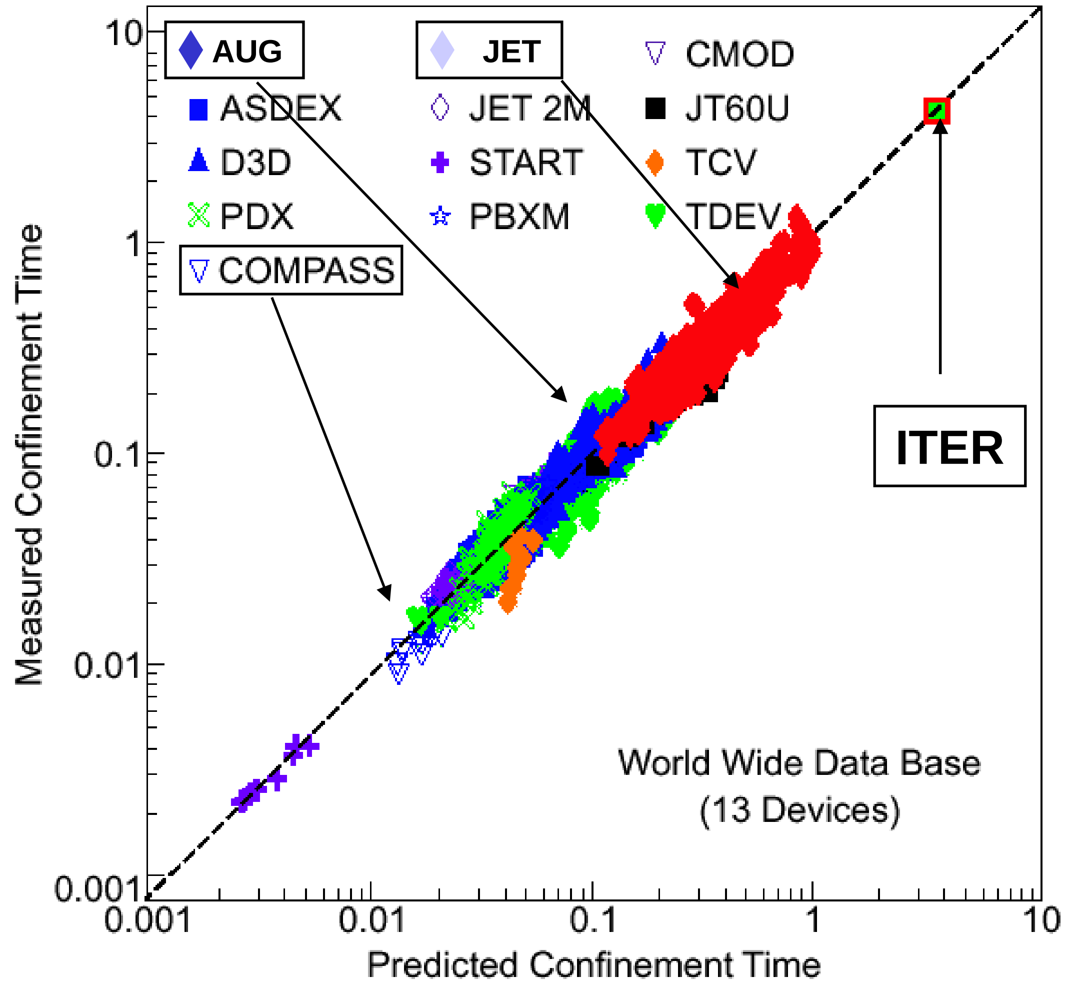

Characteristics of the bulk plasma radiation

Main plasma (JET)

Fuel ions D-D or D-T are diluted by impurities. Eg 2%C, 0.1% O, 001% Ni.

Density ~10^{20} /m^3 , Te ~ 10 keV, Ti ~ 20 keV.

Optically thick below λ ~1mm:

Emits and absorbs RF and microwave.

Optically thin above λ ~ 1mm.

Emits quasi-blackbody Bremsstrahlung spectrum peaked at few keV.

Many discrete spectral lines from fuel and impurity neutrals and ions.

Neutron and gamma emission from fusion reactions.

Active diagnostics

1 MW, 1 GHz gryrotron	Collective Thomson scatt.	Ion dynamics
mm-wave ~ 100 GHz	Reflectometry	Plasma position
FIR DCN laser 0.2 mm	Interferometer	Density profile
Ruby laser	LIDAR Thomson Scattering	Electron density and temp.
Neutral beam 100 keV	Charge exchange spectr.	Ion temp, impurity density
Lithium beam ~ 20 keV	Spectroscopy	Edge Te, Ne
Heavy ion beam	Vis spect, Mass spect	E-fields
Laser ablation	Impurity injection	Impurity transport

Passive Diagnostics

Radiation imaging possible in **blue**

Magnetics	Pick-up coils	B-fields, position, current, stored energy
RF ~ 30MHz	RF antennae	Ion cyclotron emission
mm-wave	Waveguide	Electron cyclotron emission - Te profile
IR	Camera	Tile thermography
Visible	Filters, Gratings	Edge impurity spectroscopy, vis. Brems Zeff
VUV/XUV	Grating + MCP	Impurity spectroscopy, machine protection
Soft x-ray camera	Diode array	Broadband tomography
Soft x-ray survey	Crystals + GPC	Impurity spectroscopy, machine protection
High res. X-ray	Crystal + MWPC	Doppler spectroscopy of Ti, bulk motion
Hard x-ray	Scintillators	Supra-thermal electrons
γ-ray	Scintillators	Fusion products
C-X neutrals	Mass-spec	Ion dynamics
Ions, electrons	Langmuir probe	Edge Te, Ne
Wide band	Bolometry	Total radiated power
Neutrons	Imaging, counting, spectroscopy, activation	

Impurities exist in a wide range of ionization stages, dominated by the electron temperature profile

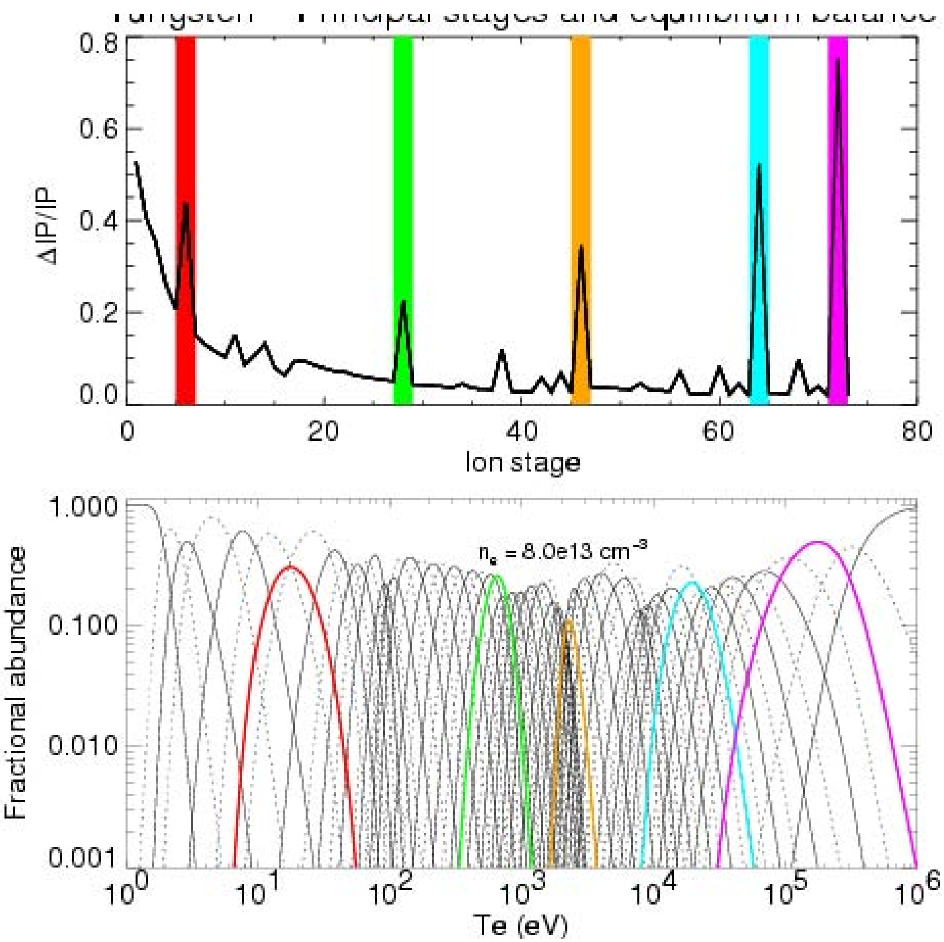

Below. Coronal fractional abundance of W ions.
Above. A guide to the shells with greatest ionization potential ranges ΔIP/IP.

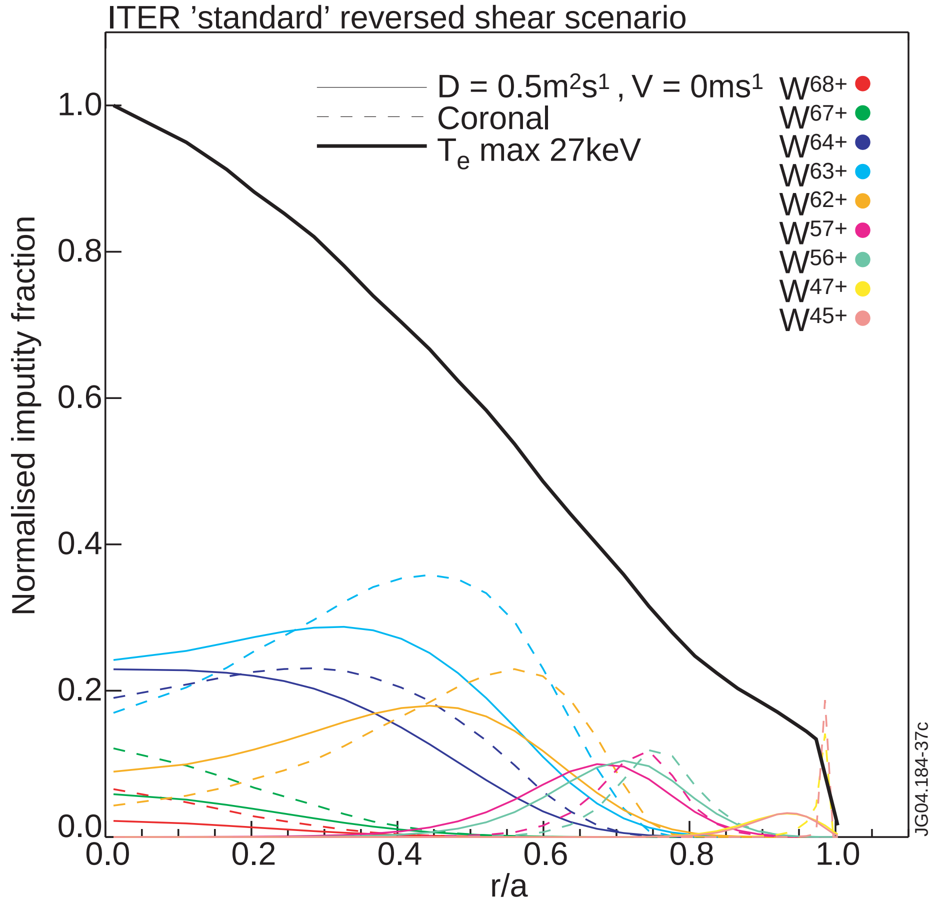

Radial profiles of W ions
Modelled for an ITER plasma

JET diagnostics

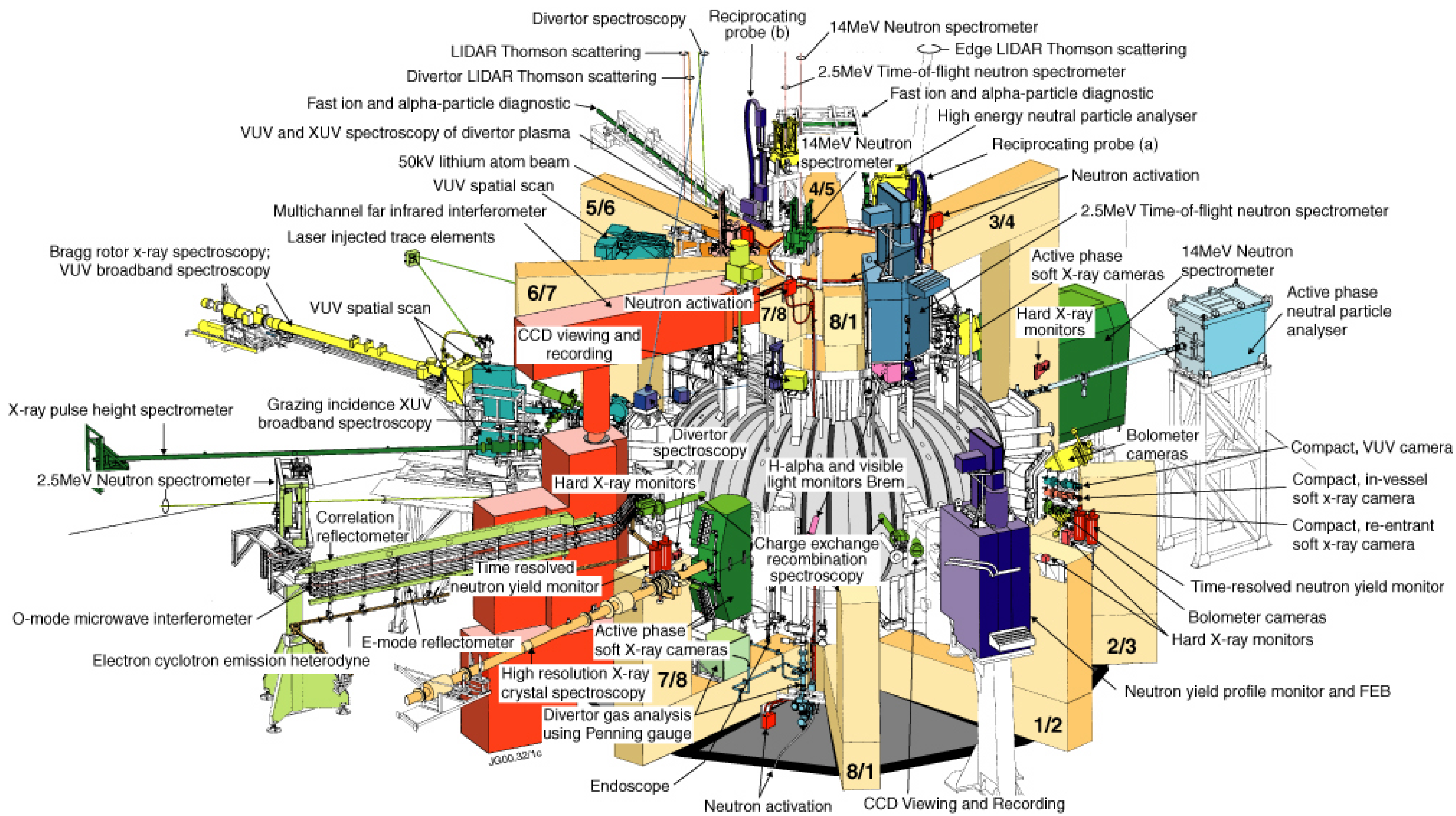

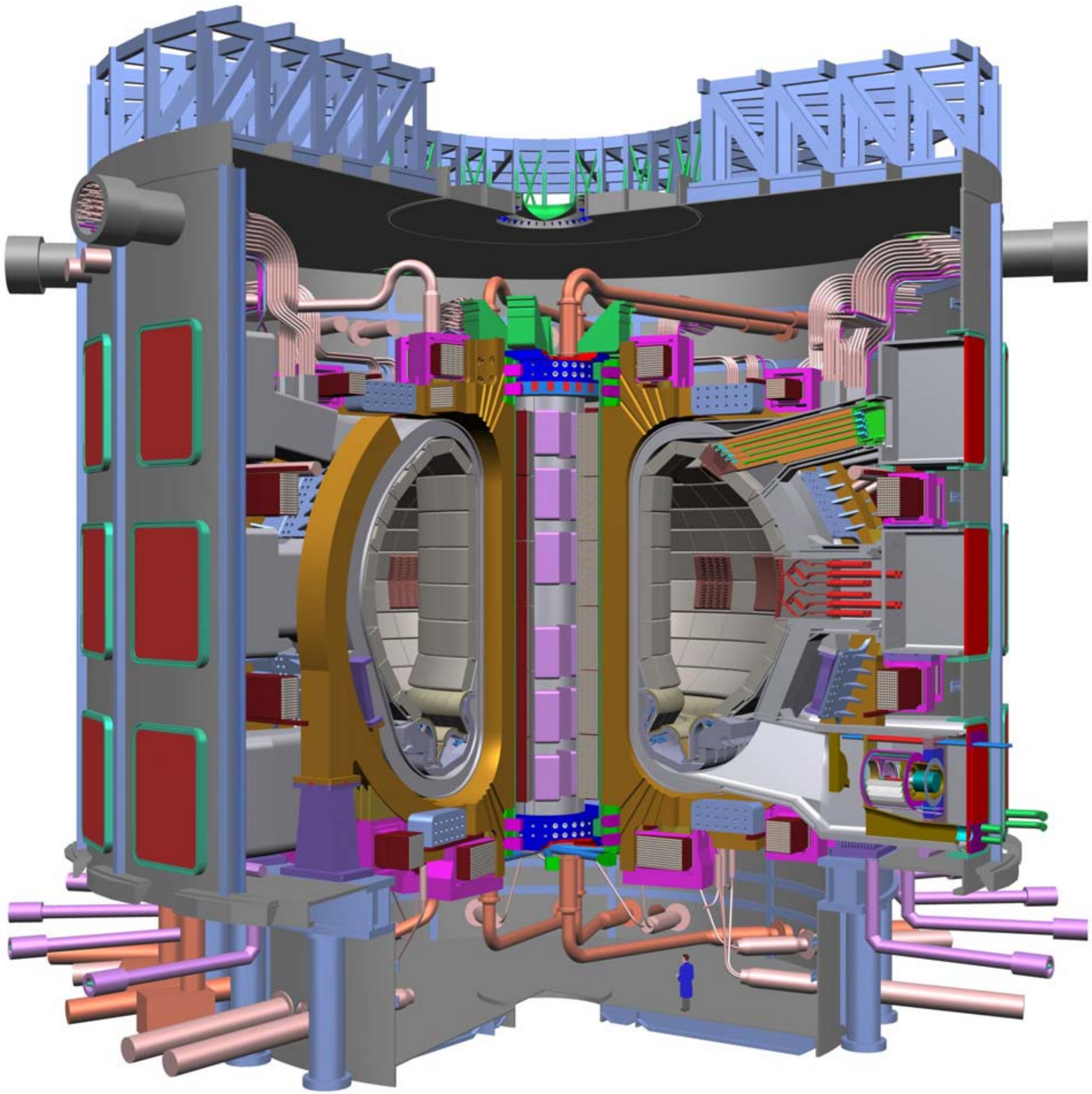

ITER (www.iter.org)

- Superconducting Tokamak
- Single-null divertor
- Elongated, triangular plasma
- Additional heating mainly from negative-ion neutral-beams

R (m)	6.2
a (m)	2
V_P (m^3)	850
I_P (MA)	15(17)
B_t (T)	5.3
δ,κ	1.85, 0.5
P_{aux} (MW)	40-90
P_α (MW)	80+
Q (P_{fus}/P_{in})	10
Prad (MW)	48

ITER cross-section

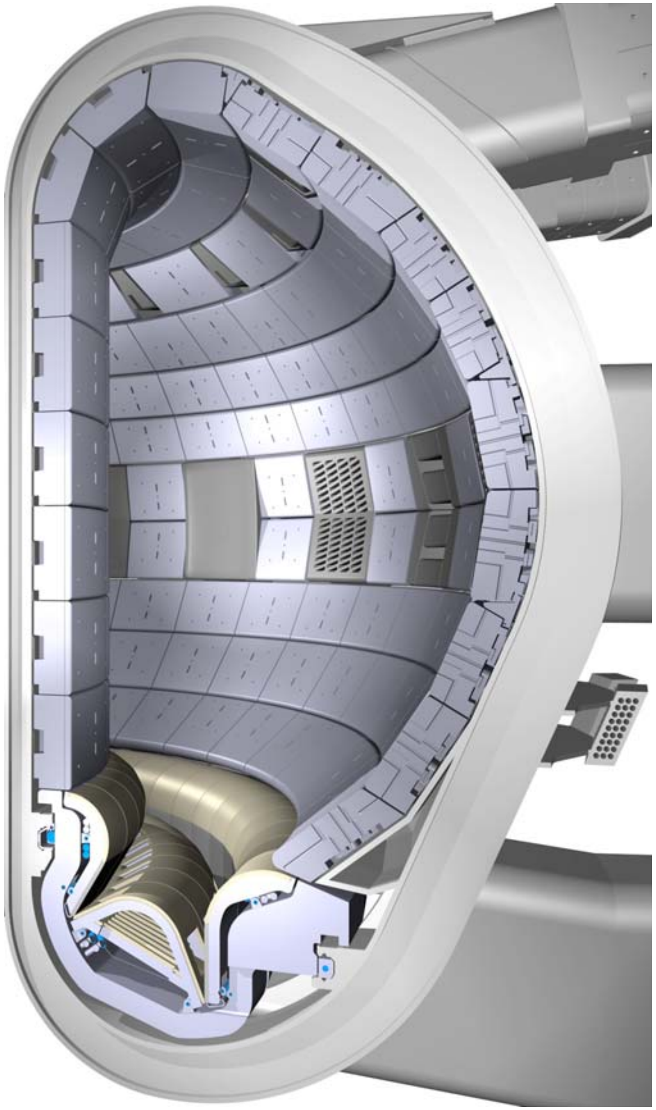

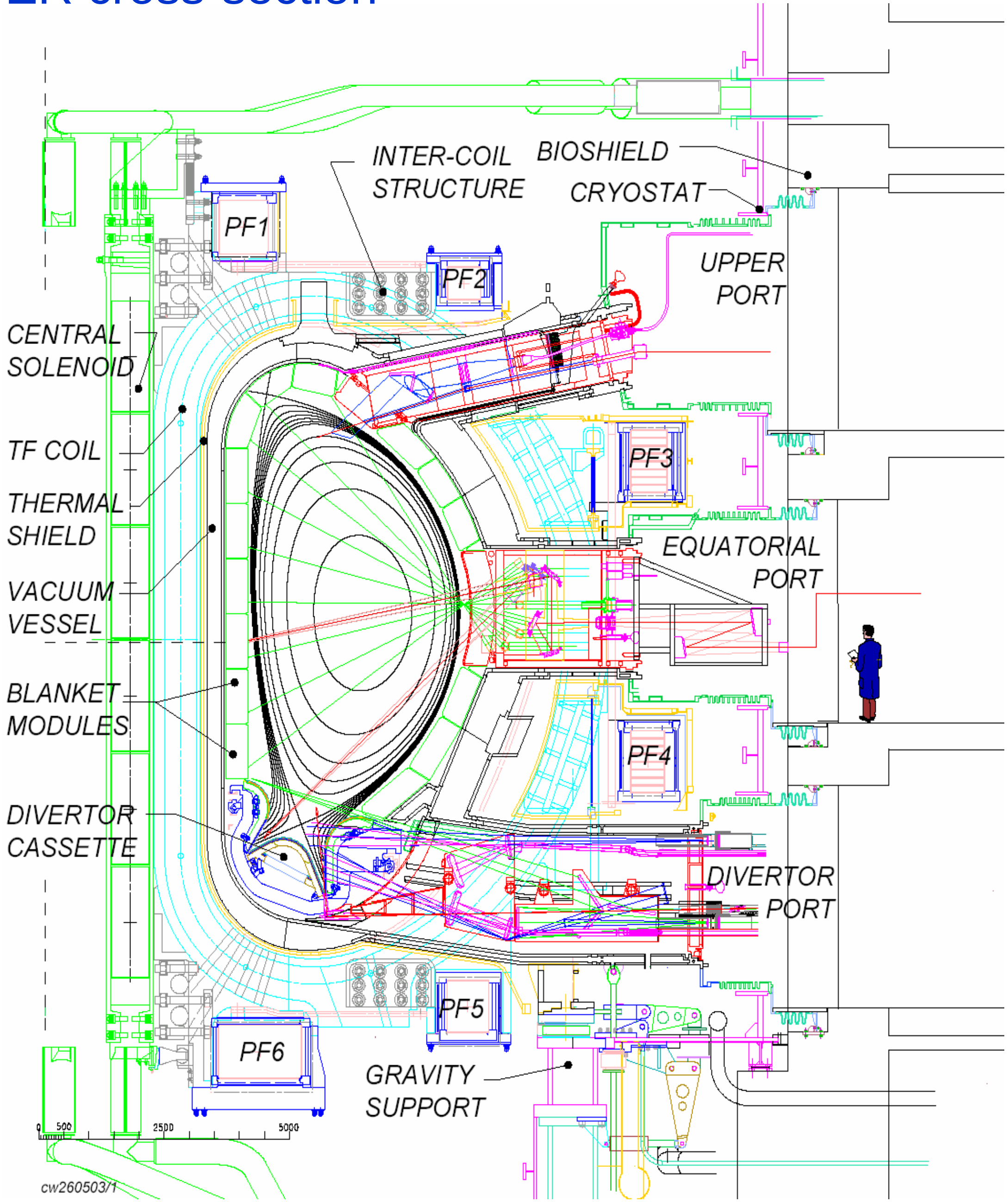

ITER Construction Schedule

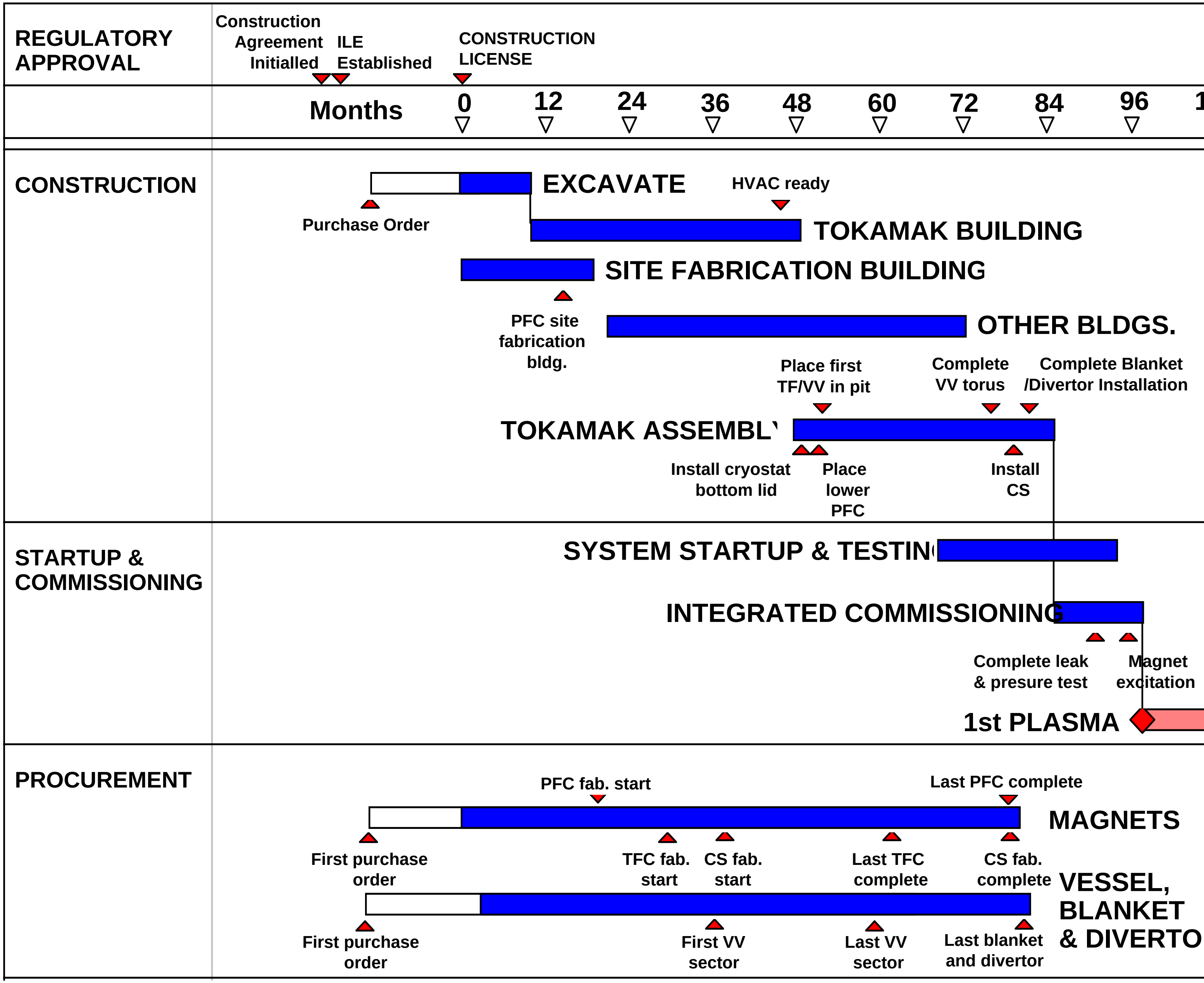

ITER Operation Schedule

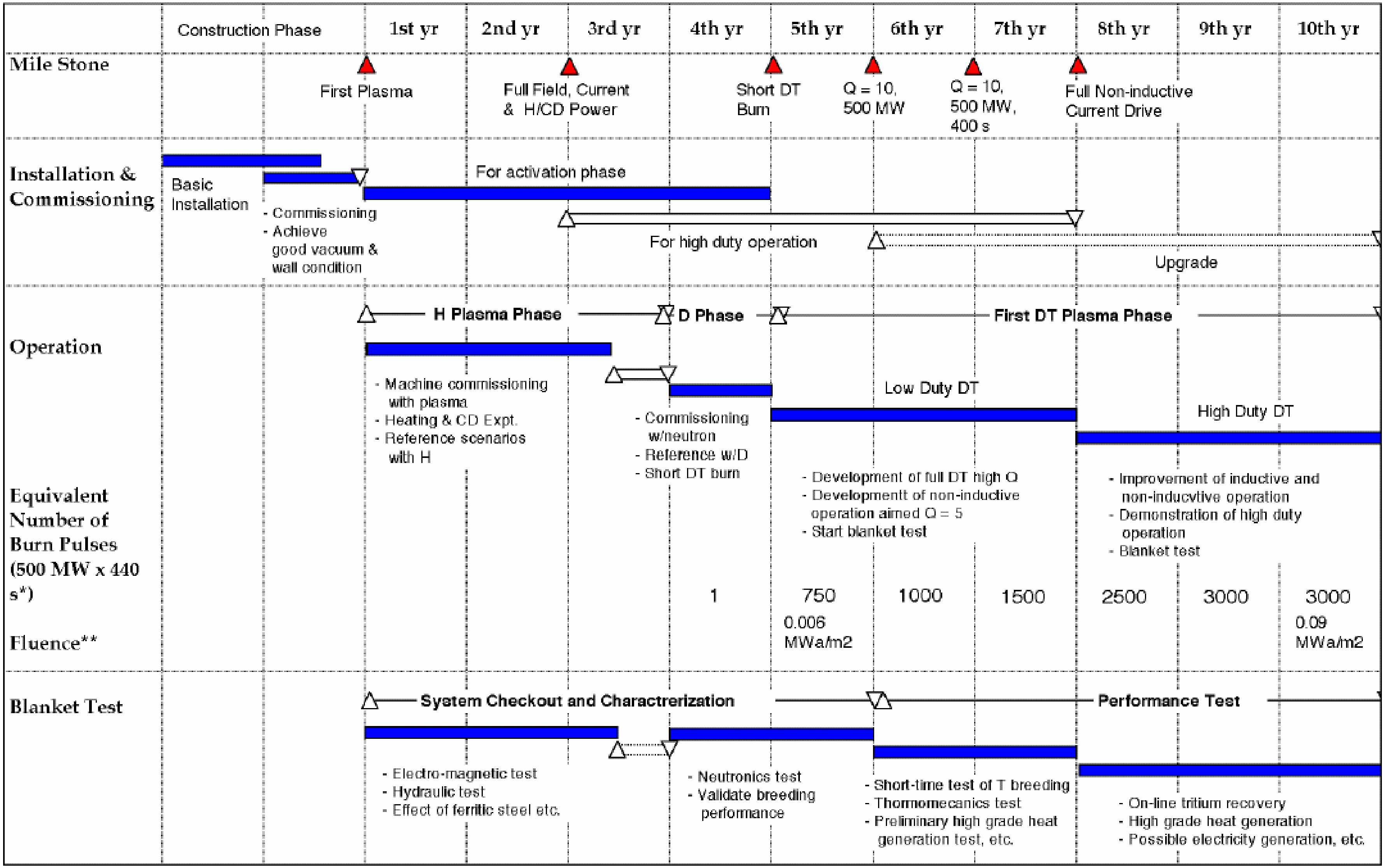

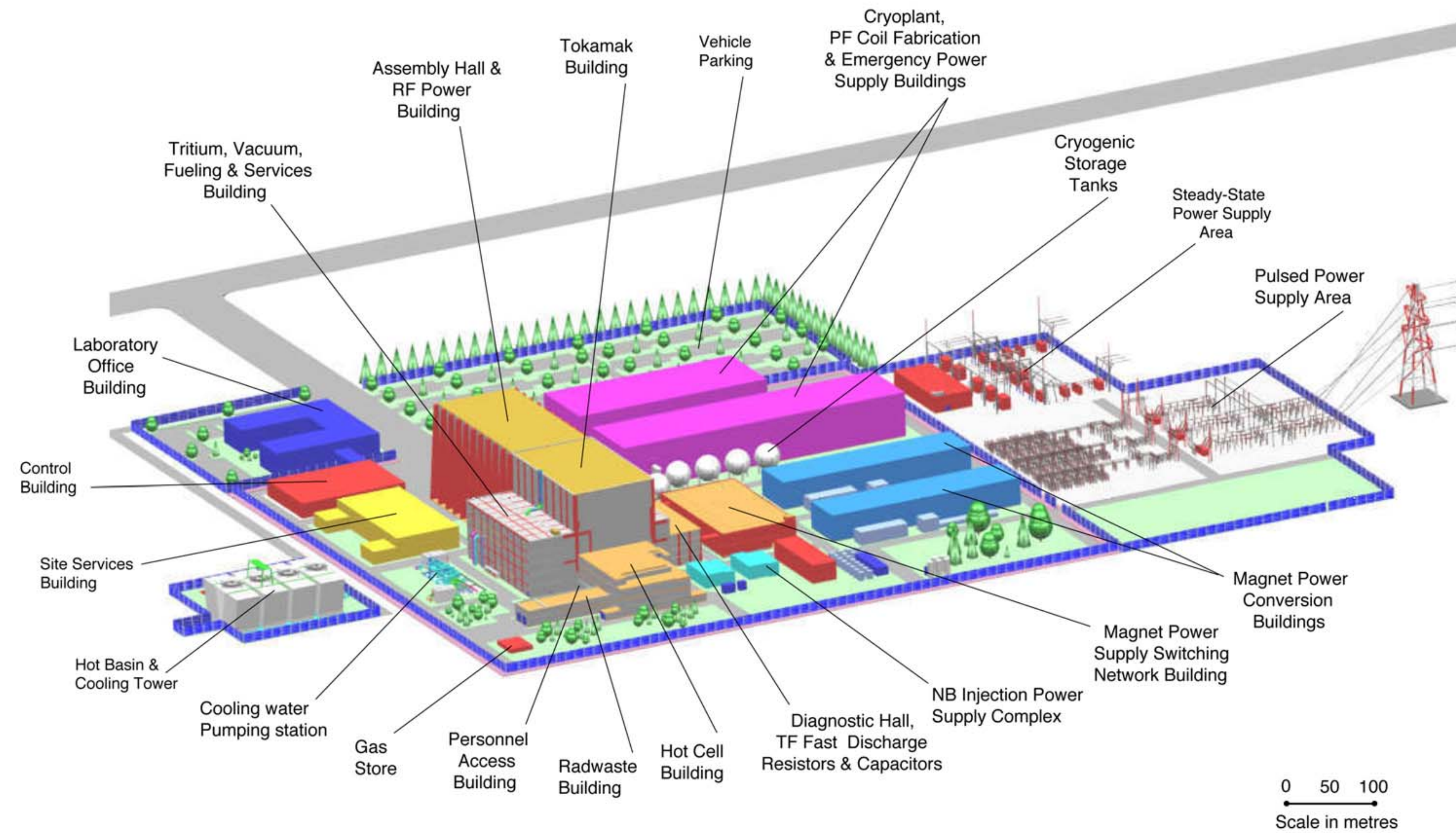

ITER Viewed From North East

ITER Diagnostic System

Magnetic Diagnostics	Spectroscopic and NPA Systems
Vessel Magnetics	CXRS Active Spectr. (based on DNB)
In-Vessel Magnetics	H Alpha Spectroscopy
Divertor Coils	VUV Impurity Monitoring (Main Plasma)
Continuous Rogowski Coils	Visible & UV Impurity Monitoring (Div)
Diamagnetic Loop	X-Ray Crystal Spectrometers
Halo Current Sensors	Visible Continuum Array
Neutron Diagnostics	Soft X-Ray Array
Radial Neutron Camera	Neutral Particle Analysers
Vertical Neutron Camera	Laser Induced Fluorescence (N/C)
Microfission Chambers (In-Vessel) (N/C)	MSE based on heating beam
Neutron Flux Monitors (Ex-Vessel)	**Microwave Diagnostics**
Gamma-Ray Spectrometers	ECE Diagnostics for Main Plasma
Neutron Activation System	Reflectometers for Main Plasma
Lost Alpha Detectors (N/C)	Reflectometers for Plasma Position
Knock-on Tail Neutron Spectrom. (N/C)	Reflectometers for Divertor Plasma
Optical/IR Systems	Fast Wave Reflectometry (N/C)
Thomson Scattering (Core)	**Plasma-Facing Components and Operational Diagnostics**
Thomson Scattering (Edge)	IR Cameras, visible/IR TV
Thomson Scattering (X-Point)	Thermocouples
Thomson Scattering (Divertor)	Pressure Gauges
Toroidal Interferom./Polarimetric System	Residual Gas Analyzers
Polarimetric System (Pol. Field Meas)	IR Thermography Divertor
Collective Scattering System	Langmuir Probes
Bolometric System	**Diagnostic Neutral Beam**
Bolometric Array For Main Plasma	
Bolometric Array For Divertor	

- **Measurements for**:
- Machine protection
- Plasma control
- Physics studies
- ~45 parameters in total

ITER diagnostics are port-based where possible

Each diagnostic port-plug contains an integrated instrumentation package

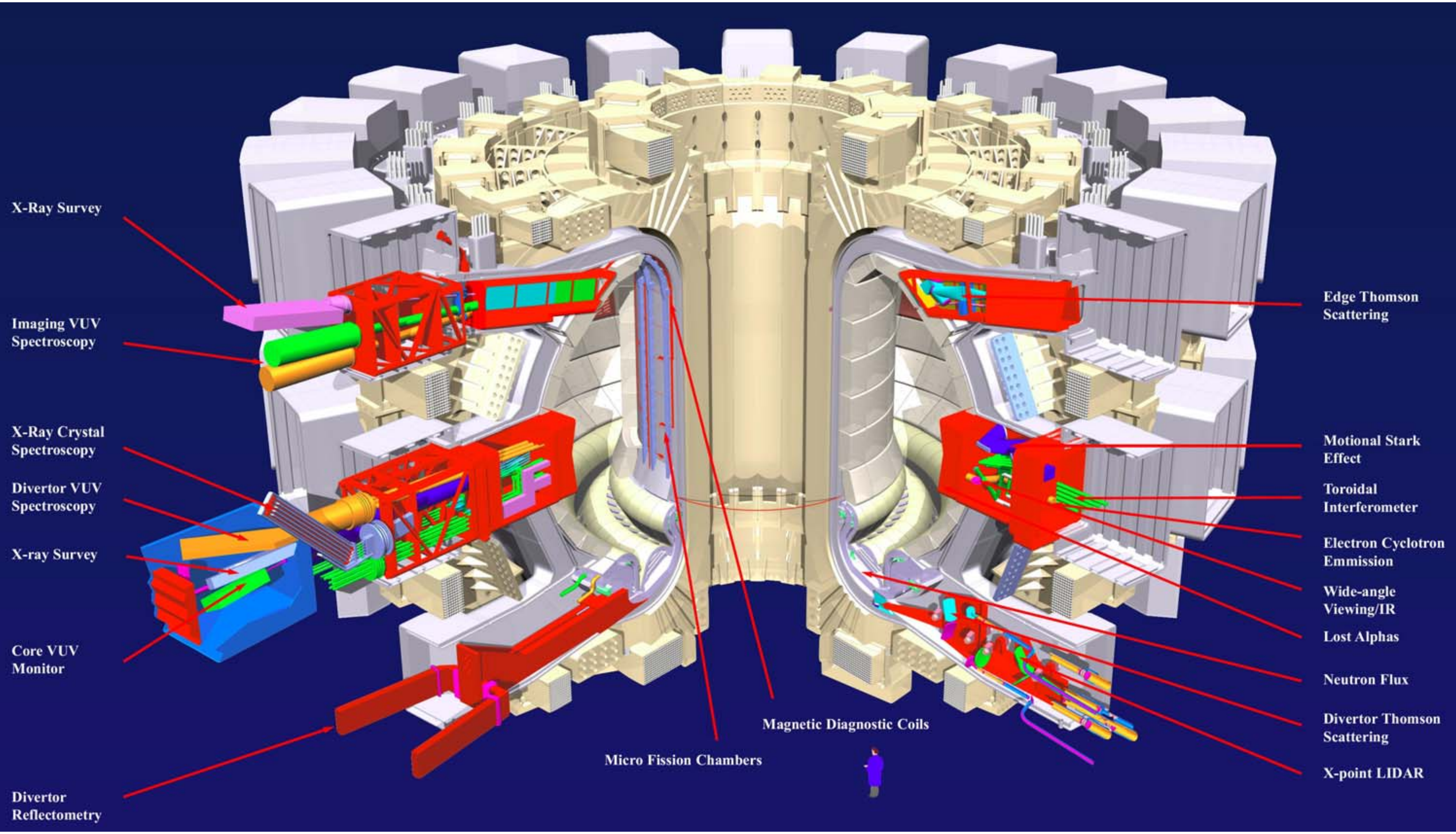

Upper & equatorial port allocations

G 55 GR 174 04-06-25 W 0.1

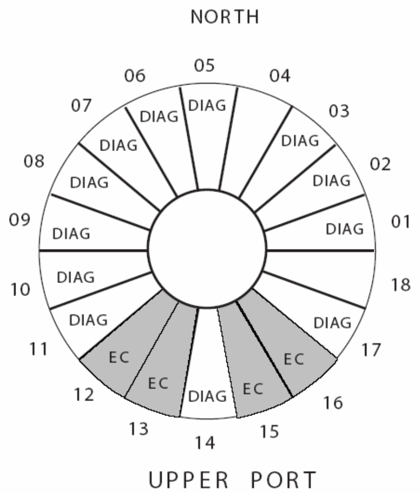

01 F03 Position Reflectometry (1 of 2)
E04 Divertor Impurity Monitor
B08 Activation System (16N, 1 of 2)

02 G10 Vis. / IR TV (1 of 6)
E02 Ha spectroscopy (divertor outer)
E02 Ha spectroscopy (outer edge)

03 E01 CXRS (on the DNB, core)
B02 Vertical Neutron Camera (1 of 3)

05 G10 Vis. / IR TV (2 of 6)
B08 Activation System (16N, 2 of 2)
B02 Vertical Neutron Camera (2 of 3)

06 E03 VUV grazing image (x 2)
B08 Activation System (foil, 1 of 2)

07 E02 Ha spectroscopy (inner edge)
E02 Ha spectroscopy (upper edge)
B02 Vertical Neutron Camera (3 of 3)

08 G10 Vis. / IR TV (3 of 6)
F09 Main Reflectometry (1 of 3)
D01 Bolometry

09 E05 X-ray Crystal Spectr (imaging)
F09 Main Reflectometry (2 of 3)

10 C06 Polarimeter

11 G10 Vis. / IR TV (4 of 6)
C02 Edge Thomson Scattering
B08 Activation System (foil, 2 of 2)

12 (EC), C07 CTS

14 G10 Vis. / IR TV (5 of 6)
E05 X-ray Crystal Spectrometry (survey)
F03 Position Reflectometry (2 of 2)

17 G10 Vis. / IR TV (6 of 6)
F02 Main Reflectometry (3 of 3)
E05 X-ray Crystal Spectrometry (graphite)
D01 Bolometry,
E07 Soft X-ray Array

G 55 GR 174 04-06-25 W 0.1

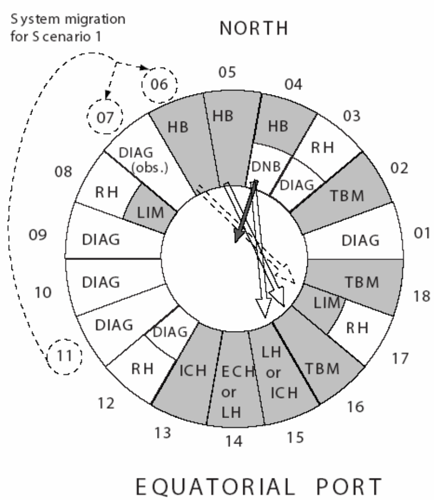

01 G01 Vis. / IR TV (1 of 4)
B01 Radial Neutron Camera
D01 Bolometry,
E11 MSE (core, HB4)
E04 Divertor Impurity Monitor
B07 Gamma Ray Spectroscopy
B11 High Resolution Neutron Spectr

03 G01 Vis. / IR TV (2 of 4)
E12 CXRS (on the DNB)
E11 MSE (edge, HB5)
E02 Ha Spectroscopy (divertor inner)

07 B08 Activation System (16N, 1 of 2)
B08 Activation System (foil, 1 of 2)
B04 Neutron Flux Monitor (DD)

08 B04 Neutron Flux Monitor (DT)

09 G01 Vis. / IR TV (3 of 4)
C05 Toroidal Interferometer/Polarimeter
E05 X-Ray Crystal Spect (Imaging)
F01 ECE,
F07 Fast Wave Reflectometry
E07 Soft X-ray Array

10 C01 Thomson Scattering main plasma)
C06 Polarimeter
C08Thomson Scattering (inner divertor)

11 E05 X-ray Crystal Spect (survey)
E03 VUV (main and divertor)
F02 Reflectometry (main plasma)
E08 NPA

12 G01 Vis. / IR TV (4 of 4)
E02 Ha Spect (upper edge)
E06 Visible Continuum Array
C07 CTS

17 B04 Neutron Flux Monitor (DT)
B08 Activation System (16N, 1 of 2)
B08 Activation System (foil, 2 of 2)

Divertor port allocations

G 55 GR 174 04-06-25 W 0.1

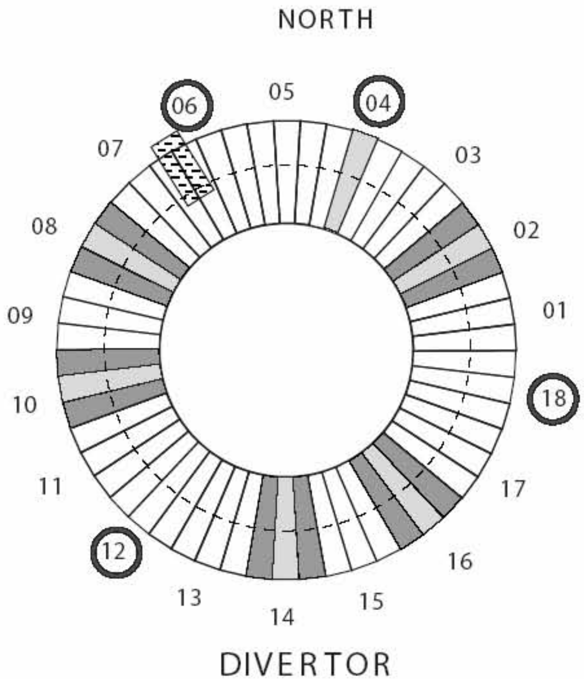

Optical access (c: centre, g: gap) & Cassette Instrumentation (i)

Cassette Instrumentation(i)

Pumping Duct Instrumentation(d)

suitable location for B02 VV Vertical Neutron Camera

02 E04 Divertor Impurity Monitor (Visible, gcg)
G07 Langmuir Probes (i)
A03 Magnetics (i)
G02 Thermocouples (i)

04 G09 Dust measurement (c)
A03 Magnetics (i)
G03 Pressure Gauges (i)
G04 Pressure Gauge(d), RGA (d)

06 B08 Activation System (foil, 1/3)
G04 Pressure Gauge (d), RGA (d)

08 F10 Reflectometry/Interferometry (gg)
E10 LIF (c)
A03 Magnetics(i)
D01 Bolometry(i),
G03 Pressure Gauges(i)

10 C03 X-point Thomson Scattering (c)
D04 Divertor Thomson Scattering (outer leg,g)
E02 Ha Spectroscopy (g)
G07 Langmuir Probes (i)
A03 Magnetics (i)
D01 Bolometry (i),
G03 Pressure Gauges (i)

12 B08 Activation System (foil, 2/3)
G04 Pressure Gauge (d), RGA (d)

14 F04 Reflectometry/Interferometry (gg)
G08 Plate Erosion (c)
G07 Langmuir Probes (i)
A03 Magnetics (i)
G02 Thermocouples (i)

16 E04 Divertor Impurity Monitor (VUV, gg)
G06 IR thermography (c)
A03 Magnetics (i)
D01 Bolometry (i),
G03 Pressure Gauges (i)

18 B08 Activation System (foil, 3/3)
G04 Pressure Gauge (d), RGA (d)

ITER Equatorial port #11

Eq	11
E05	X-Ray Crystal Spectrometry (Survey)
E03	VUV Spectroscopy (main)
E04	VUV Spectroscopy (divertor)
F02	Refl, Doppler Reflectometry
E08	**Neutral Particle analyser (NPA)**

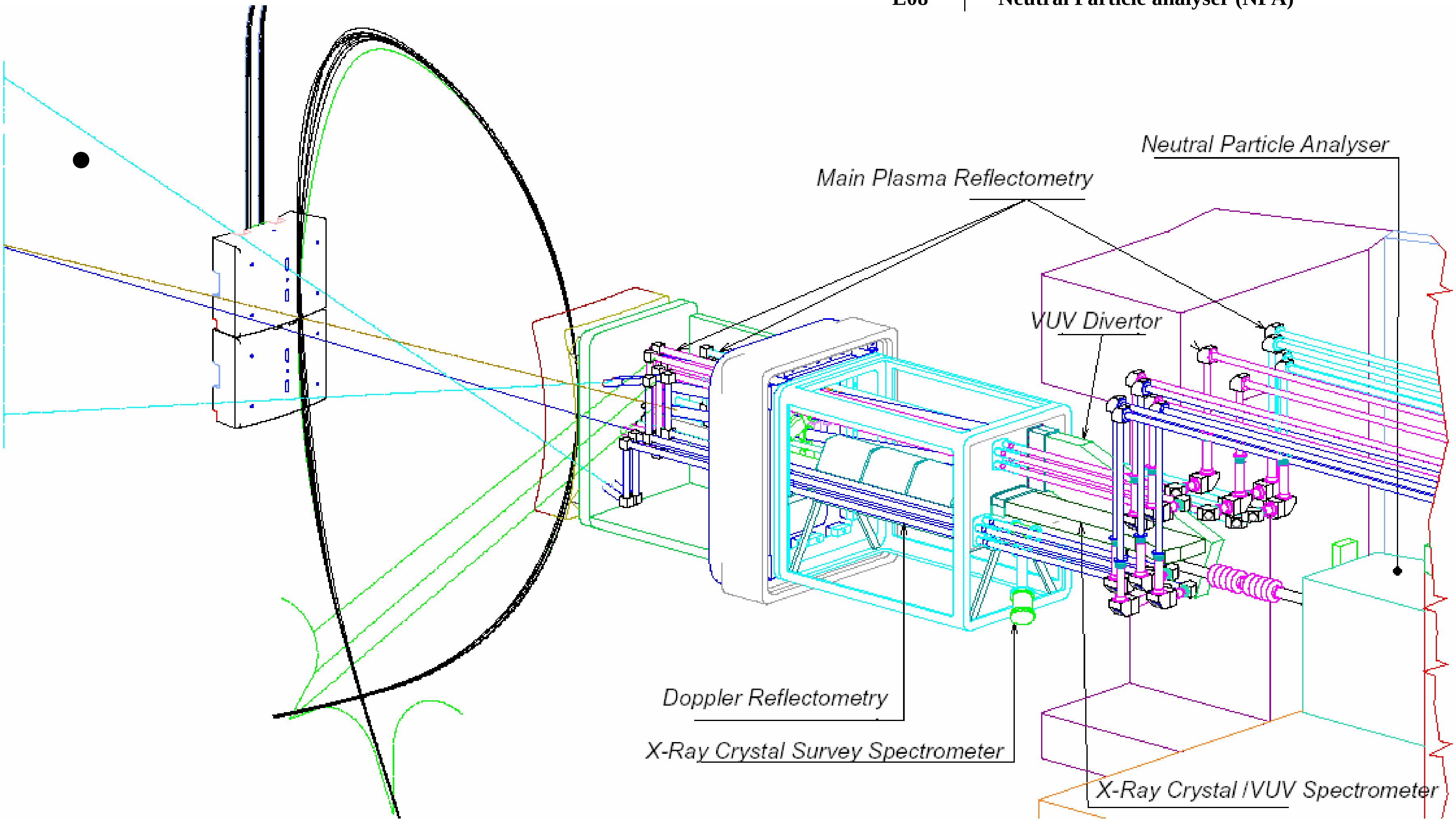

Eq#11

- Diagnostic Modules
- Waveguides suggest possibly longitudinal segmentation
- Port Plug Flange
  - Vacuum extensions
  - Waveguide windows
  - Shielded interspace structure

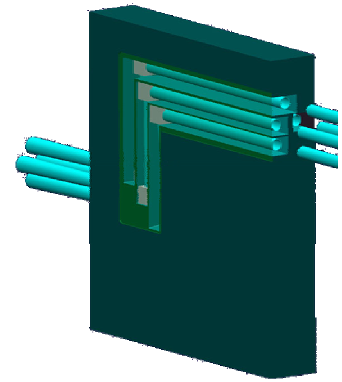

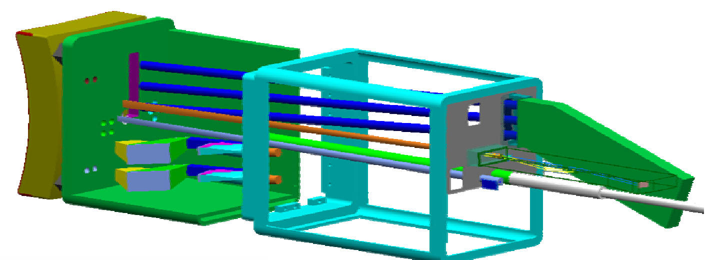

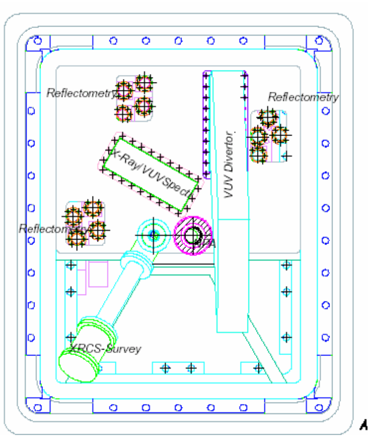

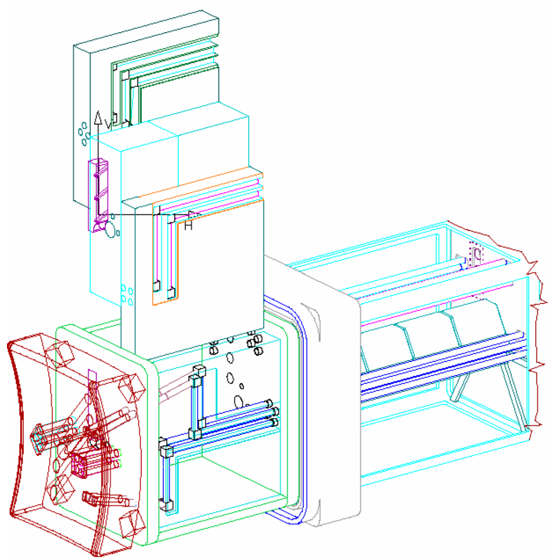

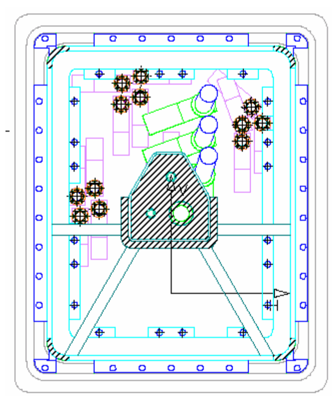

- Bio-shield penetration
- VV movement relative to building
- Port Cell layout
- Removable equipment
- Extended vacuum boundary
- Pumping
- Pressure boundary
- Wall penetration

Eq#11

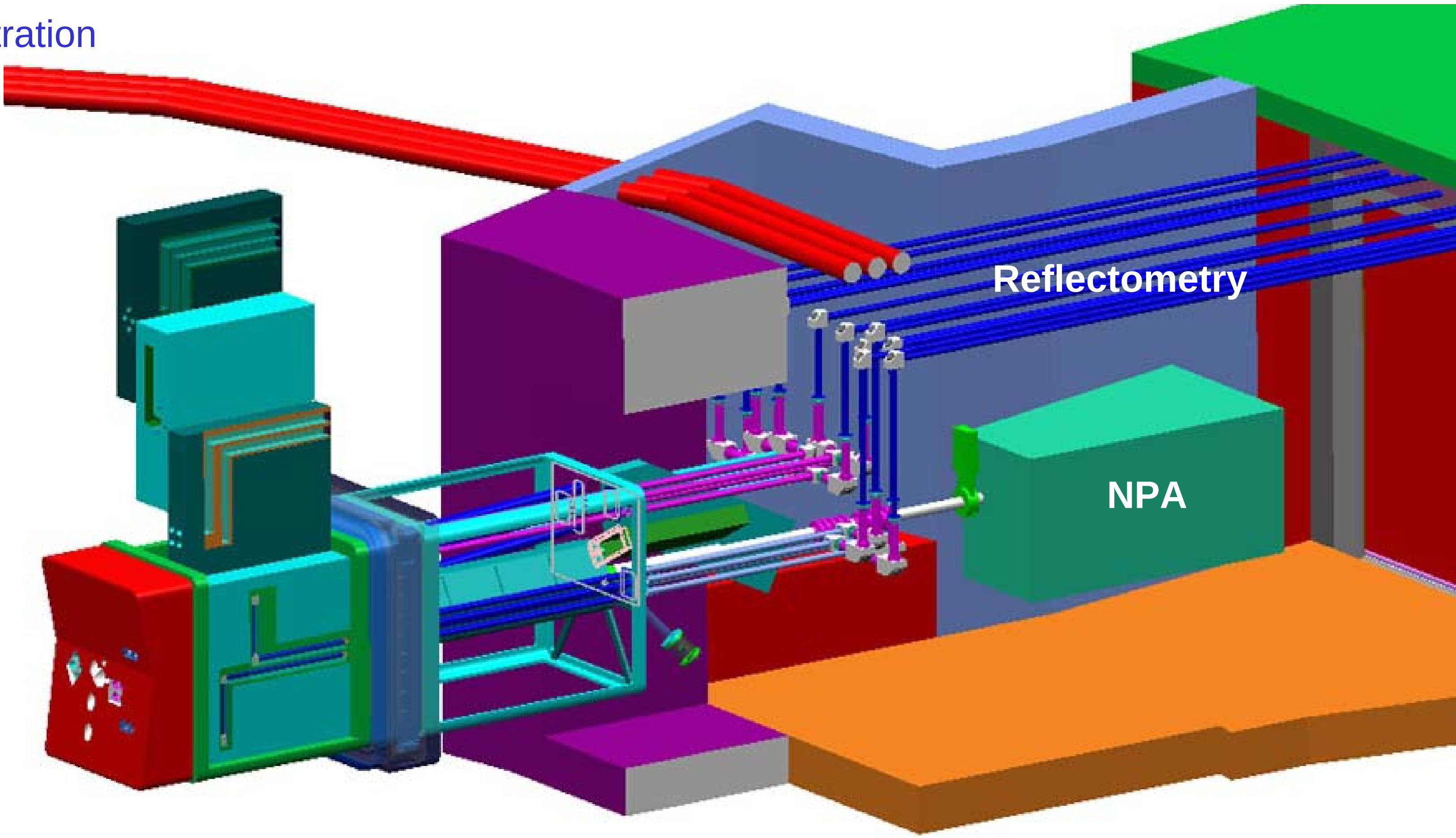

Exploded view of ITER equatorial port #1

Lead diagnostic is the radial neutron camera

Port Plug (green) Interfaces with

- Diagnostic Components (coloured)
- Other ITER (grey)
- Standard Port Plug Structure
- With Common cut-outs

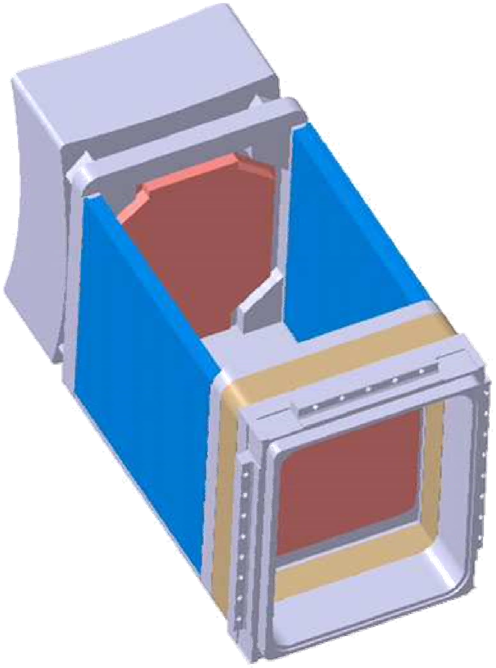

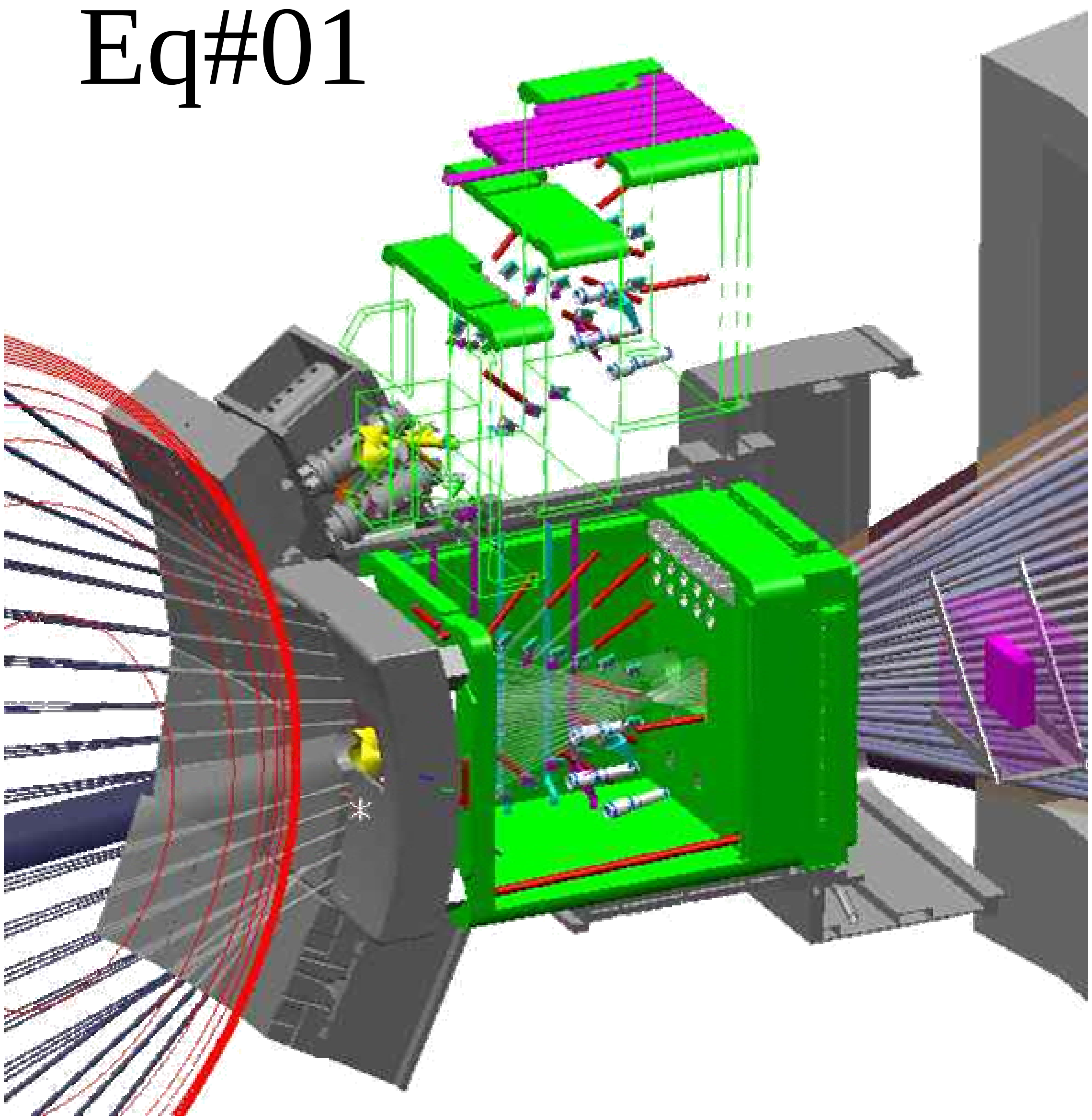

Neutronic analysis of core CXRS optics on ITER upper port #3

G.E.Shatalov, S.V.Sheludiakov, Kurchatov Inst. Moscow

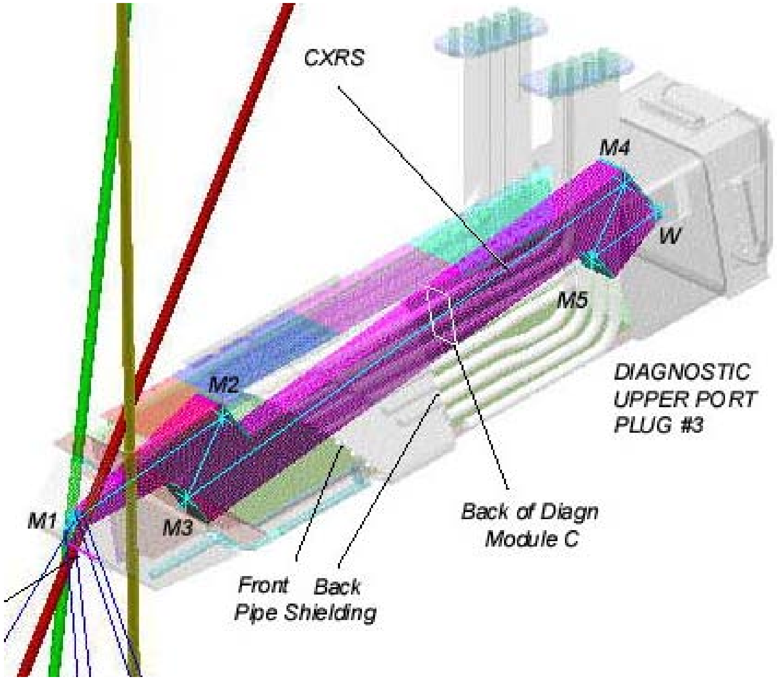

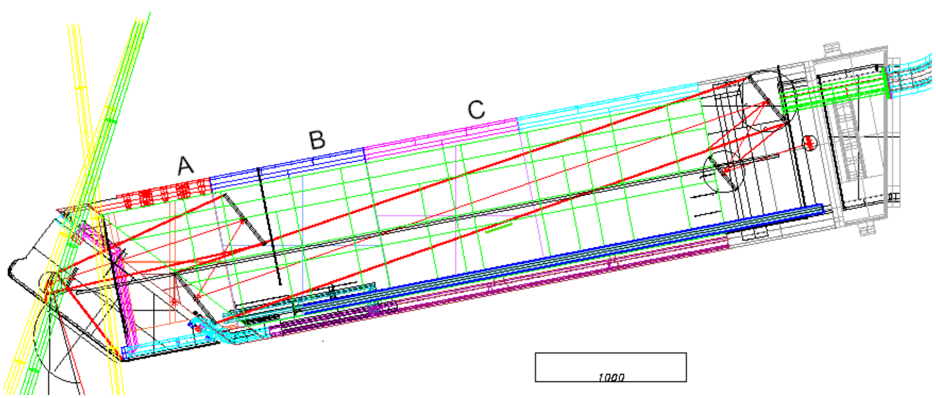

The neutron environment ranges from mild behind the port-plug to severe at the blanket.

StSt:H_2O 80:20,
Allowable activation
at Flange <100 uSv/hr
behind BioSh <10 uSv/hr

Normalized to 500 MW fusion power
Neutron flux at flange ~ 1. 10^7 n/cm^2 s^{-1}
This is less than inside JET torus hall.

Equivalent to
local dose <5 uSv/h (10 days after s/d)

Total nuclear heating power to:

BSM	420 kW
A	58 kW
B	0.43 kW
C	9W

Addition power deposition in TFC ~10W
M1 Heating ~2W/cc
Total Neutron flux ~6.10^{13} n/cm^2 s^{-1}

Infra-red thermography of walls and divertor targets

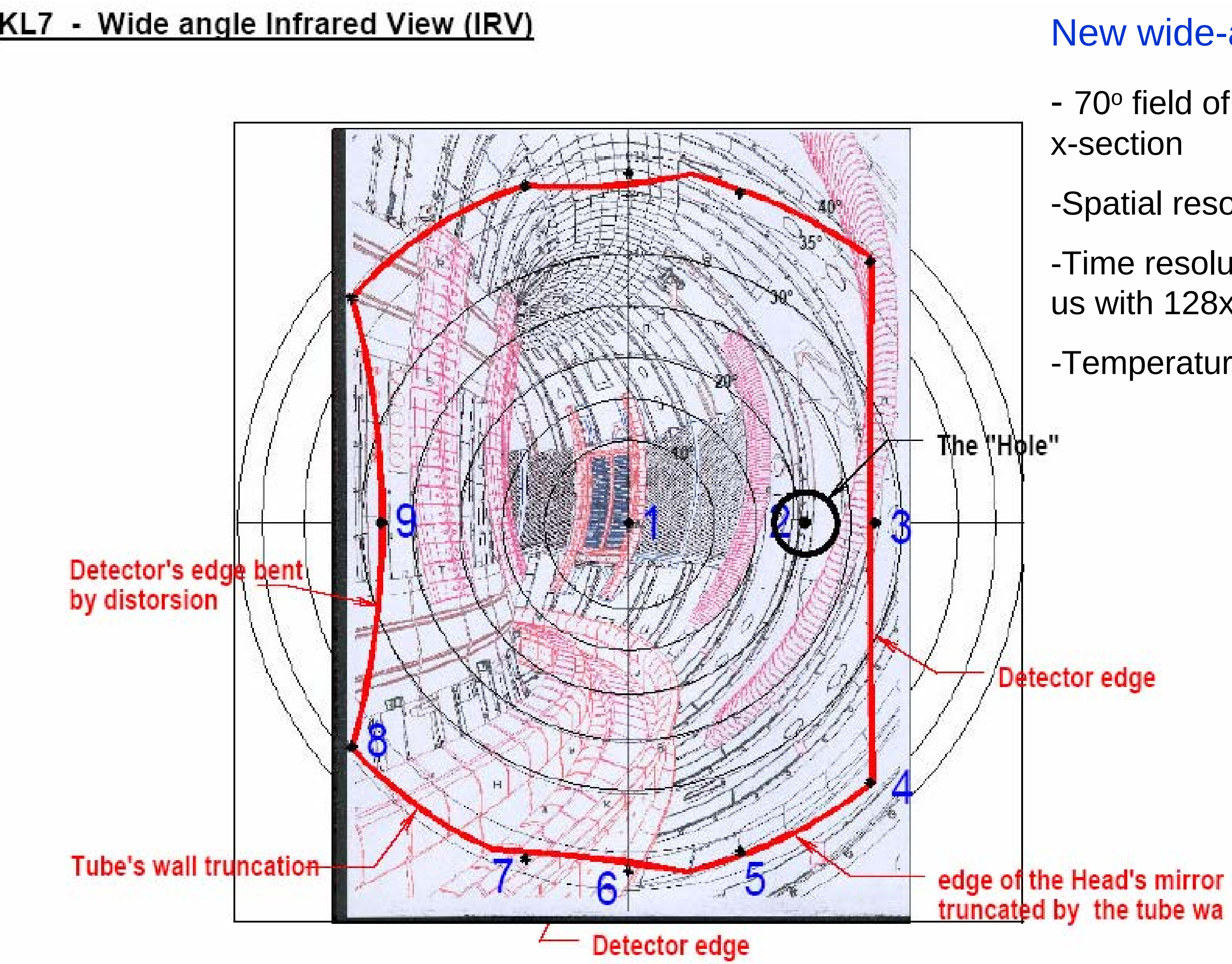

New wide-angle IR camera for JET

- 70º field of view covers full poloidal x-section

-Spatial resolution 10-20 mm

-Time resolution 10 ms, 640 x 512, 100 us with 128x8 window

-Temperature range 200 - 2300º C

New wide-angle IR camera for JET

E Gauthier (CEA), P Andrew (UKAEA)

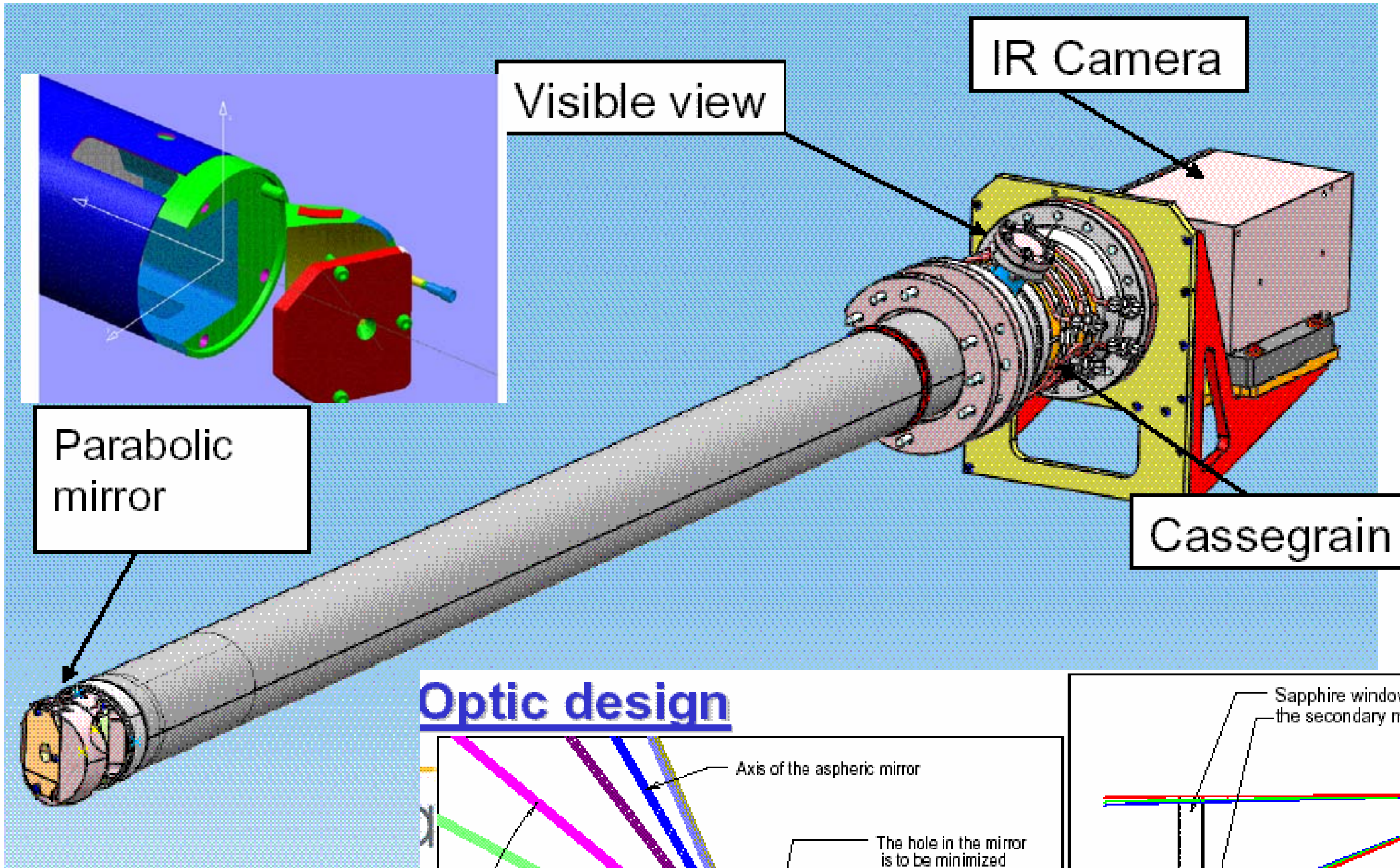

Optic design

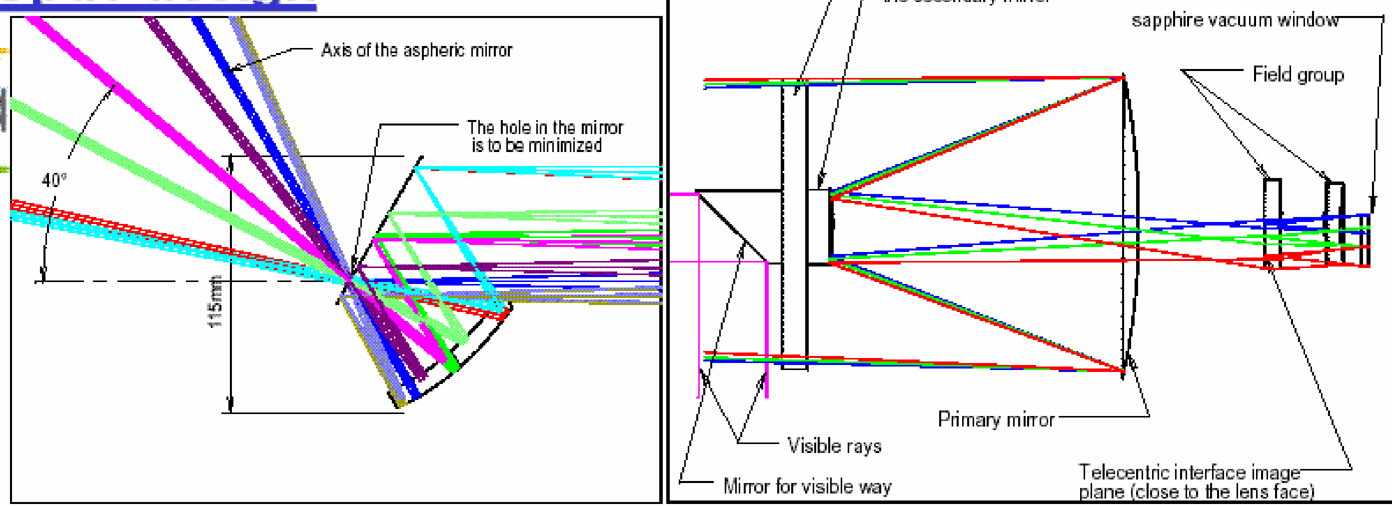

JET Bolometer camera

K McKormick (IPP,Garching), A Huber (FZK)

- Bolometers measure plasma radiation profile and total radiated power P_{rad}.
- Ideally 100% absorption from IR to 100keV.
- Essential for machine protection and power balance (P_{rad} ~ 0.2 . P_{in}).
- Present technique: Resistance thermometers Au or Pt meander on Mica foil.
- 4 foils per channel in bridge to cancel neutrons etc. and eddy currents.
- Requires many in-vessel cables.
- Gold not useable on ITER : transmutes to Hg.

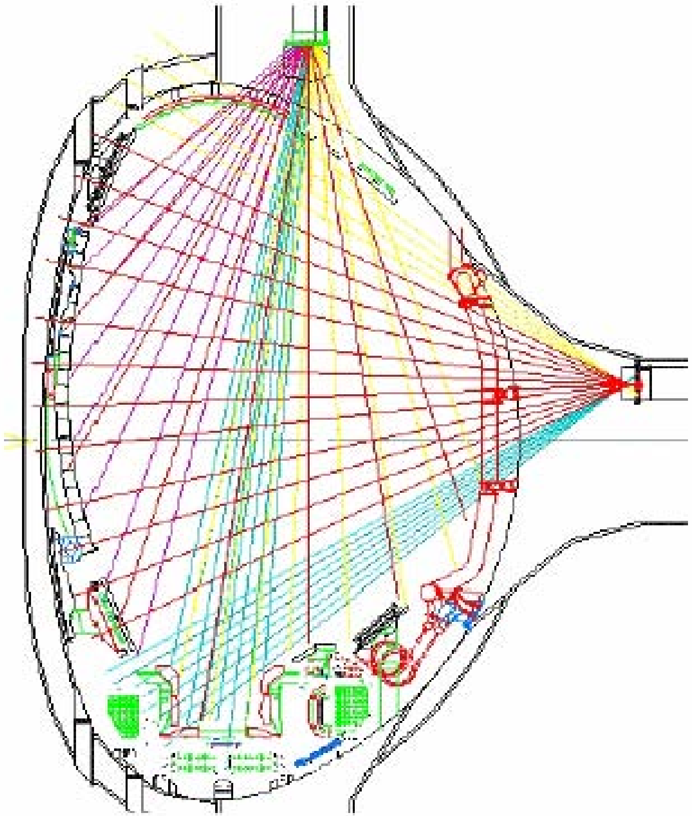

Imaging Bolometer on JT-60U (JAERI, Naka, Japan)

B.J. Peterson, et al., 30th EPS, ECA 27A P-4.067

Features:

- Pin-hole image of plasma onto gold foil
- Foil re-radiates in infra-red
- **Remote** IR camera measures heat pattern
- Solve thermal transport in foil to recover image

Design:

- IR camera: Indigo/Omega 85 mK, 30 Hz, 160 x 128 pixels, 14 bit
- Foil: Au, 0.0025 x 70 x 90 mm, E_{ph} < 8 keV
- Bolometer: 33 ms, 12(tor) x 16 (pol) = 192 ch NEPD = 300 mW/cm^2, S/N <60

Cross-section of JT-60U

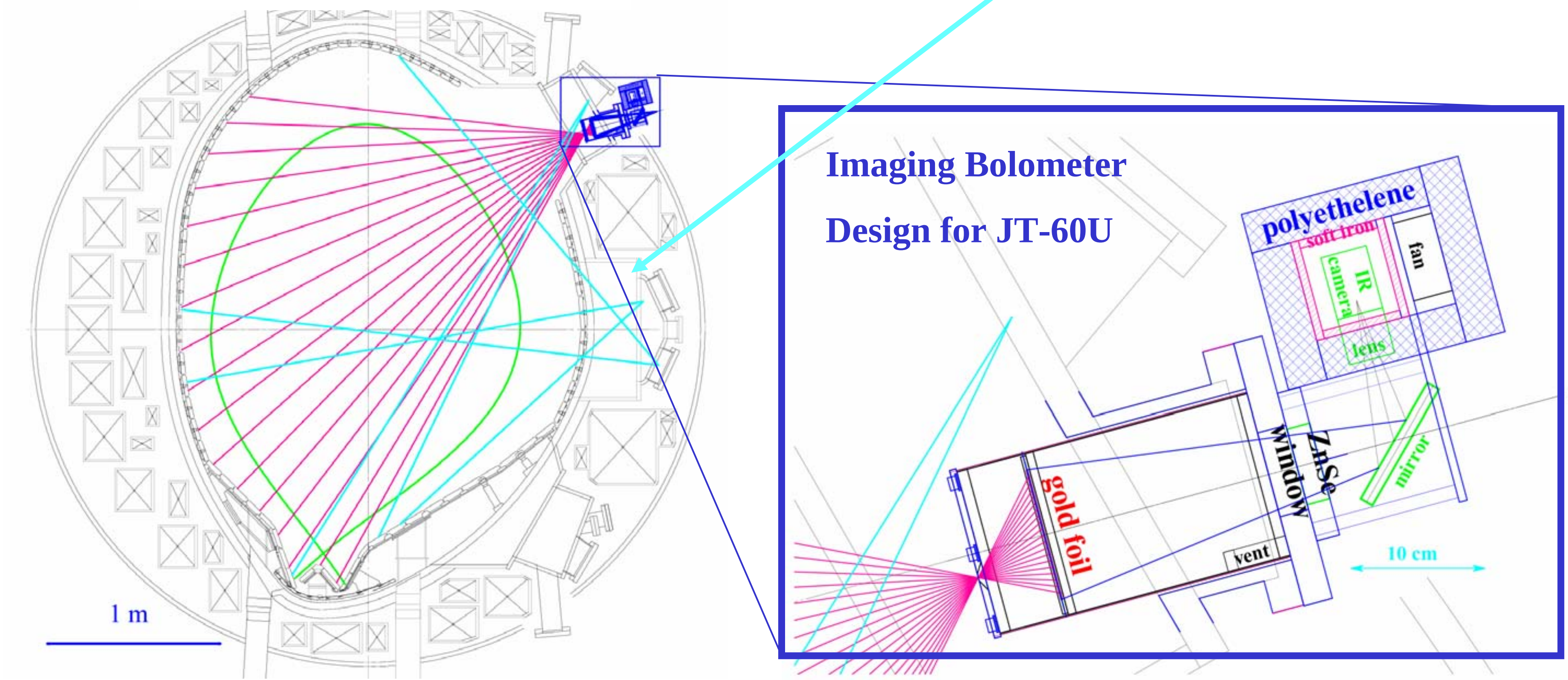

IRVB Data Analysis

B.J. Peterson et al., IEEE Trans. Plasma Sci. **30** (2002) 52-53.

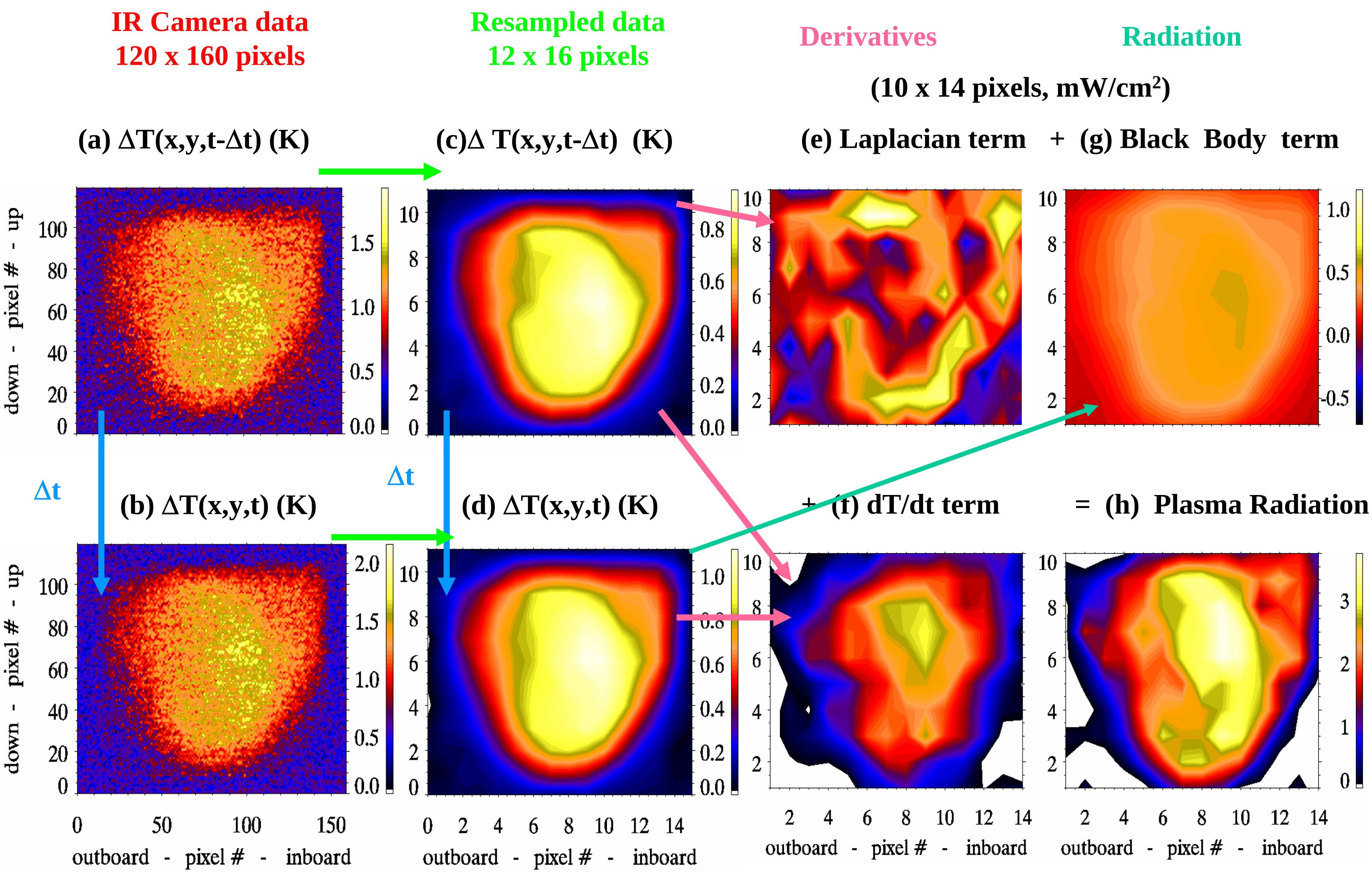

First Images from an Imaging Bolometer on a Tokamak

TV view of IRVB FOV in JT-60U

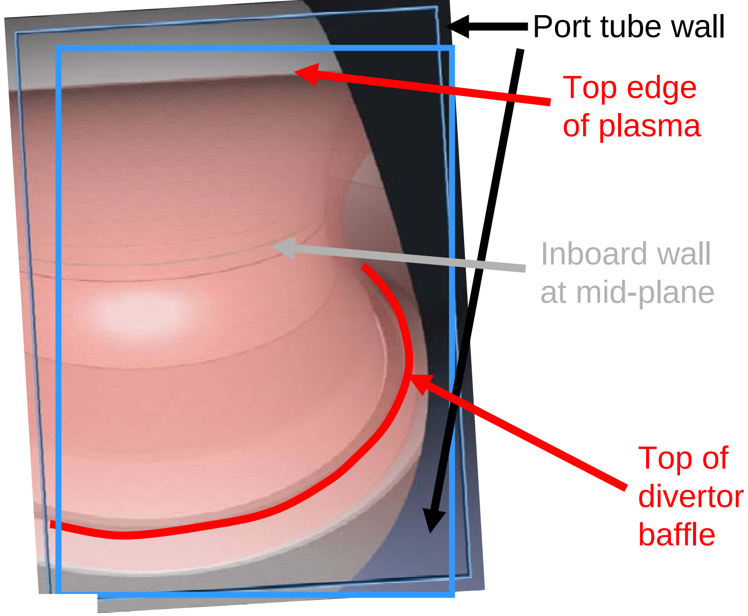

Sequential images of IR radiation from foil during disruption of Ohmic plasma

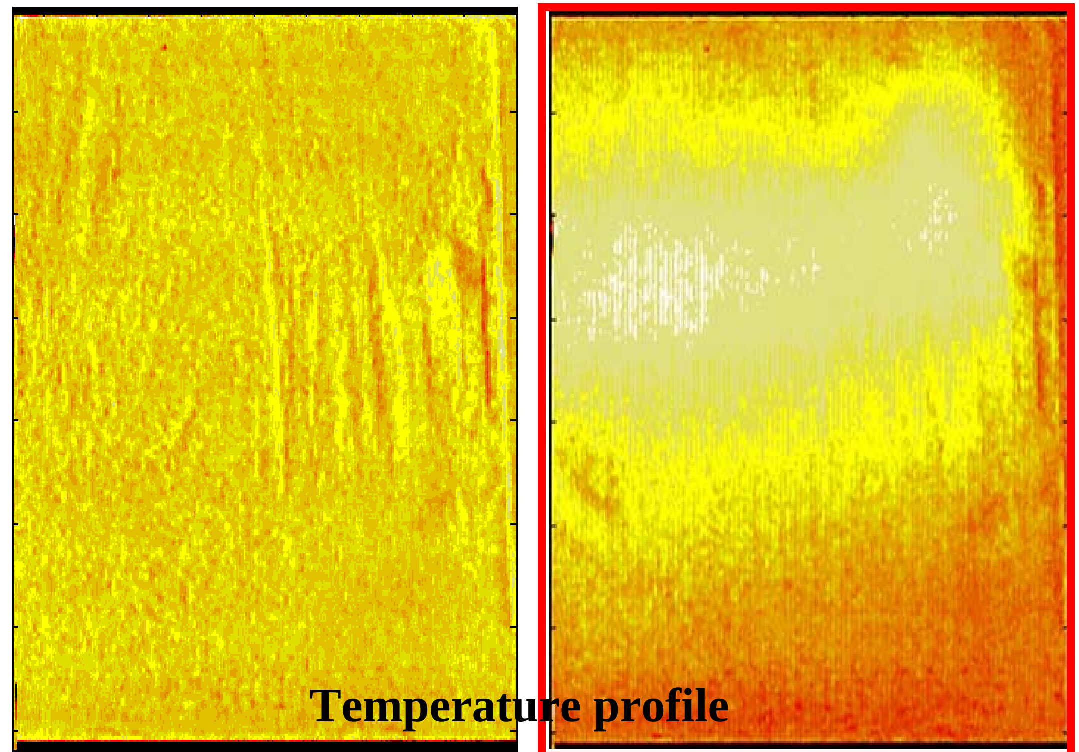

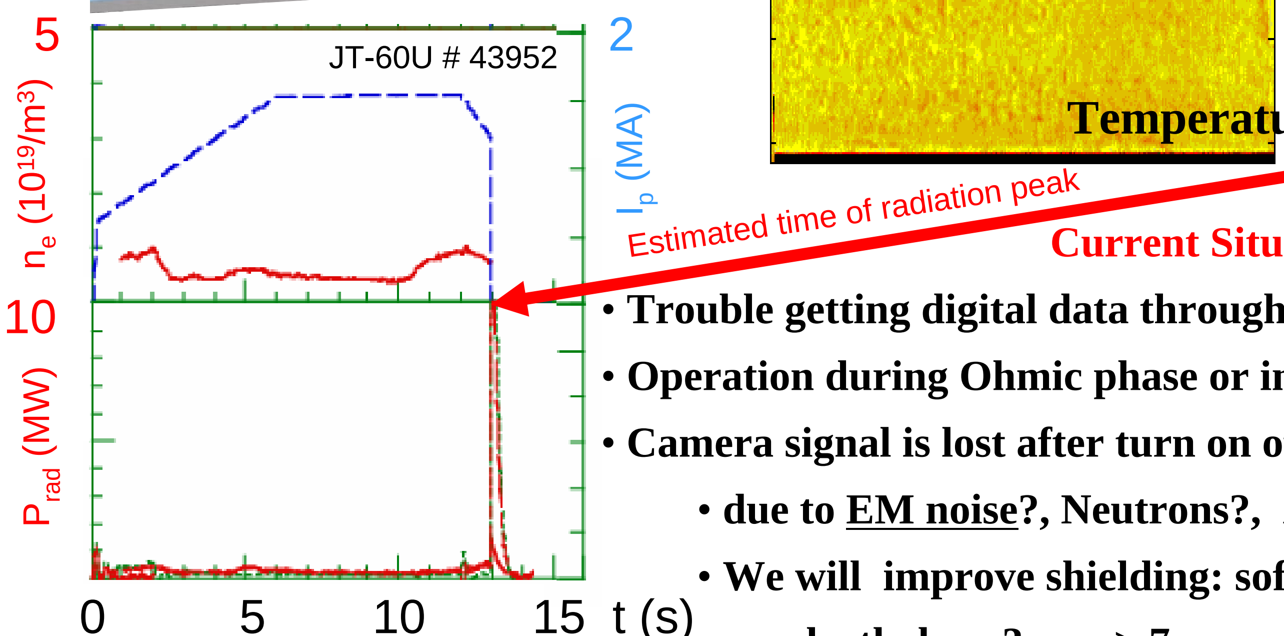

Current Situation:

- **Trouble getting digital data through Firewire link with long cables**
- **Operation during Ohmic phase or in H plasma is usually ok**
- **Camera signal is lost after turn on of high powered NBI**
  - **due to <u>EM noise</u>?, Neutrons?, X-rays, gammas?**
  - **We will improve shielding: soft iron 6 mm -> 12 mm polyethylene 3 cm -> 7 cm, add 1 cm lead**

Charge-exchange recombination spectroscopy gives **local** measurement

Based on charge exchange between heating neutral beam and fully stripped impurity ions.

eg $D + C^{6+}$ > $D^{+} + C^{5+*}$ > C^{5+} + $h\nu$

Line width > Ion temp. **Line shift** > plasma motions. **Intensity** > impurity concentrations

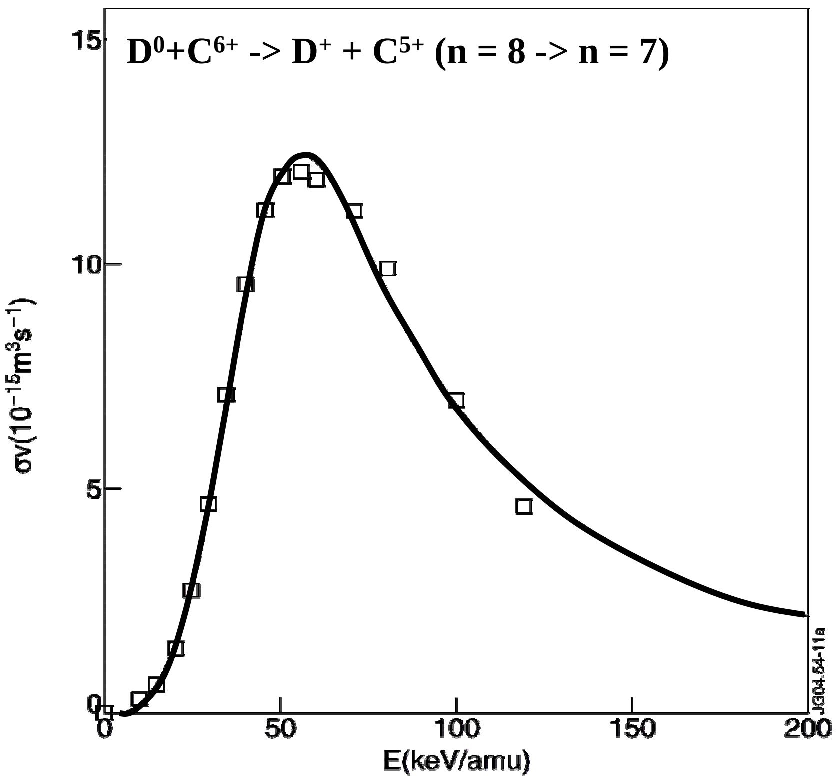

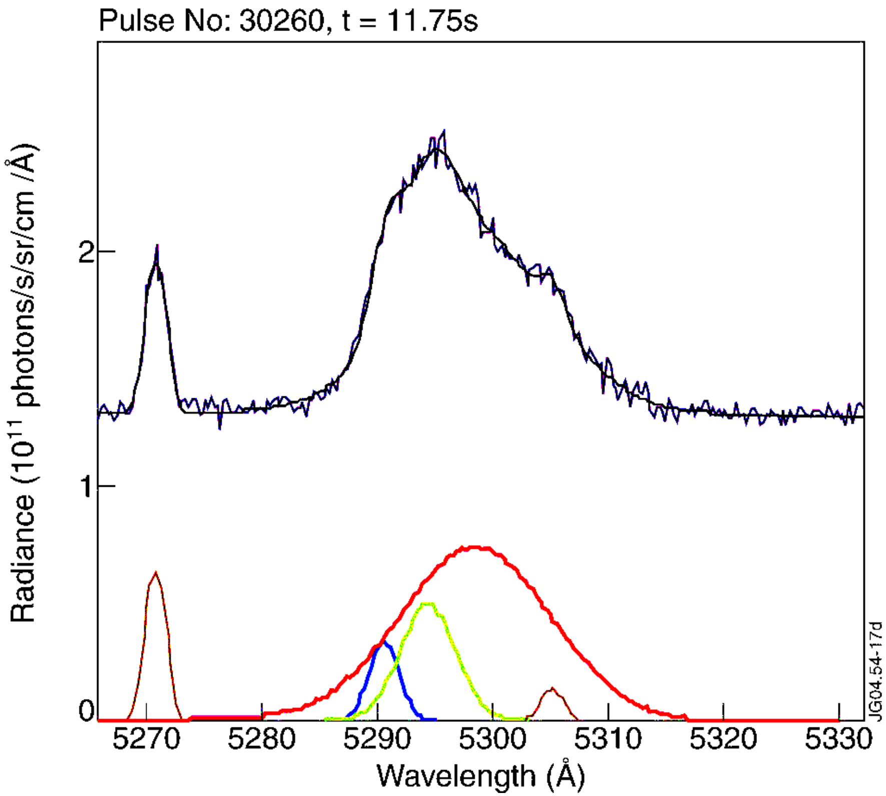

Above: Measured spectrum, Fitted spectrum

Below: C^{5+} CX from Deuterium heating beam.
Electron impact excitation of C^{5+} in edge plasma.
C^{5+} CX from edge neutrals.
Background lines Be^{+} 5271 & C^{2+} 5305

Peak CX cross-section is around 60 keV – typical of heating beams on current machines.

ITER has 1 MeV heating beams, and requires a diagnostic neutral beam for CXRS

Charge-exchange recombination spectroscopy (CXRS) at JET

K-D Zastrow, A Meigs, C Negus,C Giroud, M Stamp (UKAEA), D Hillis (ORNL), R Bell and D Johnson (PPPL)

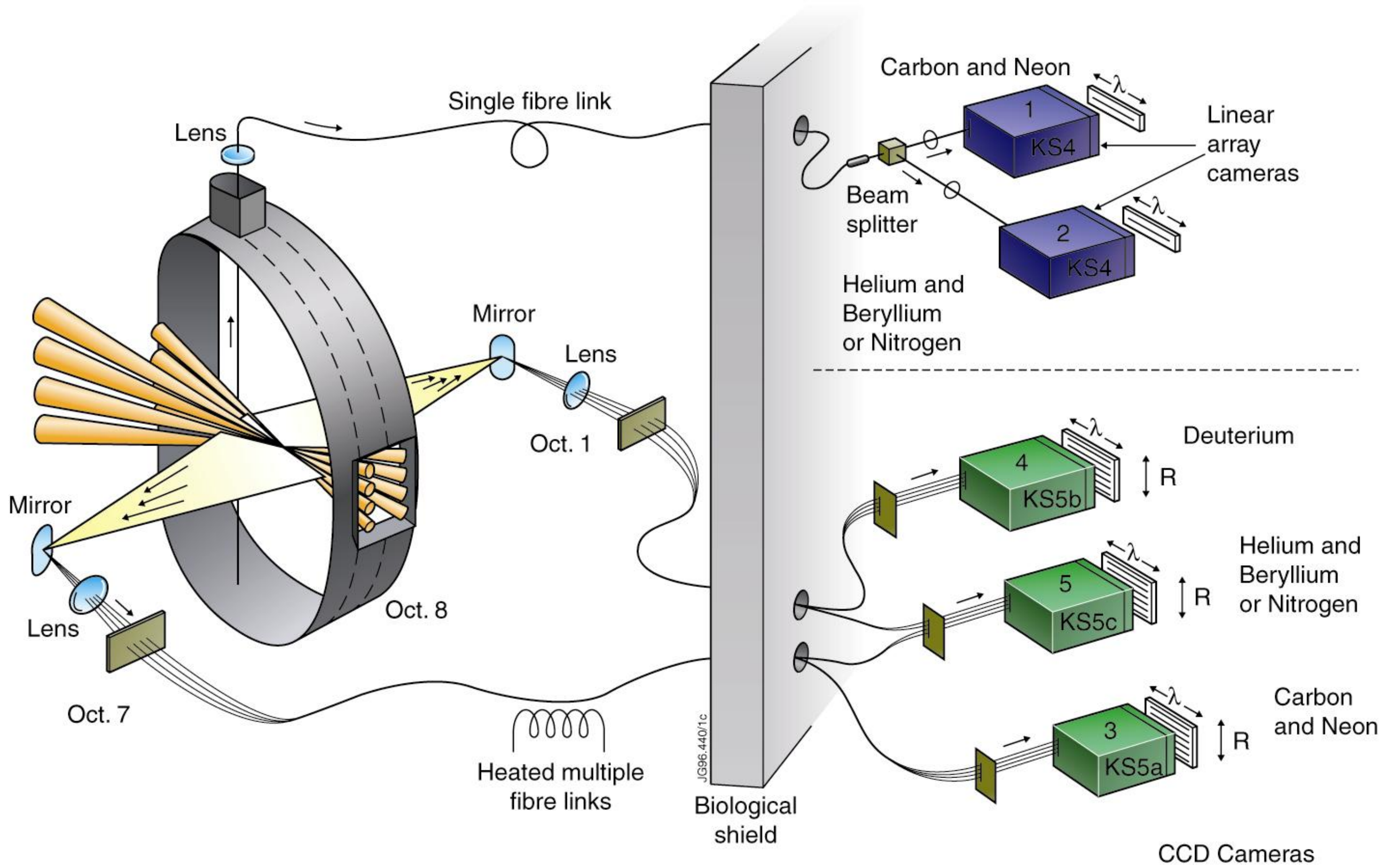

- Periscopes image the neutral beam onto the spectrometer slits via fibre bundles
- Each fibre produces a separate spectrum “track” on a visible CCD camera

Example of the use of Charge Exchange measurements on JET

Internal transport barrier **#51976**

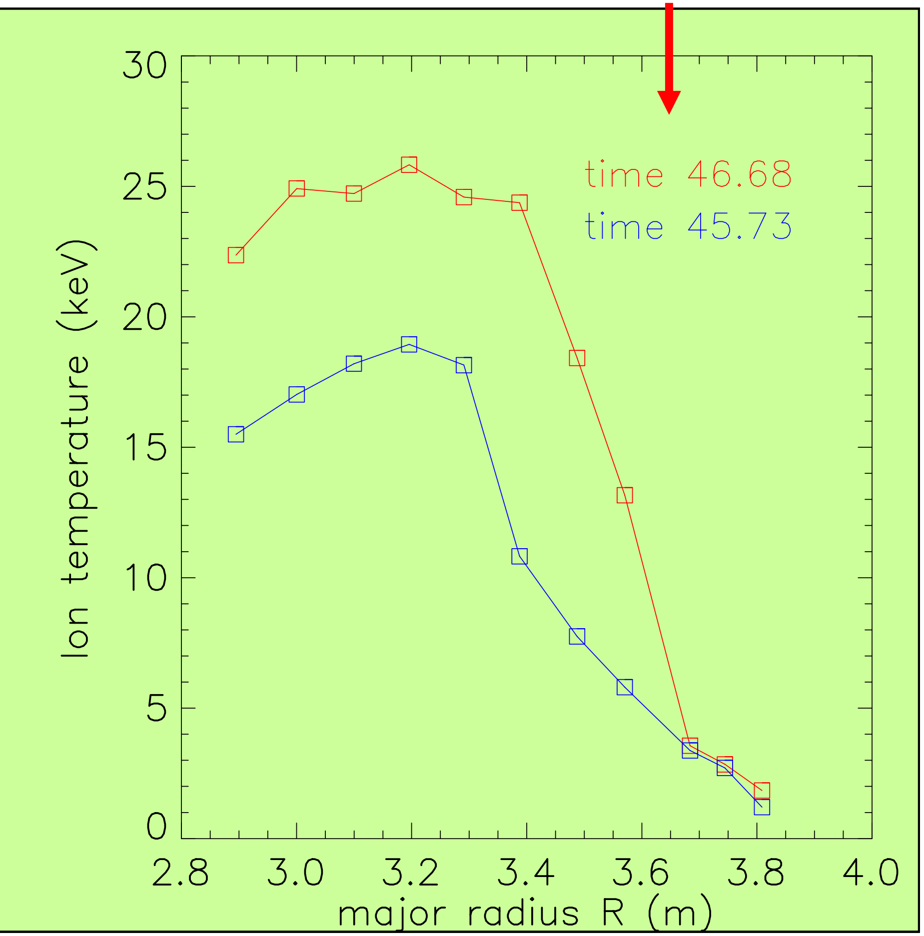

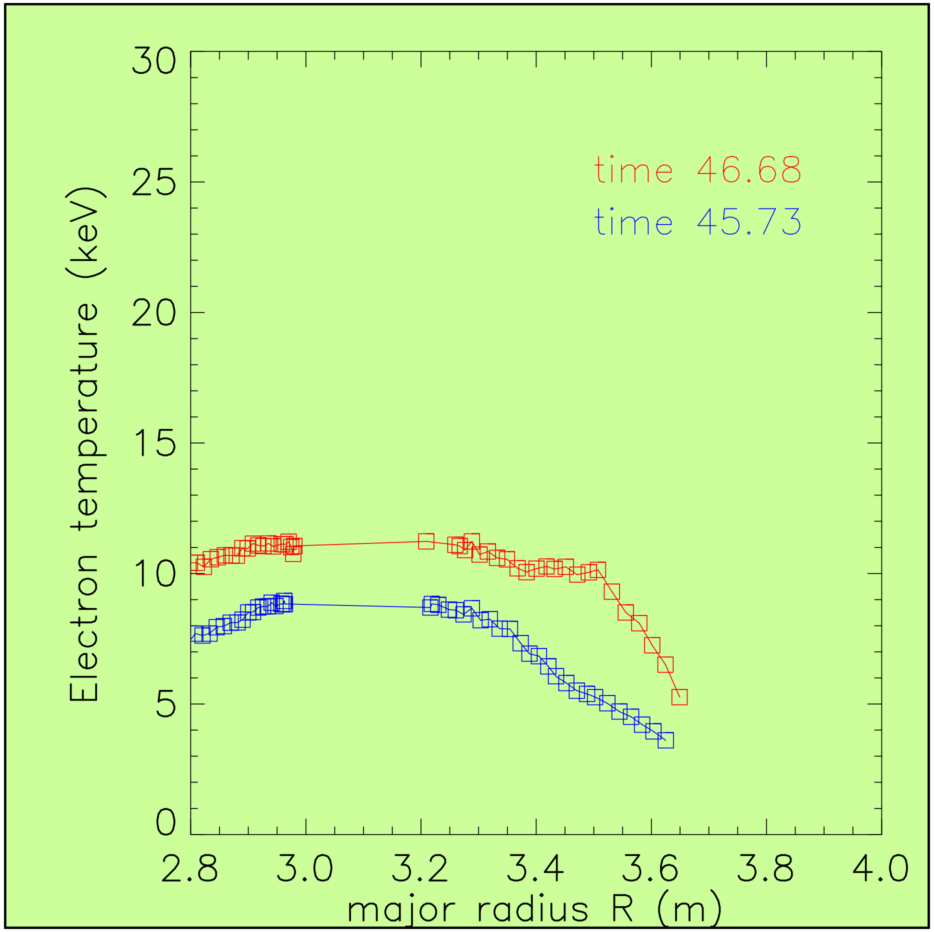

Example of Ion temperature and toroidal velocity measurement by CXRS

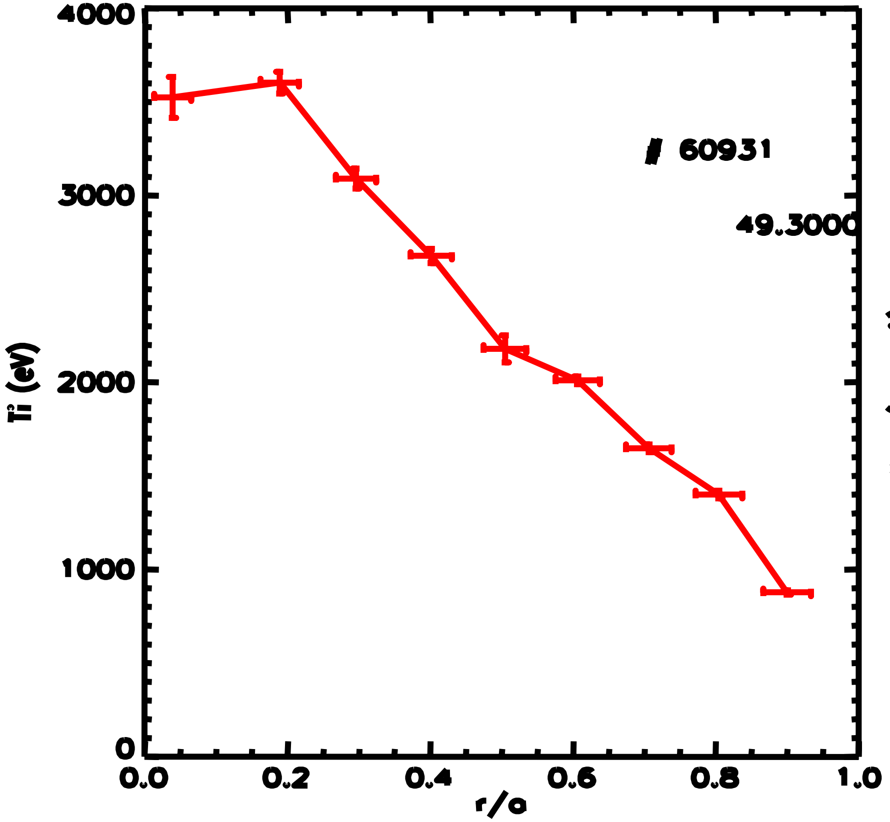

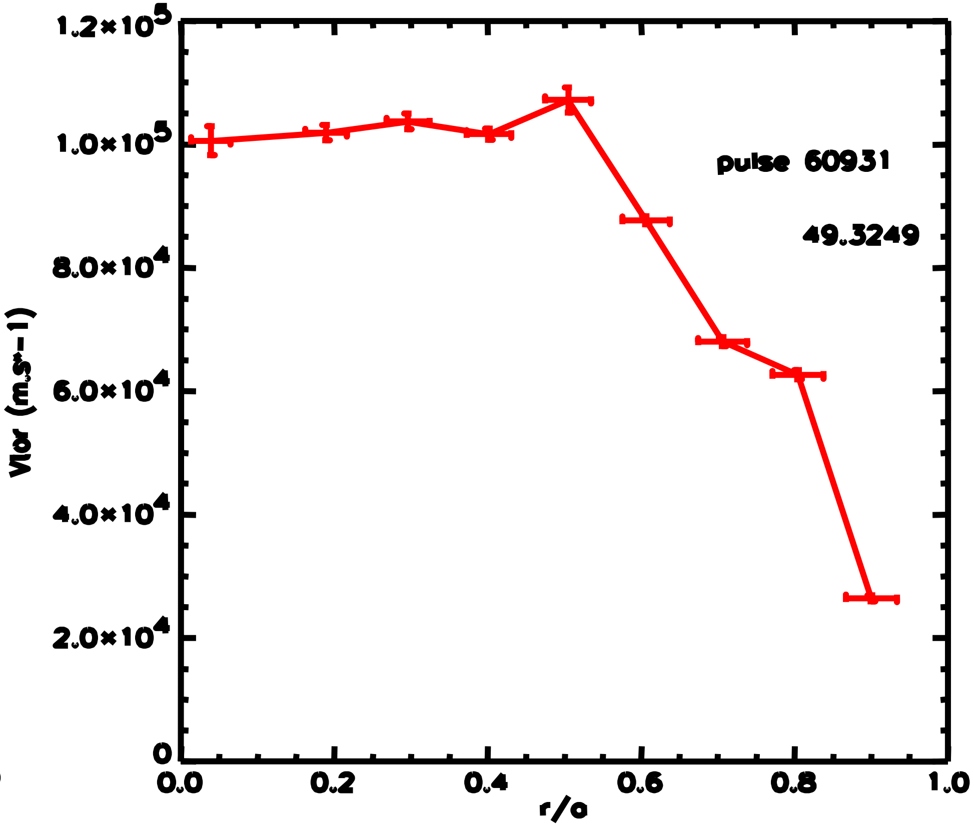

VUV spectroscopic imaging is important for the edge and divertor plasmas

- Monitor impurity influxes in real time
- Study transport

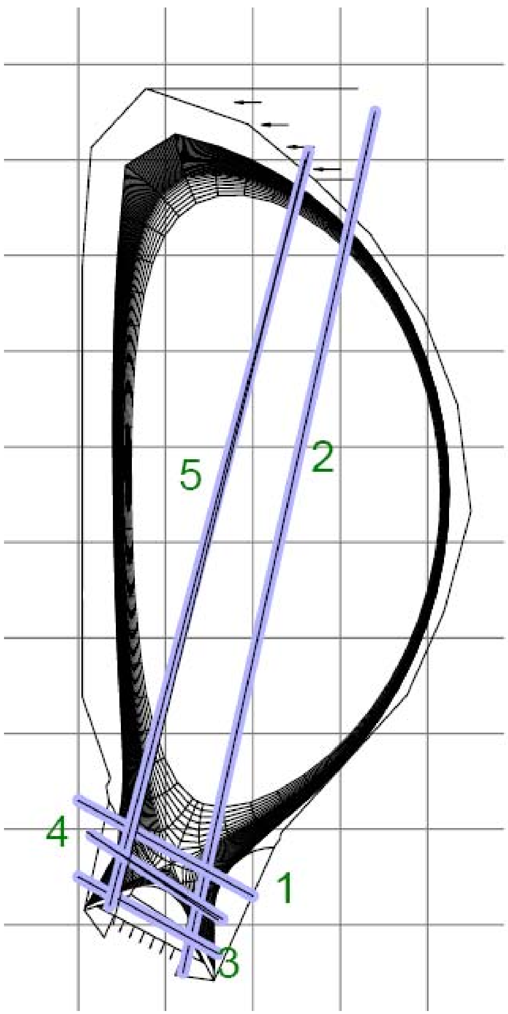

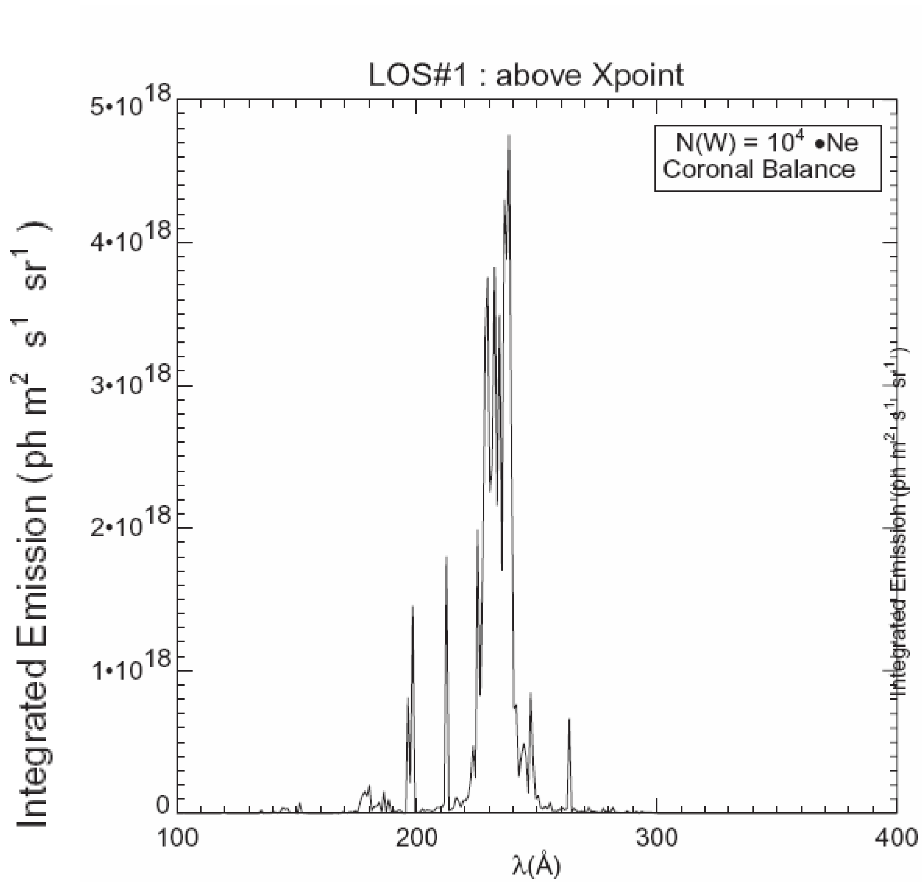

Modelled tungsten spectrum integrated along one line-of-sight in the ITER divertor plasma

JET Real-time X-ray/VUV Data

Comprehensive x-ray VUV survey spectroscopy is essential for machine protection, and to achieve burning plasma - Zeff < 2

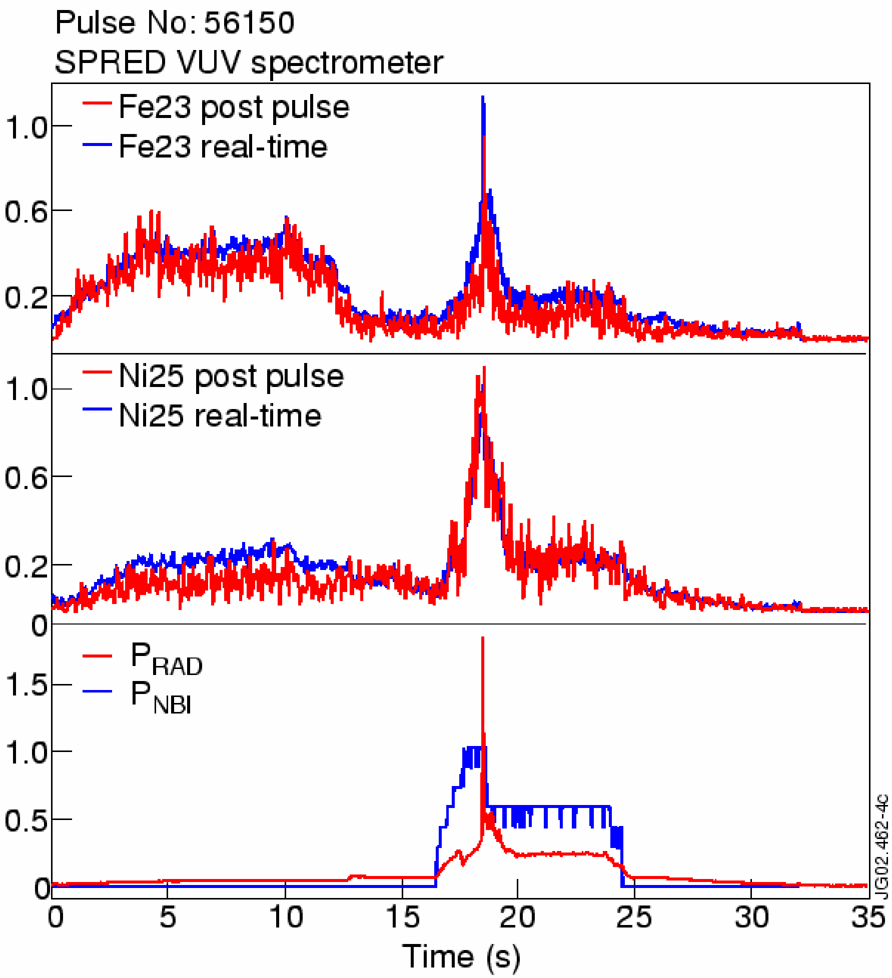

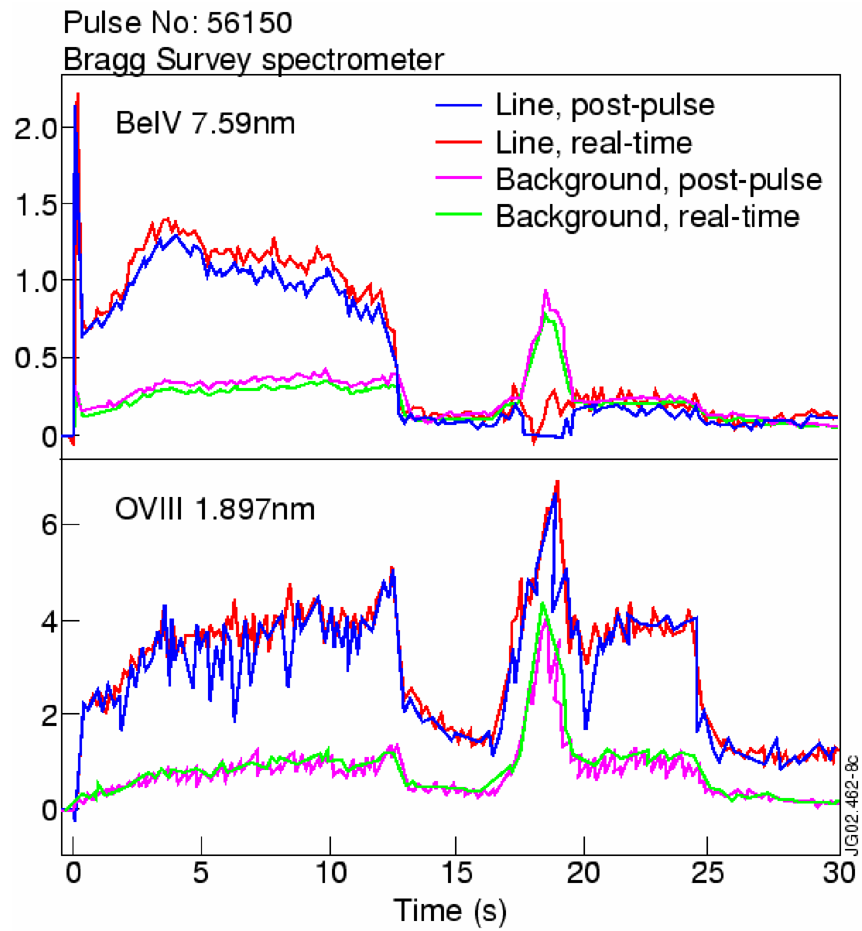

Real-time Fe XXIII and Ni XXV signal from the VUV spectrometer, compared with post-pulse values.
To prevent damage to the lower hybrid current drive launcher, operation of LHCD is interlocked to the RT Fe XXIII signal

Real-time signals from the x-ray survey spectrometer, showing line intensities and associated continuum background for Be VI and O VIII.
Most intrinsic and injected impurities can be monitored.

General layout of VUV spectrometers

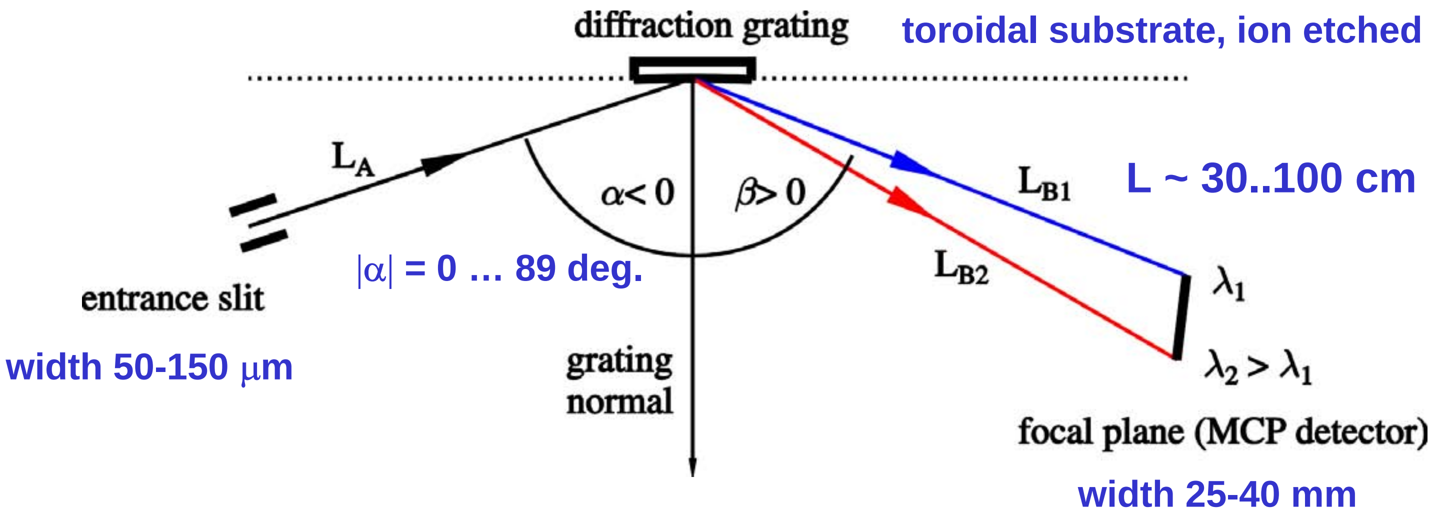

Fonck R J et al, Appl. Opt. **21** 2215 (1982)
Biel W et al., Rev. Sci. Instrum. **75** 3268 (2004)

Spectrometer design issues:

- incidence angle (reflectivity, diffraction efficiency)
- large etendue (but good wavelength resolution)
- The grating is optimized match the detector resolution

Imaging VUV spectrometer for ITER

Grating is designed to match a given detector

This design is for a conservative 100um: MCP -> phosphor –> CCD

Ray-Tracing calculations for toroidal grating ITER Imaging Dr. W. Biel, IPP, FZ Juelich

(All dimensions given are in mm, angles in degrees, origin located in the grating centre)

G = 2292.00 / mm, α= -60.000, L_A = 1300.00, rs0 = 1300.00. MCP angle = 54.00

β_1 = 54.875, β_2 = 53.750, L_{B1} = 1293.03, L_{B2} = 1292.89

Slit height 6.0, width 0.06. Grating height 16.0, width 36, aperture 50.00, Light source extended

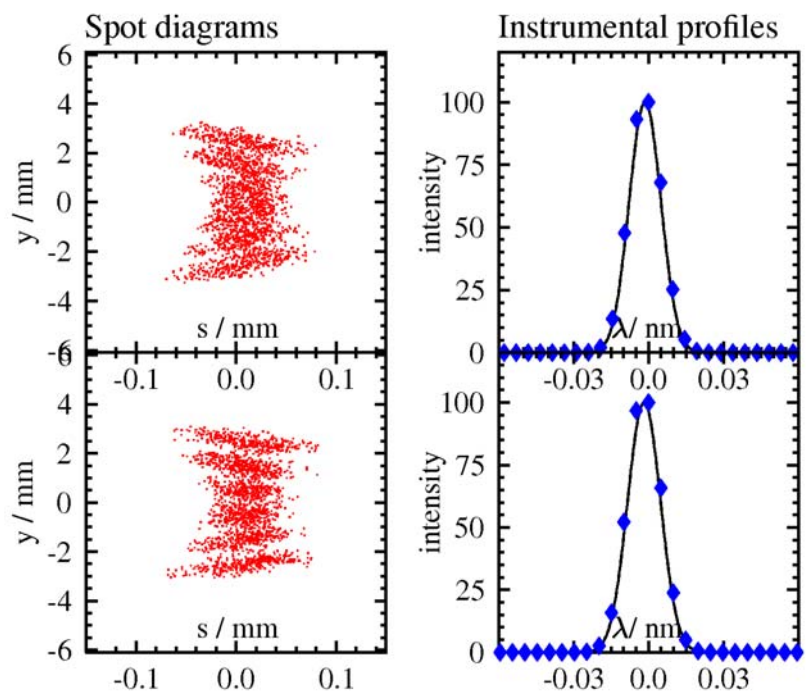

λ= 21.00 nm :
Imaging line width = 0.0117 nm
Bandpass line width = 0.0134 nm
Detected line width = 0.0149 nm
Etendue = 6.0649E-005 mm^2 sr
Transmission = 0.17549
TH = 0.99366
Dispersion = 0.19412 nm/mm

λ= 26.00 nm :
Imaging line width = 0.0123 nm
Bandpass line width = 0.0139 nm
Detected line width = 0.0155 nm
Etendue = 6.1153E-005 mm^2 sr
Transmission = 0.17695
TH = 0.99980
Dispersion = 0.19955 nm/mm

Average line width: from imaging = 0.0120 nm, mean camera output width = 0.0152 nm
Mean Resolution = 1550, mean Etendue = 6.1156E-005 mm^2 sr

Relatively high resolution
$\lambda/\lambda\delta$ ~ 1500

Relatively narrow
Wavelength range
21 nm – 26 nm

Angle of incidence:
α = 60 degrees

Relevant spectral lines:

He II	25.632 nm
Be IV	25.627 nm
C V	22.279 nm
O V	21.515 nm
Kr XXVI	22.00 nm
Ar XV	22.115 nm
Cr XXII	22.290 nm
Fe XXIV	25.509 nm
Ni XXVI	23.420 nm
Ni XVII	24.918 nm
Cu XVIII	23.424 nm

ITER Imaging VUV spectrometer in Upper Port #06
(Similar system for divertor)

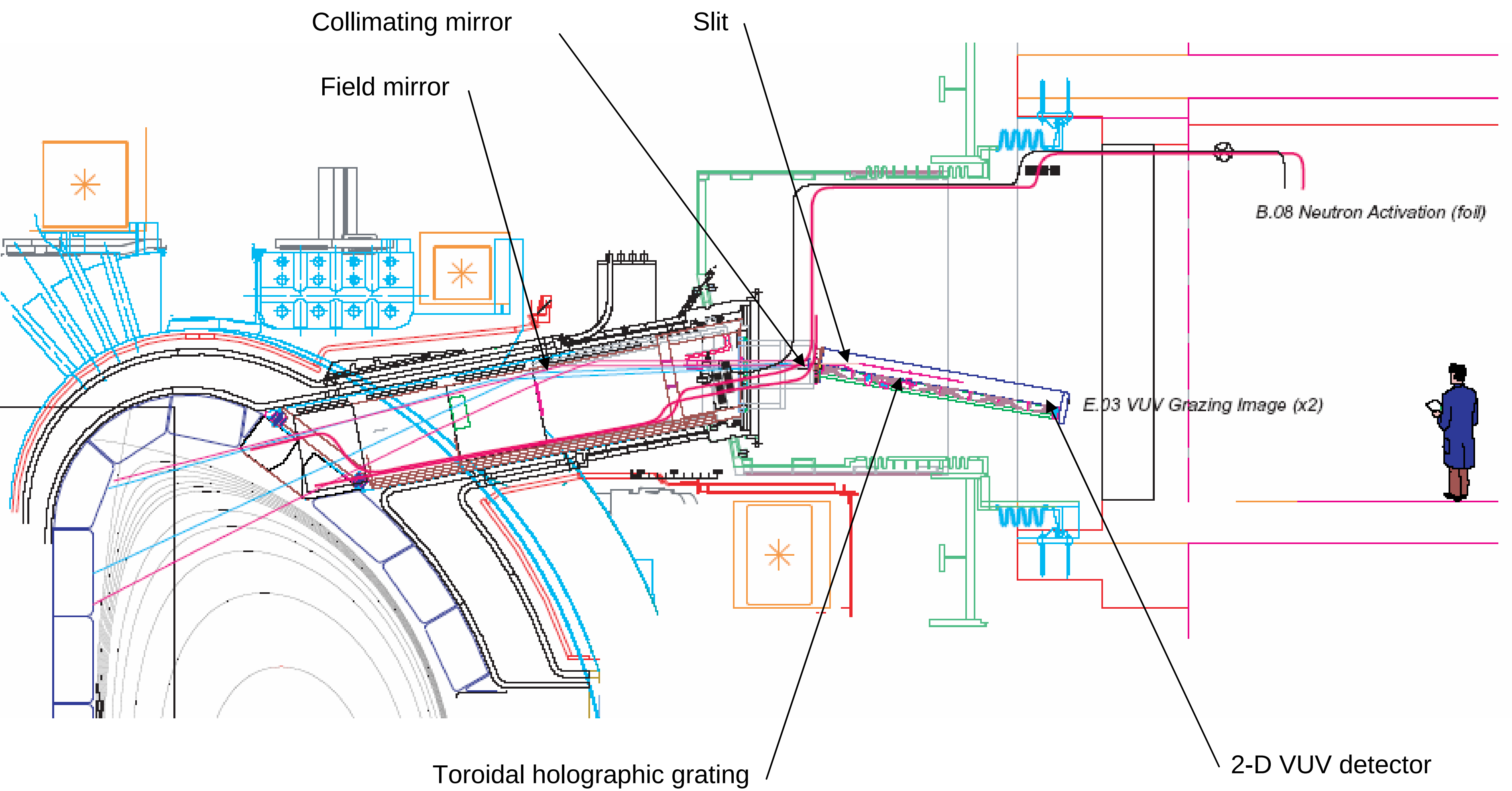

Upgrade to JET scanning VUV spectrometer for 2005

Addition of a collimating mirror:

Allows for a much smaller scanning mirror, now behind a valve.

Improve spatial resolution for 20 cm to < 1cm

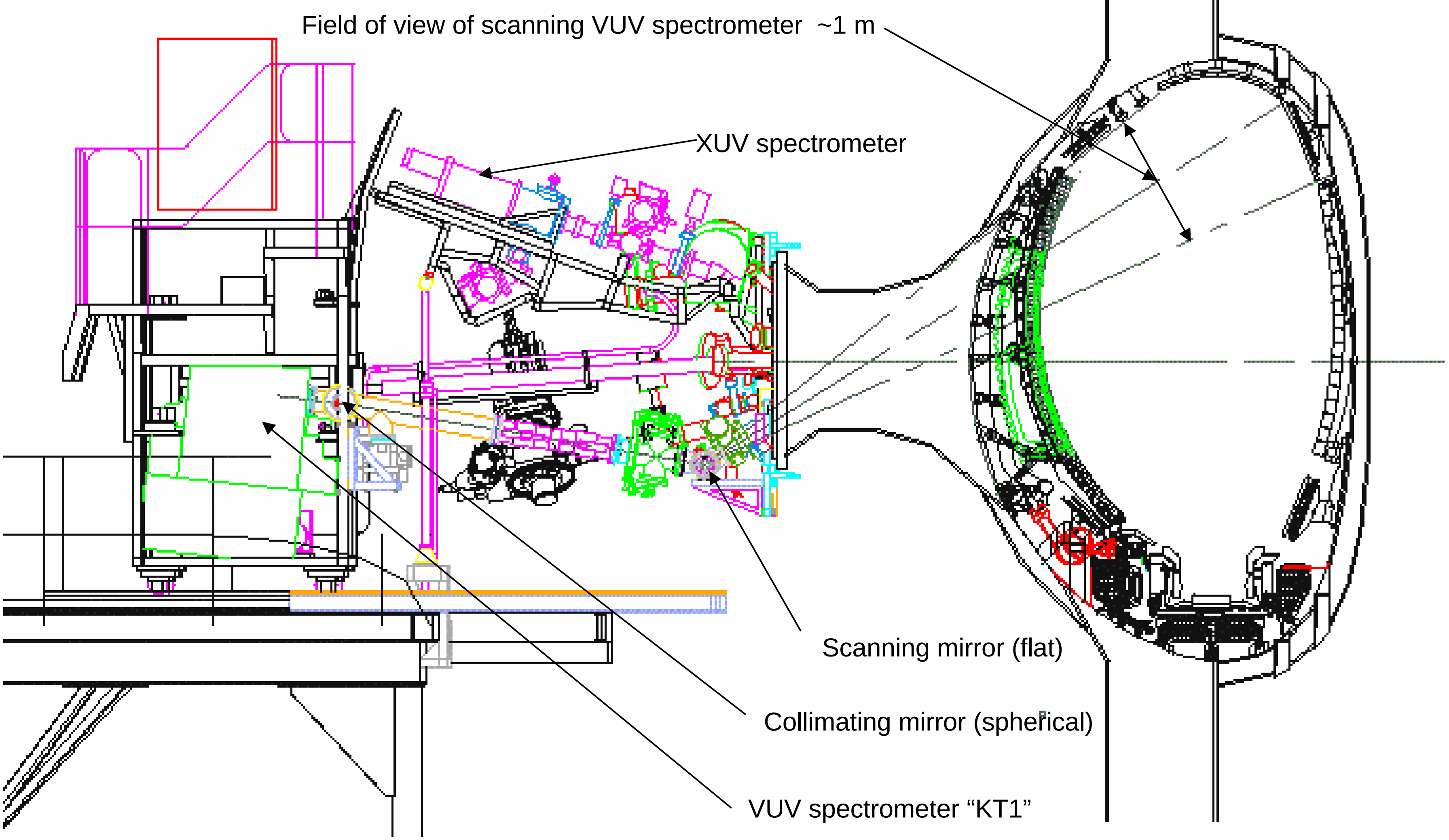

The JET D-T compatible soft x-ray cameras

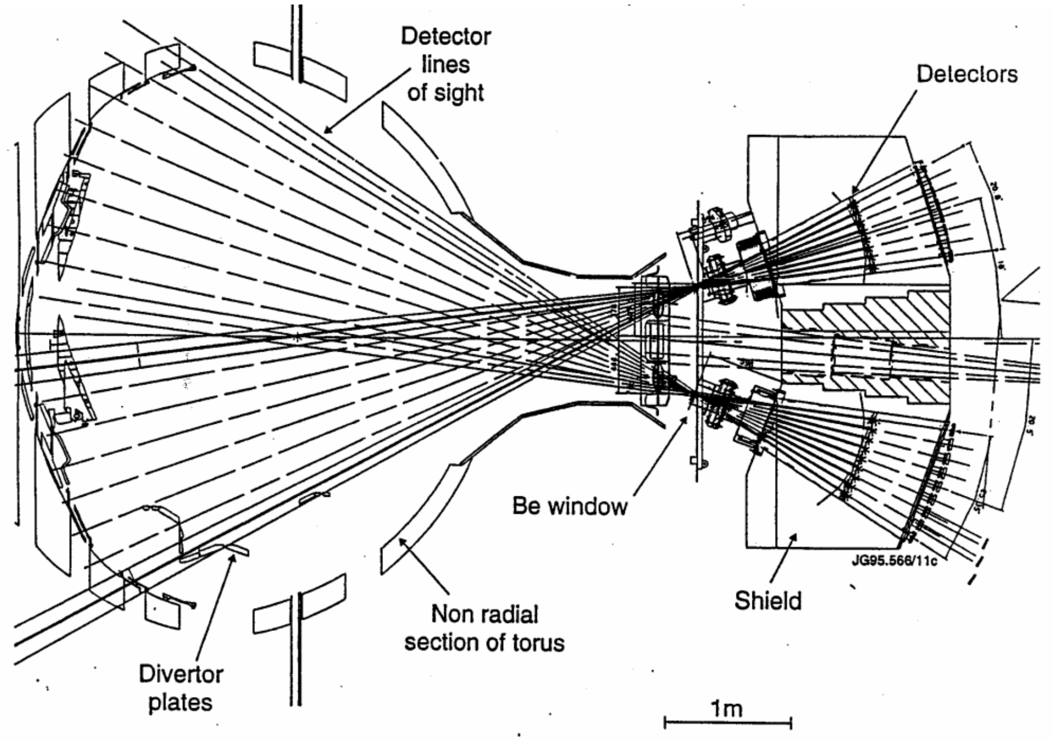

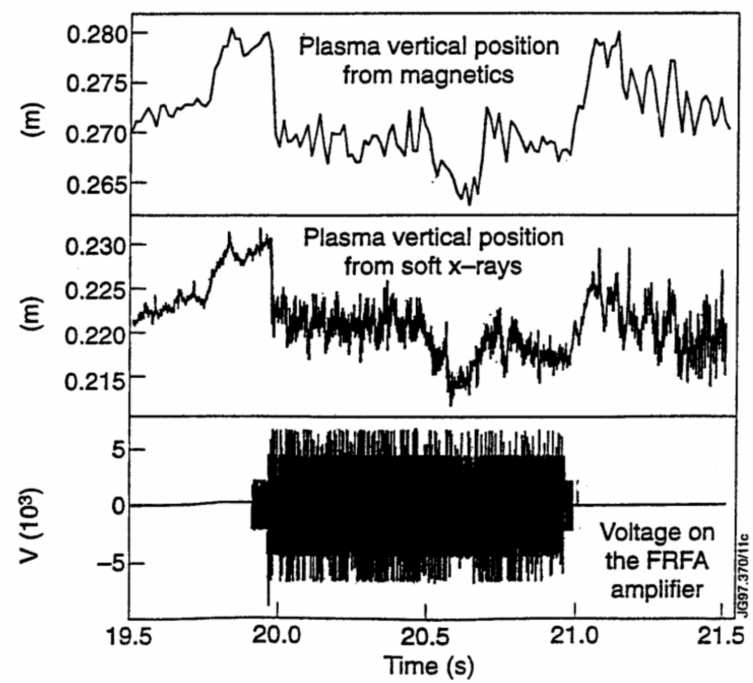

Demonstration of plasma vertical stabilization from 20 - 21 s, using the soft x-ray control signal.

ENERGY-RESOLVED FAST 2-D X-RAY IMAGING

D Pacella ENEA – Frascati , Italy. APS – HTPD , 19-22 April 2004 , San Diego, CA, USA

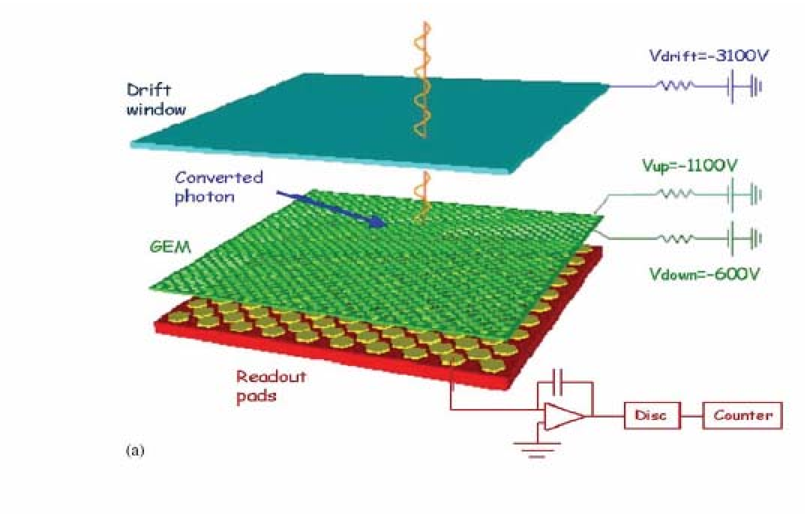

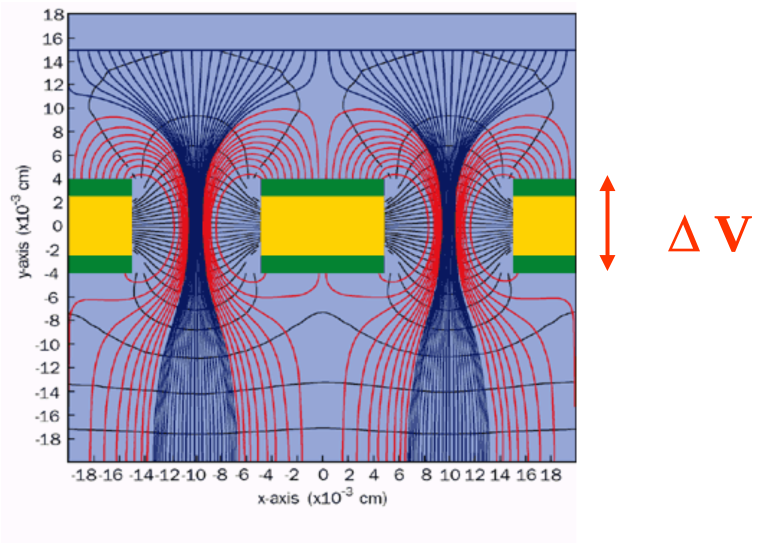

Prototype GEM detector. PIXCS-128 128 pixels

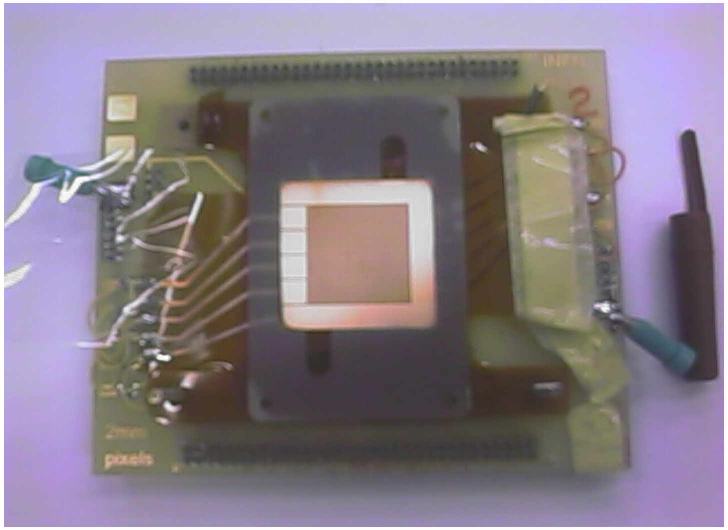

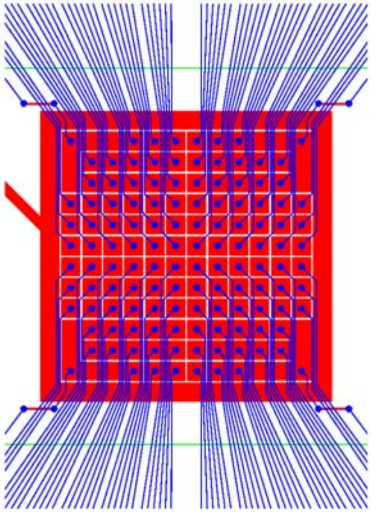

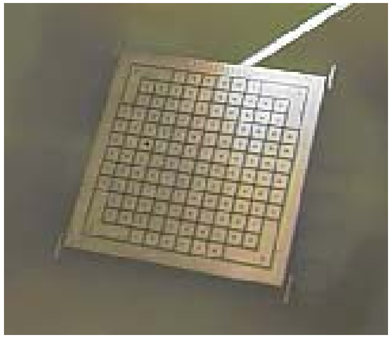

Energy resolution on each pixel in a wide energy range
Independent window analyzer on each pixel, capable of > 10^6 count/s

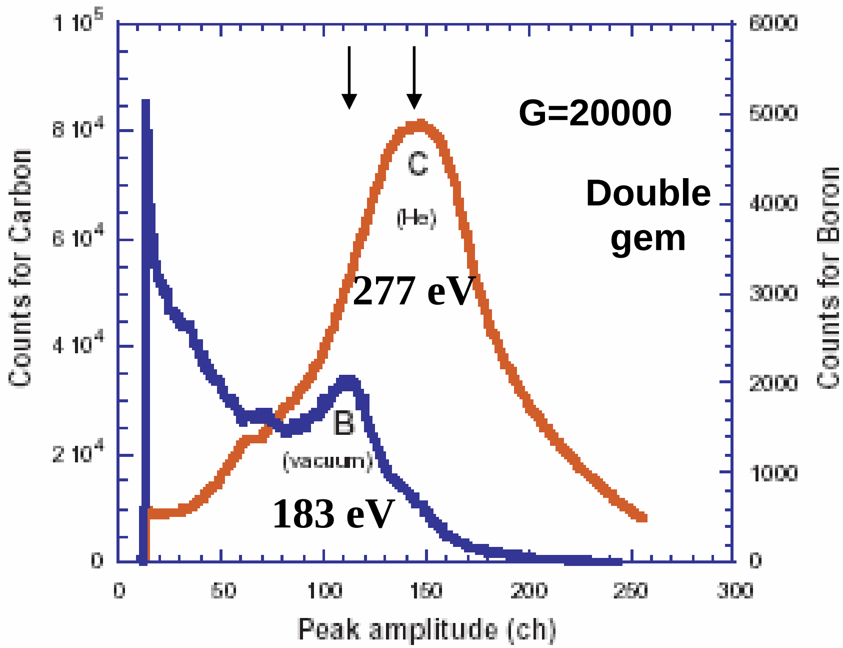

Fig. 4. Spectrum of carbon (277 eV, right axis) with double GEM and He between source and detector. Spectrum of boron (183 eV, left axis), with double GEM and vacuum between source and detector.

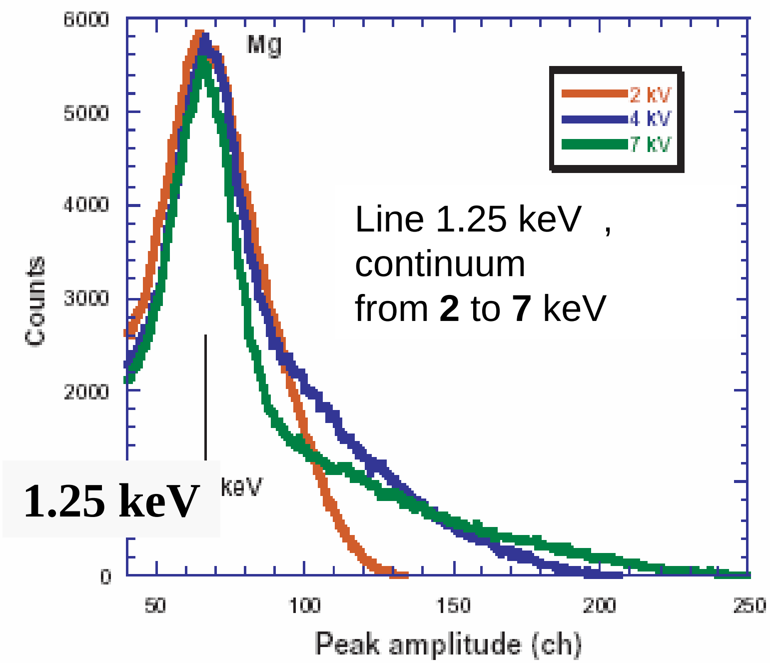

Fig. 5. Spectra of Mg (1.25 keV) with different Voltages for the anode of the X-ray source: 2.5 kV (red), 4 kV (blue), 7 kV (green). Spectra are normalized to the peak emission of the K feature.

Steerable, “zoomable” x-ray pin-hole camera with tangential view
Fast spectroscopic imaging is valuable to study cross-field transport

Tangential views of NSTX plasma (Madison, Wisconsin)

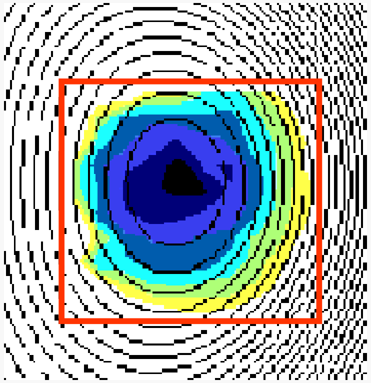

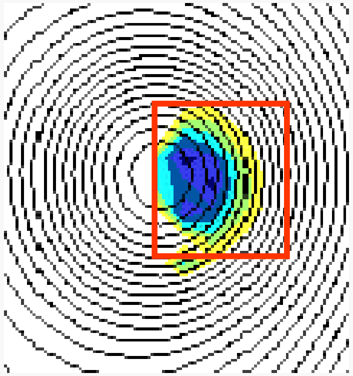

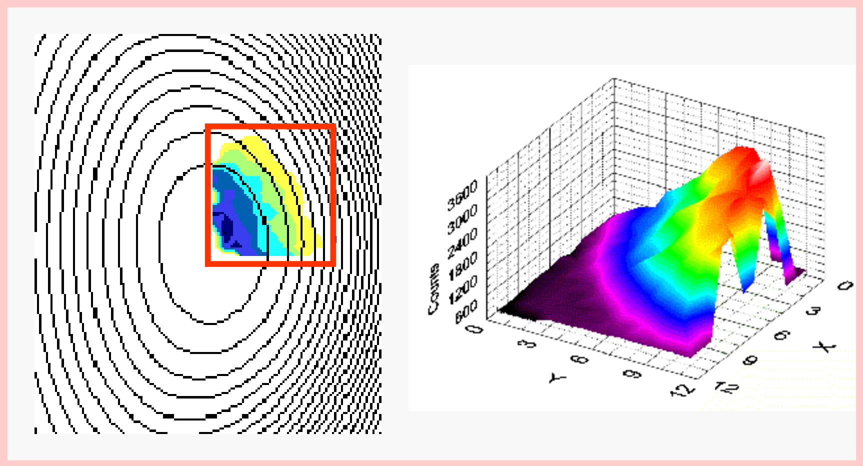

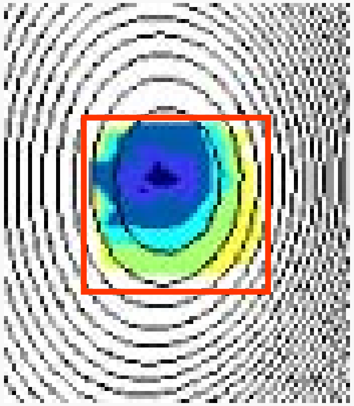

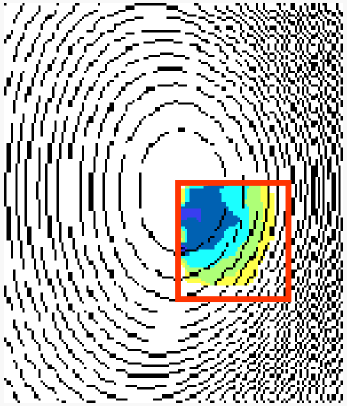

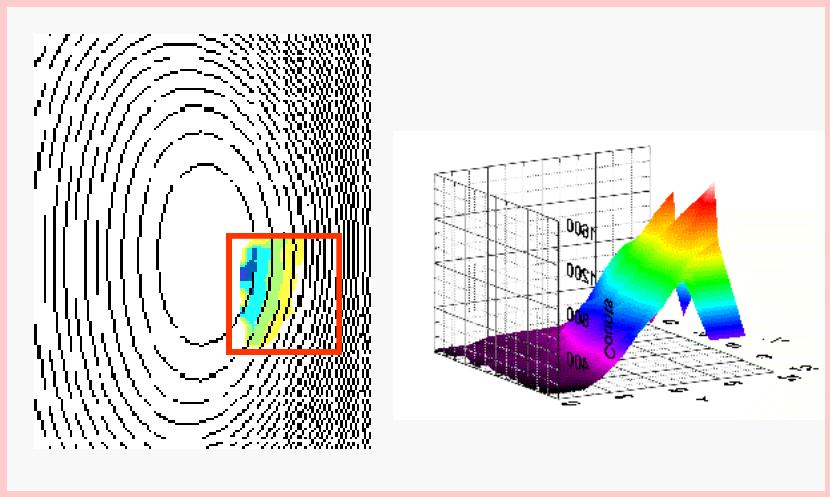

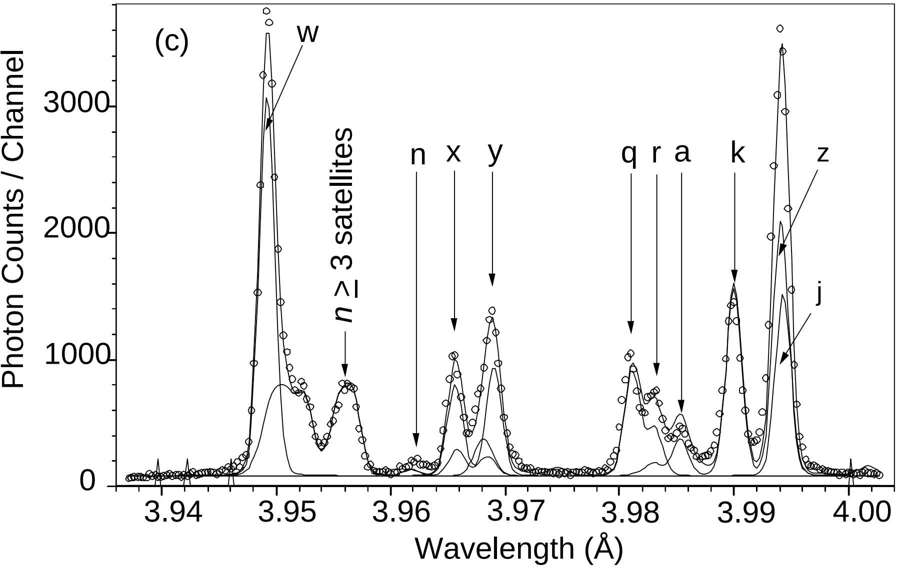

Te = 0.58 keV from <u>all</u> diel. satellites & line **w**; Ti = 0.45 keV

ArXVII spectrum from NSTX - Manfred Bitter

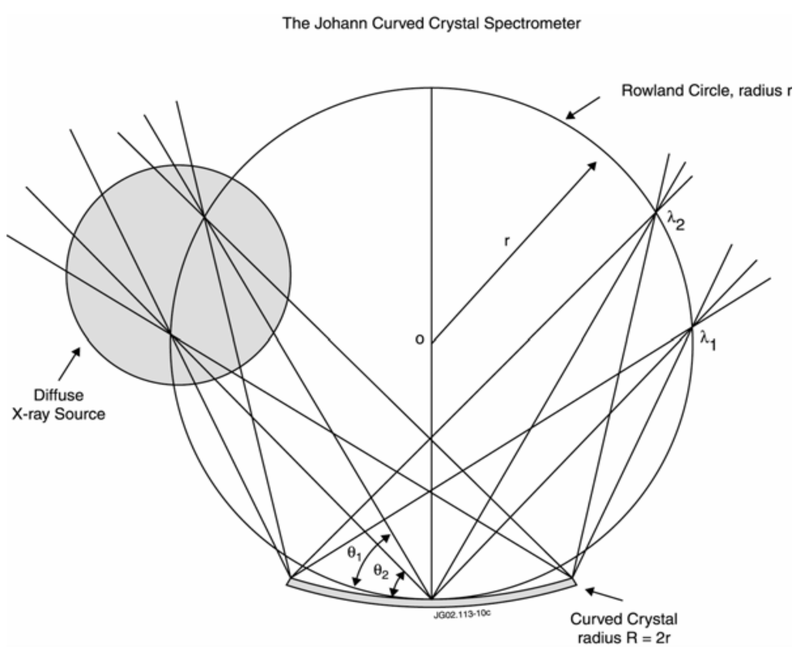

High-resolution x-ray spectroscopy

Extensively, but not exclusively, He-like ions.

~Te/Z: 250eV: Ne, 500eV,:Ar, 2keV: Fe-Ni, 10keV:Kr

Requires $\lambda/\delta\lambda$ >~ 5000, hence λ < 1.3 nm for crystals

Ti:	Doppler broadening
Vtor/pol:	Doppler shift
Te	Dielectronic satellite ratio
ne	Forbidden line ratio z/(x+y) (sometimes)
Zeff	Continuum τimp Impurity injection
nimp	Absolute calibration

Simple and reliable - bent crystal & pos. sens. detector.

Crystals are cheap dispersive elements, eg Si < 1kEur

Energy resolving detector makes it doubly dispersive, with excellent signal-to-noise ratio.

All crystal-window-detector processes are volume effects, leading to calculable and stable calibration. (1 mm Carbon ~ transparent at 10 keV).

Detector developments have been the key to progress:

1st gen.	Photographic film
2nd gen.	Multiwire prop. counter, ~ 3 - 25 m radiius
3rd gen.	Solid state eg CCD, 0.5 - 2 m radius
4th gen.	**Imaging with fast 2-d detector**

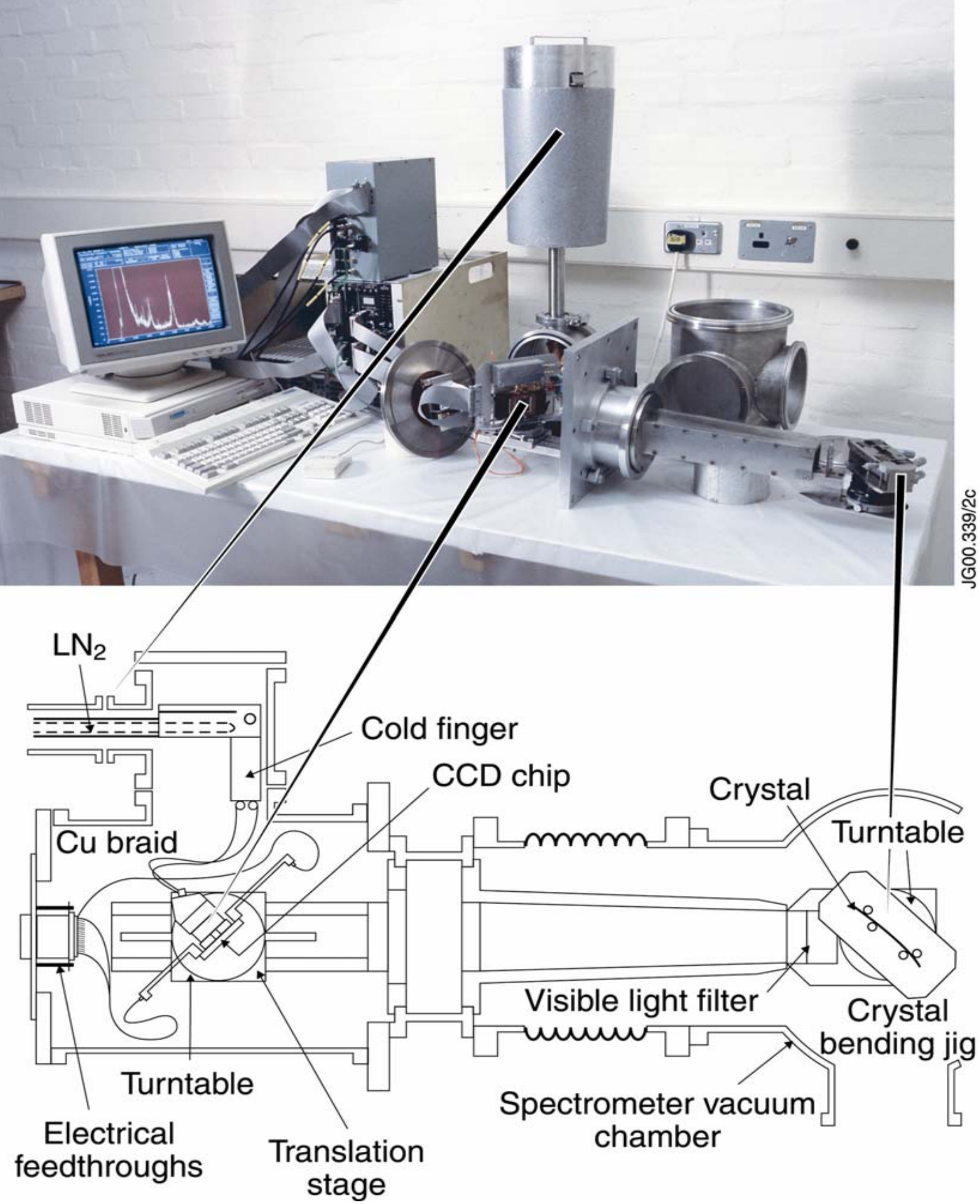

Portable Johann-CCD spectrometer

R Barnsley et al, Rev Sci Instr. April 2003

Deployed on several tokamaks:

- DITE, COMPASS, MAST, JET

and other sources:

- Laser produced plasma (photo film)
- Oxford Univ. Electron-beam ion trap

High resolution crystal spectrometer on the MAST tokamak. M Nelson et al, HTPD 2004

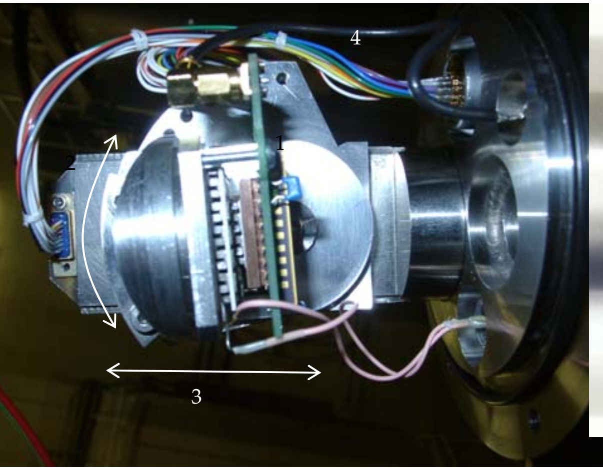

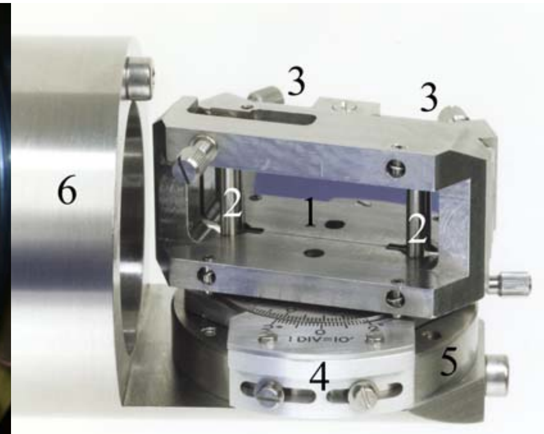

Peltier-cooled x-ray CCD, 1024x256
$\Delta E \sim$ 150 eV at low count-rate
8 ms readout with vertical binning

4-pillar crystal bender
Fits inside ϕ 65 mm tube
Bakeable to 100° C

Compact Johann-CCD spectrometer

- Shares sight-line of toroidally & poloidally scanning NPA
- Si(111) crystal for He-like Ar at 0.399 nm
- Built and installed on MAST in 6 months

ITER prototype in preparation - imaging

- Spherical crystal already obtained
- Initial tests to be with existing CCD (slow)
- **Fast 2-d detector required….**

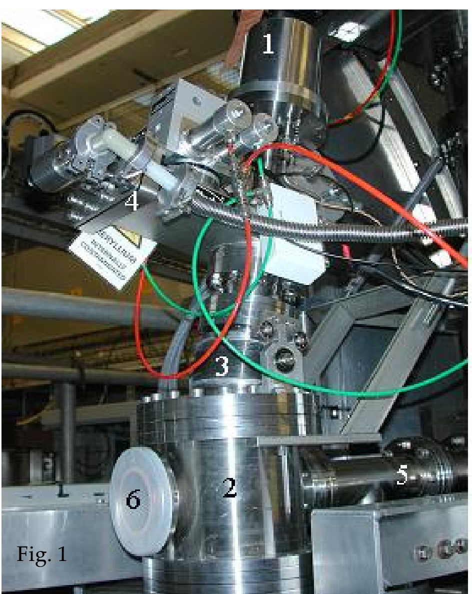

Fig. 1

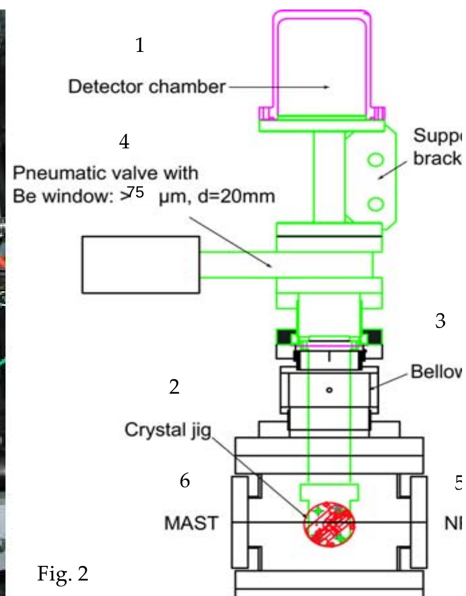

Fig. 2

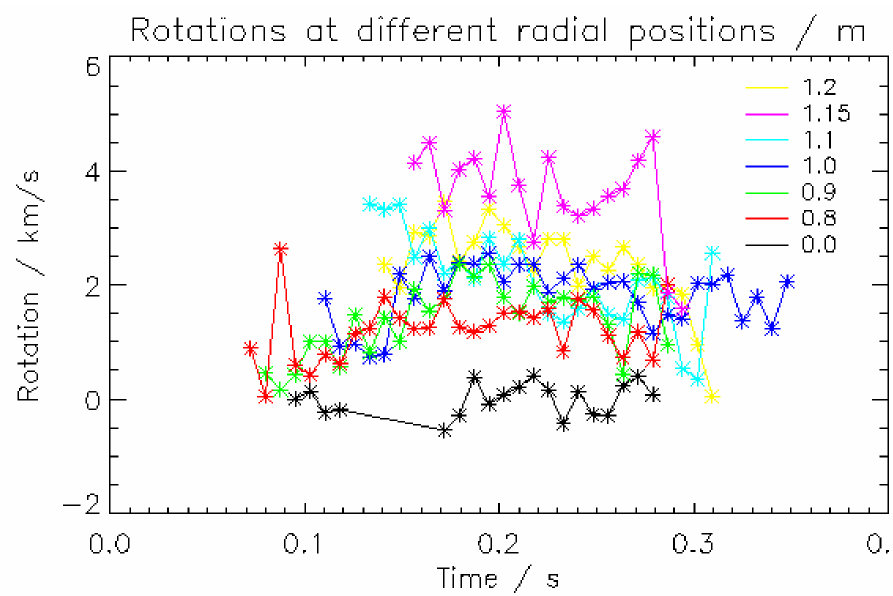

JET high-resolution crystal spectrometer - XCS

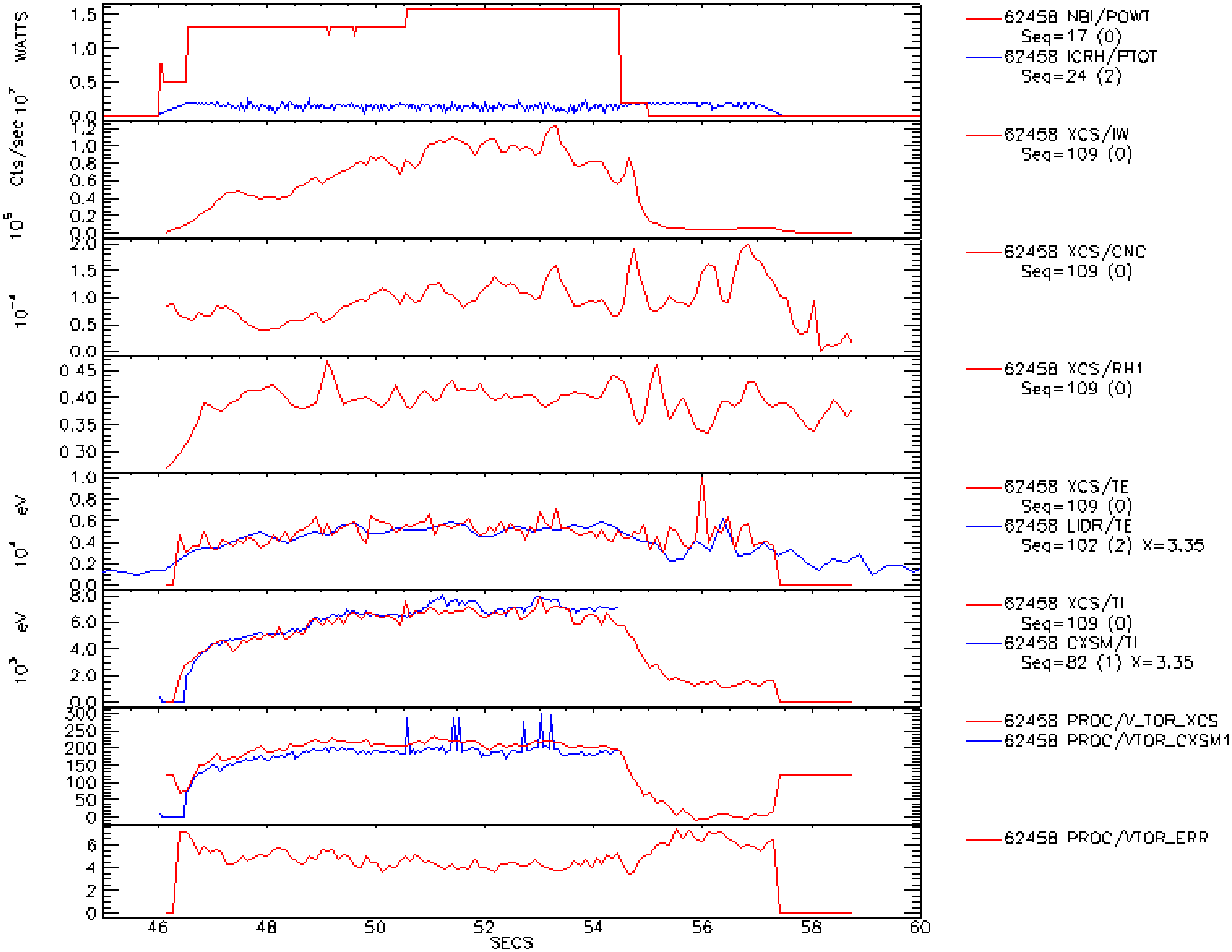

1) NBI & RF heating

2) Ni XXVII count-rate

3) Ni concentration

4) r/a of Ni peak emission

5) Te at same r/a XCS LIDAR

6) Ti, XCS CXRS

7) Vtor, XCS CXRS

8) Error on Vtor XCS

25 m Johann spectrometer with multi-wire proportional counter. Single-chord only.

One of the original JET diagnostics, with data from ~ 50 000 pulses

Doubly-curved crystal optics

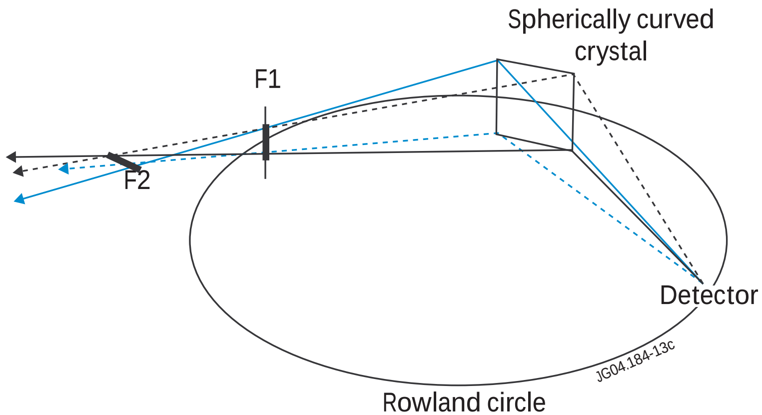

Fig.14a. Spherical crystal optics

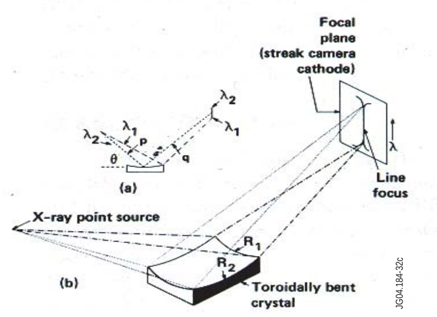

Fig.14b. Toroidal crystal optics

+ Spherical or toroidal crystal allows plasma imaging

+ Improves S/N ratio with smaller entrance aperture

and smaller detector

$f_s/f_m = -1/\cos(2\theta_B)$

- No real focus for $\theta_B < 45°$

f_s: Sagittal focus f_m: Meridional focus θ_B: Bragg angle

A new Instrument for simultaneous Measurements of Profiles of the toroidal and poloidal plasma rotation velocities

M. Bitter, K. W. Hill, L. Roquemore, B. Stratton Princeton University
S. G. Lee, Korea Basic Sicence Institute, J. E. Rice MIT

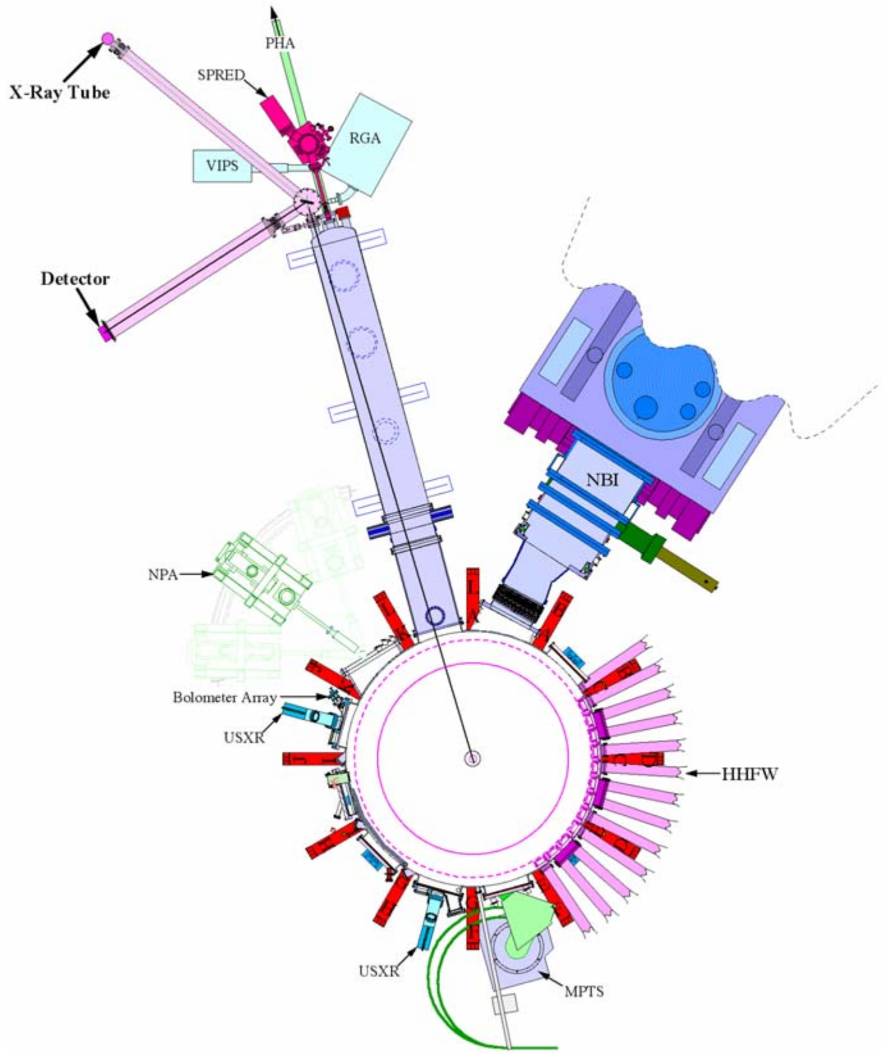

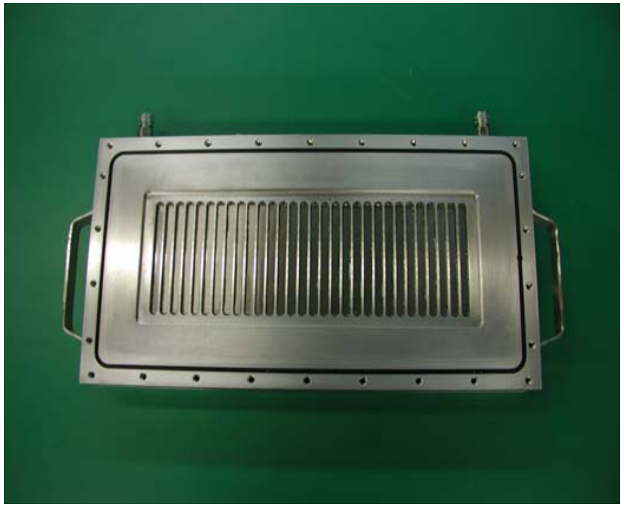

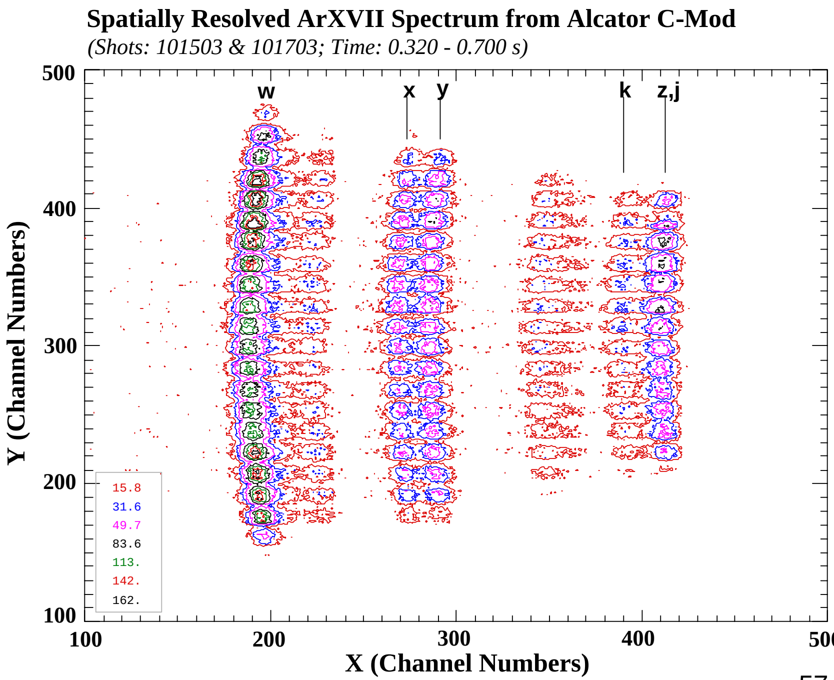

ITER impurity line emission and spectrometer signals

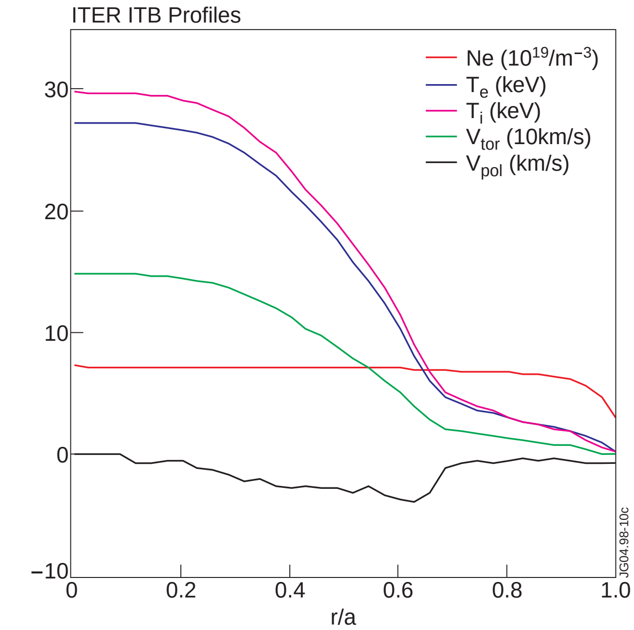

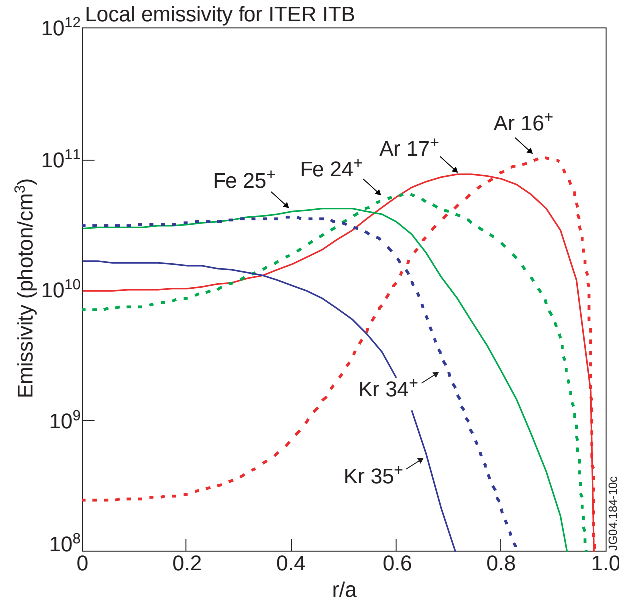

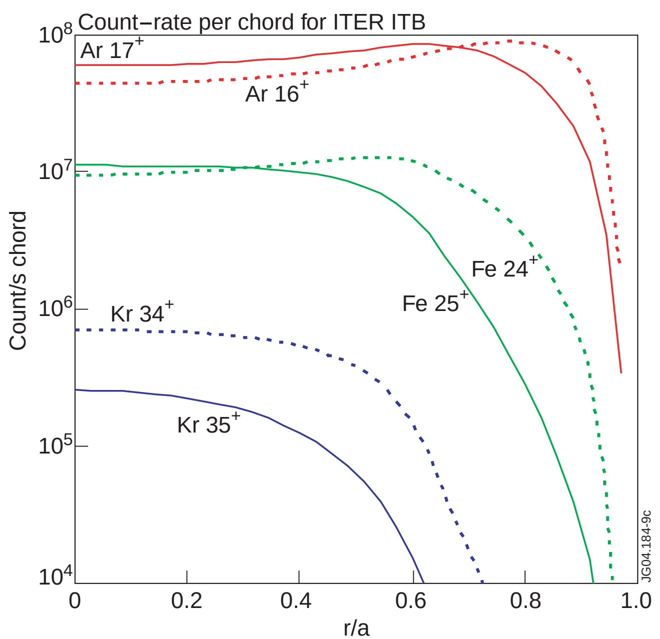

Top left Modelled ITER radial profiles

Top right Local emissivity of impurity spectral lines

Bottom Simulated signals for imaging x-ray crystal spectrometer

Incremental radiated powers for added impurity concentrations of $10^{-5}.n_e$ are:

Ar 0.25 MW Fe 0.8 MW Kr 1.4 MW

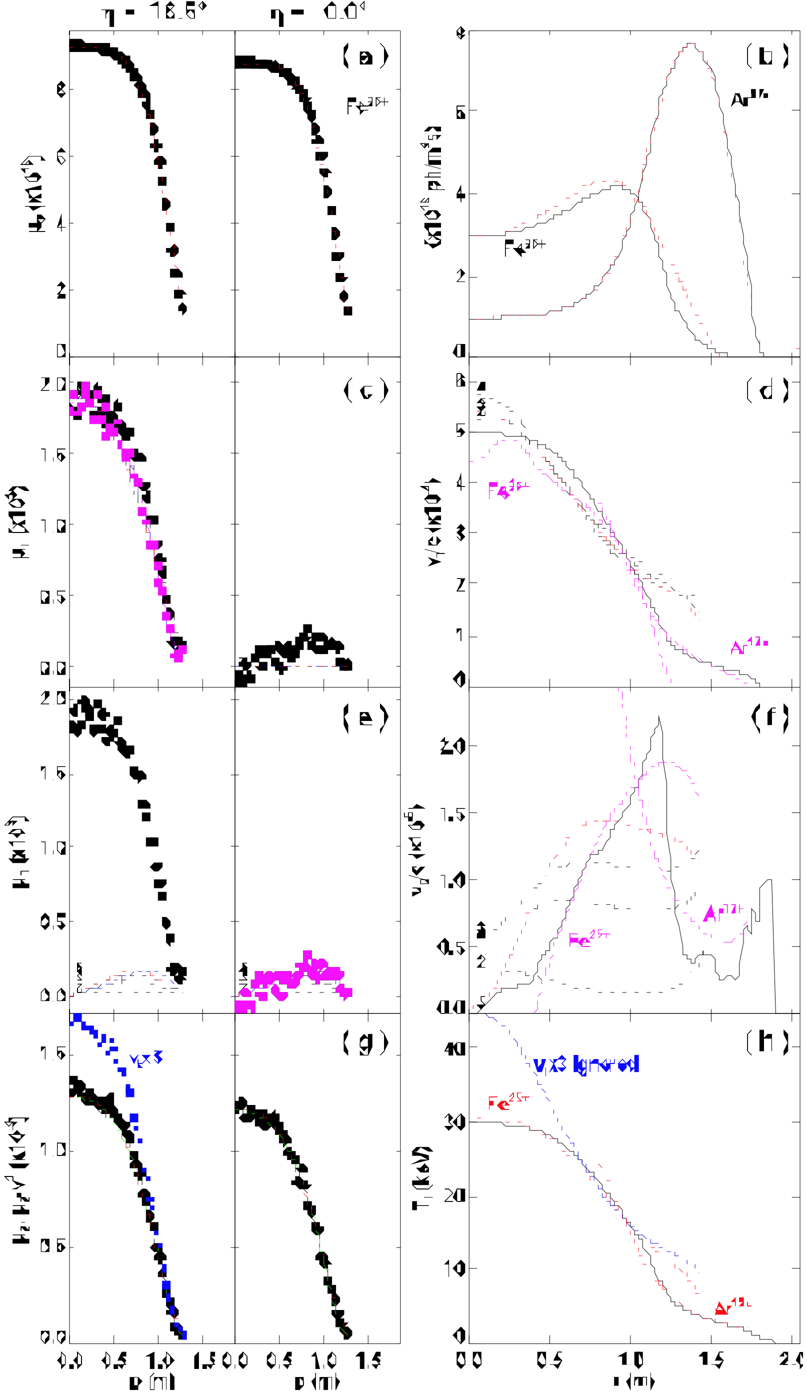

Simulation results for ITER ITB
C Ingesson et al HTPD 2004

- Fe concentration of 10^{-5}
- H-like line at 1.784 Å
- Integration time of 0.3 s

Two views of the top half of the plasma were assumed measuring at toroidal angles *h* = 0° and 18.5°.

Left-hand column: moments calculated from the simulated measurements (solid circles) and backcalculated moments from the reconstruction (curves).

Right-hand column: input profiles of the simulation (solid curves) and reconstructed profiles (dotted lines).

Rows, from top to bottom:
emissivity, toroidal rotation, poloidal rotation and T_i.

Design for ITER imaging x-ray crystal spectrometers

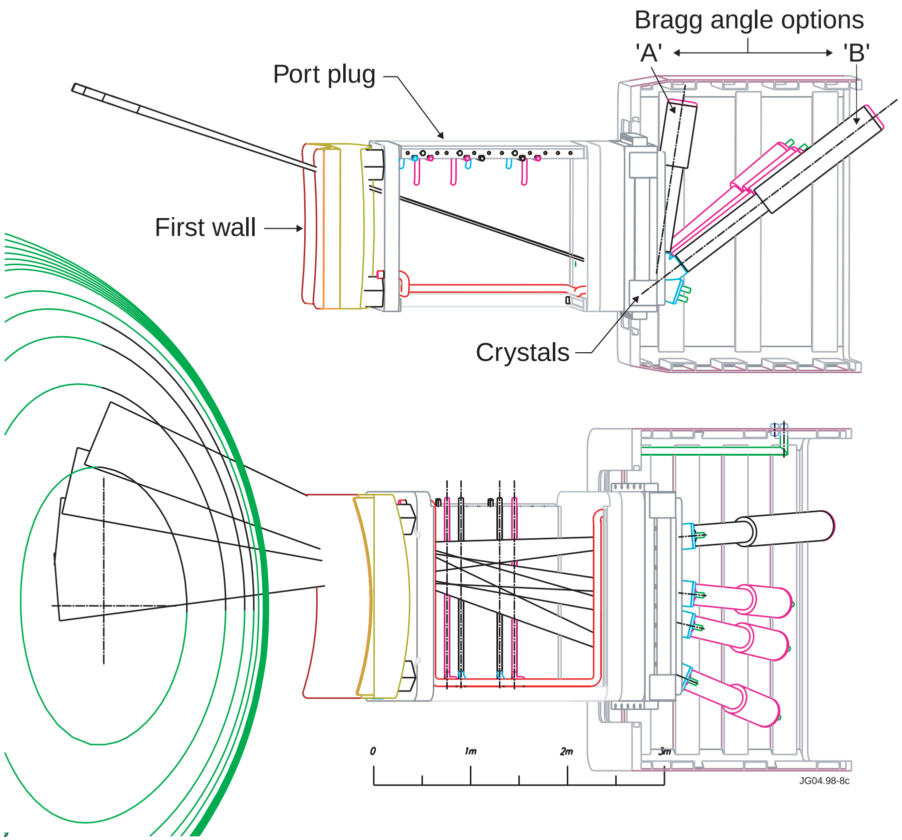

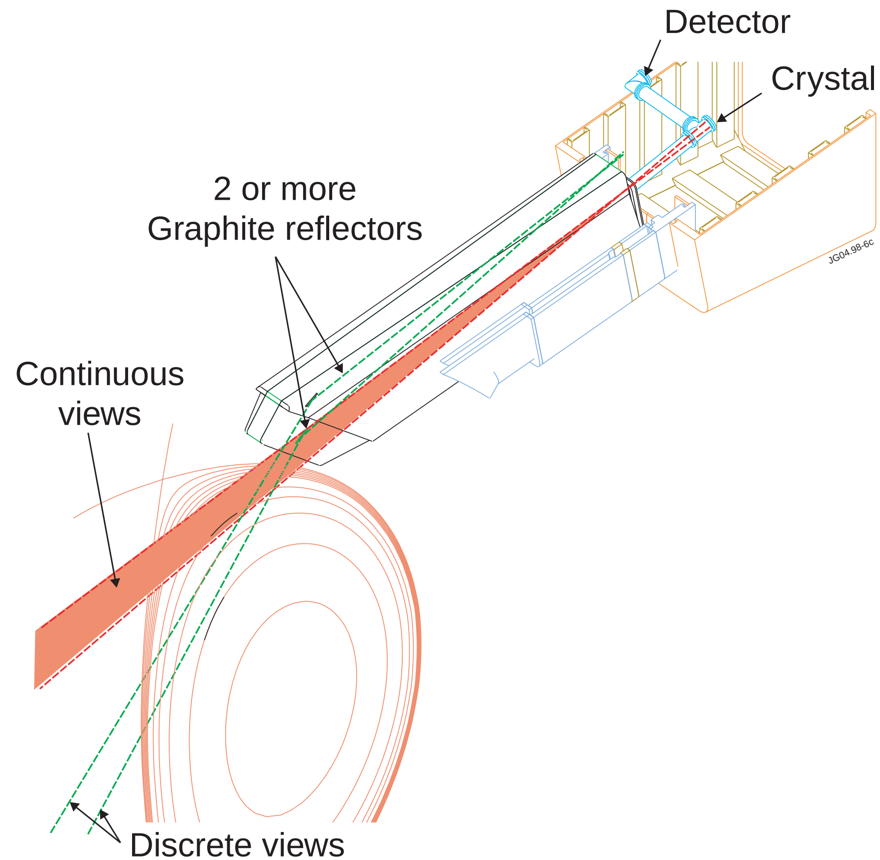

Equatorial port:options
“A”: Spherical crystals - better optically
“B”: Toroidal crystals - better S/N
~ 3m crystal radius:
- Could use gas or solid state detector

Upper port
Part of plasma cannot be viewed directly
- graphite reflectors are used.
- ~ 1m crystal radius
- Dispersion too low for gas detector,
ideal for solid-state pixel-detector

Modelled neutron levels for the ITER upper port imaging crystal spectrometer.

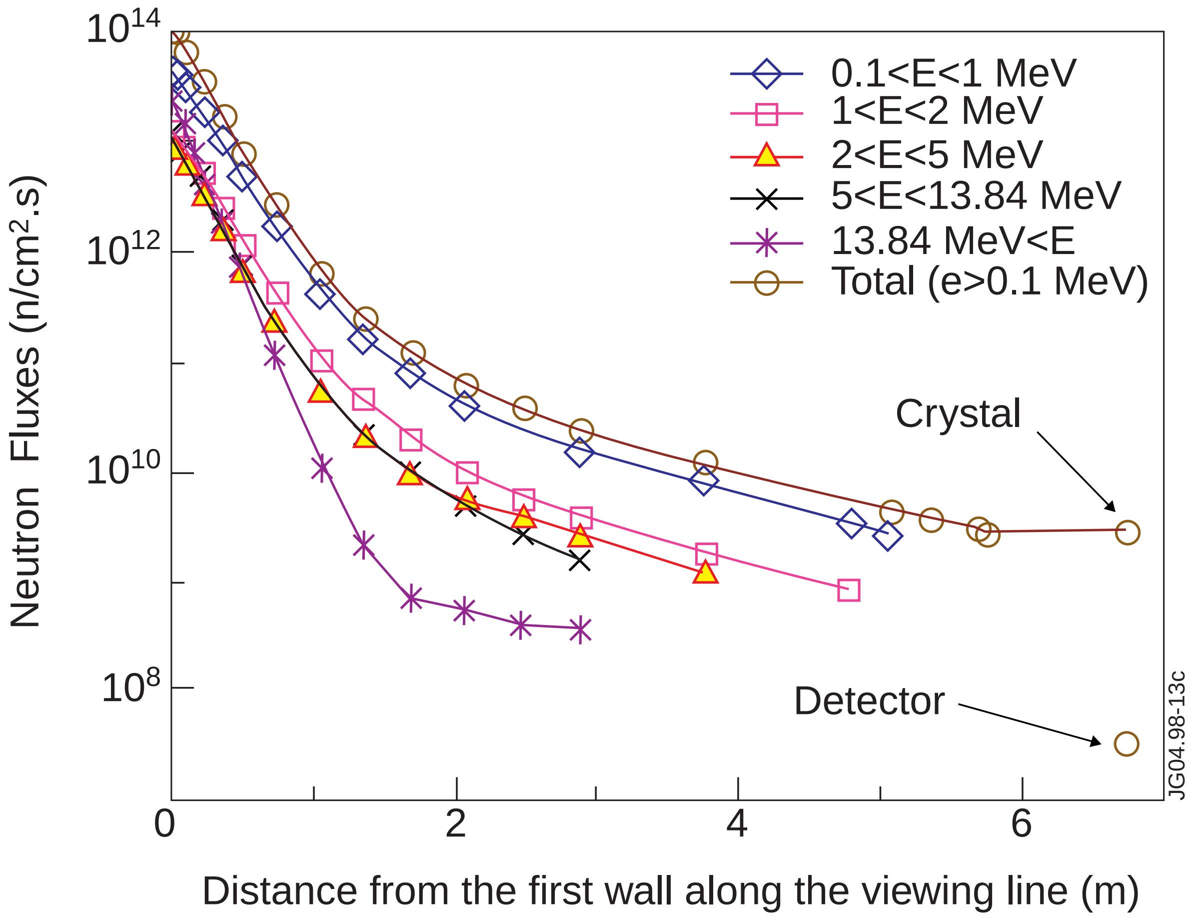

ITER imaging x-ray crystal spectrometer

- Combined radial and 19° tangential views

- Separation of toroidal and poloidal rotation components

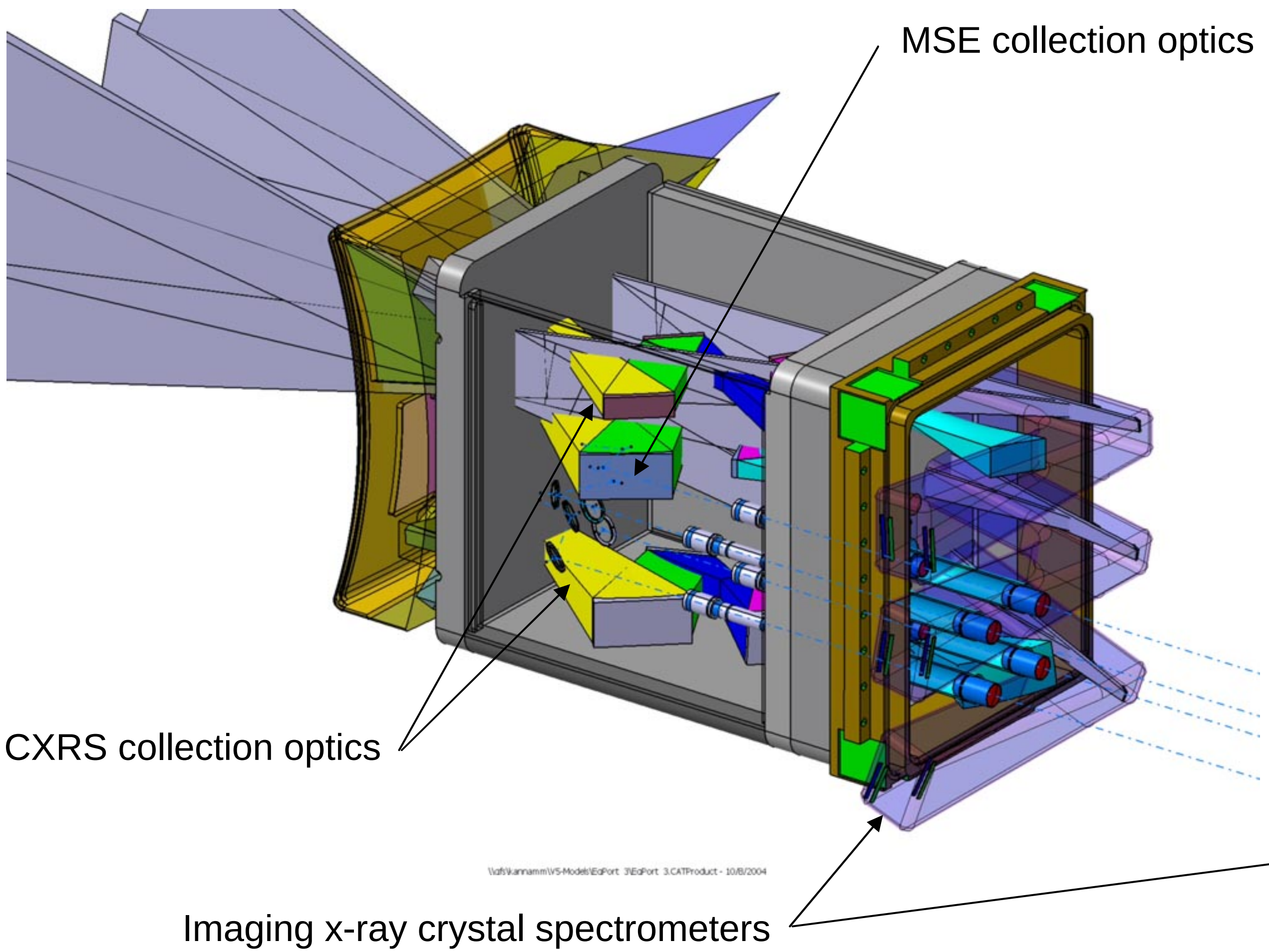

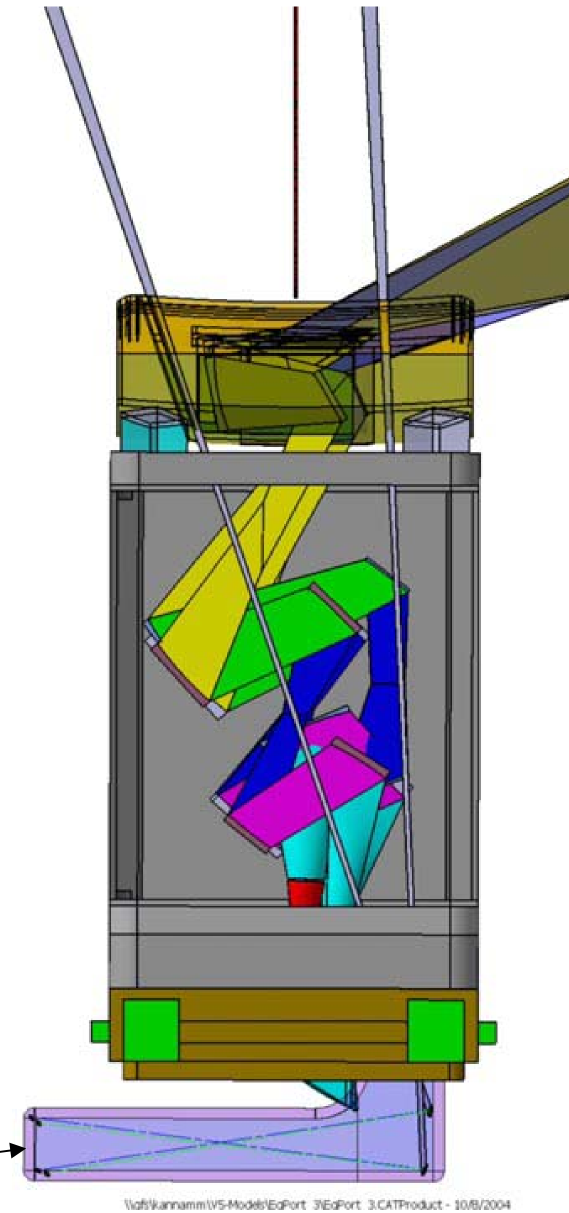

Optical parameters and detector requirements for
equatorial and upper port imaging crystal spectrometers

Port location	Equatorial		Upper	
Crystal curvature	Spherical	Toroidal	Spherical	Toroidal
Central Bragg angle	54.0°	27°	48.0°	27°
Plasma – crystal (m)	7		7	
Imaged plasma height (m)	~ 3.5		~ 0.5	
Demagnification	0.21	0.36	0.14	0.18
Crystal – detector (m)	1.5	2.5	1	1.3
Crystal radius/radii (m) R r	2.0	5.5 1.7	1.3	2.9 1.0
Port – detector (m)	<0.5	~ 2.3	<0.5	~ 1.5
Detector width (mm) for 1% band-width	27	28	15	15
Total detector height (mm) Number of detectors	750 3 - 4	1250 4 - 5	70 1	93 1
Detector resolution (mm) for $\lambda/\delta\lambda = 10^4$	0.27	0.28	0.15	0.15
Detector resolution (mm) for $\rho/\delta\rho = 100$	8	14	6	7.5
Detector travel (mm) for 10% tuneable band	300	300	150	150
Bragg angle range for 10% tuneable band	7.4°	1.4°	5.3°	1.4°

Outline detector specification for imaging x-ray spectrometer

Total detector height (~200 - 750 mm) = observed plasma height (~4 m) x demagnification (~0.05 - 0.2)

Individual detector height:	~ 70 - 250 mm for 3-5 detectors
Detector width in λ direction:	~15 – 30 mm
Vertical resolution:	~2 - 5 mm, for >100 total resolvable lines of sight
Horizontal resolution:	~0.1 mm
QDE / Energy range:	> 0.7, 3 – 13 keV
Average count rate density:	~10^6 count/cm^2.s
Peak count rate density:	~10^7 count/cm^2.s
n-γ background count density:	~10^5 count/cm^2.s
	(flux of 10^6 n-γ/cm^2.s, 10% sensitivity. 90% shielding)

Candidate detectors

This performance is typical of detectors in use or in development for high-flux sources such as synchrotrons.

- Gas-microstructure proportional counters.

- Solid state arrays. CCD or pixel.

γ-ray imaging of fast ions in JET

V Kiptily, 31th EPS Meeting, London, 2004

Gamma-ray camera - shared with neutron camera

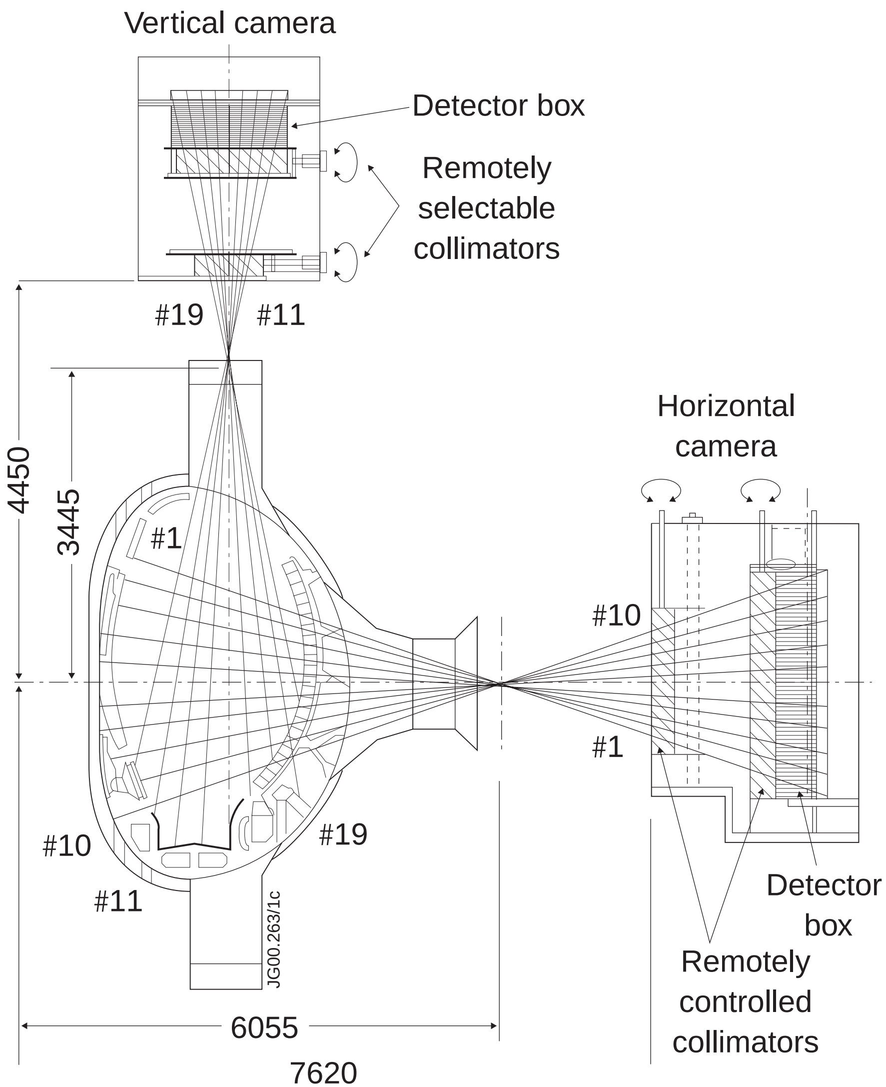

On JET γ -ray emission profile measurements provide information about spatial distribution of fast alphas

- **vertical camera - 9 lines-of-sight**
- **horizontal camera - 10 lines-of-sight**
- **Collimators: Ø10 and 21 mm**
- **Space resolution: 10 cm in centre**
- **γ-Detectors: 10x10x15 mm CsI-diodes**

Gamma-ray spectroscopy of nuclear reactions on JET

At JET γ -ray spectrometry provides information on distribution function of charged fast particles

γ -ray emission is produced by

- fusion products: p(3 MeV, 15MeV), T (1 MeV), ^{3}He(0.8 MeV), α (3.5 MeV)
- ICRF-driven ions: H, D, T, ^{3}He, ^{4}He

due to nuclear reactions with fuel and with the main impurities, Be and C

α-particle diagnosis at JET is based on the nuclear reaction ^{9}Be(α,nγ)^{12}C

Nuclear reactions observed in JET involving fast ...

deuterons

^{9}Be(d,pγ)^{10}Be
^{9}Be(d,nγ)^{10}B
^{12}C(d,pγ)^{13}C

protons

D(p,γ)^{3}He
T(p,γ)^{4}He
^{9}Be(p,γ)^{10}B
^{9}Be(p,p'γ)^{9}Be
^{9}Be(p,α γ)^{6}Li
^{12}C(p,p'γ)^{12}C

tritons

T(d,γ)^{5}He
^{9}Be(t,nγ)^{11}B
^{12}C(t,γ)^{15}N
^{12}C(t,nγ)^{14}N
^{12}C(t,$\alpha\gamma$)^{11}B

^{3}He

D(^{3}He,γ)^{5}Li
^{9}Be(^{3}He,pγ)^{11}B
^{9}Be(^{3}He,nγ)^{11}C
^{9}Be(^{3}He,dγ)^{10}B
^{12}C(^{3}He,pγ)^{14}N

^{4}He and α's

^{9}Be(α,nγ)^{12}C

$^{9}Be(\alpha,n\gamma)^{12}C$ reaction

The nuclear reaction between **fast alphas** and **Be** impurity leads to:

- Excitation of high-energy levels in $^{13}C^*$ nucleus
- De-excitation by emission of **neutron** with population of low-lying levels in $^{12}C^*$
- Further de-excitation by **3.21-MeV** and **4.44-MeV gammas** to ground state of ^{12}C nucleus

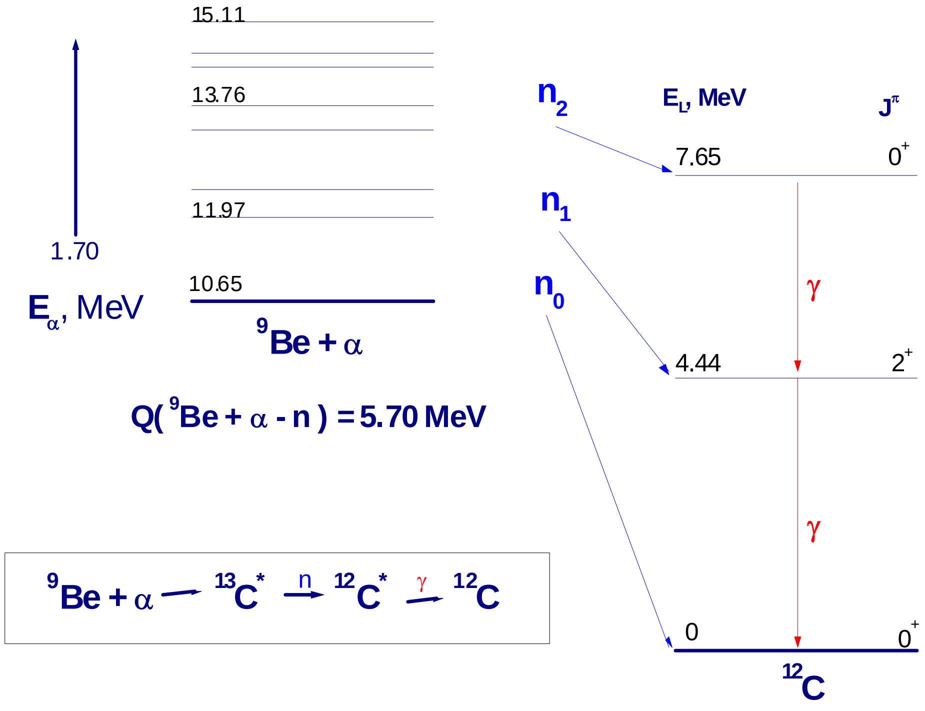

The γ-ray emission from this reaction are determined by the specific reaction cross-section :

4.44-MeV γ's (level 4.44 MeV) are produced by α's with E_α > 1.7 MeV

3.21-MeV γ's (level 7.65 MeV) is produced by α's with E_α > 4 MeV,

...and by the α-particle distribution function, $F(E_\alpha)$

The reaction $^{9}Be(\alpha,n\gamma)^{12}C$ can be used to measure changes in the density of the fast α-particles.

Reaction cross-section

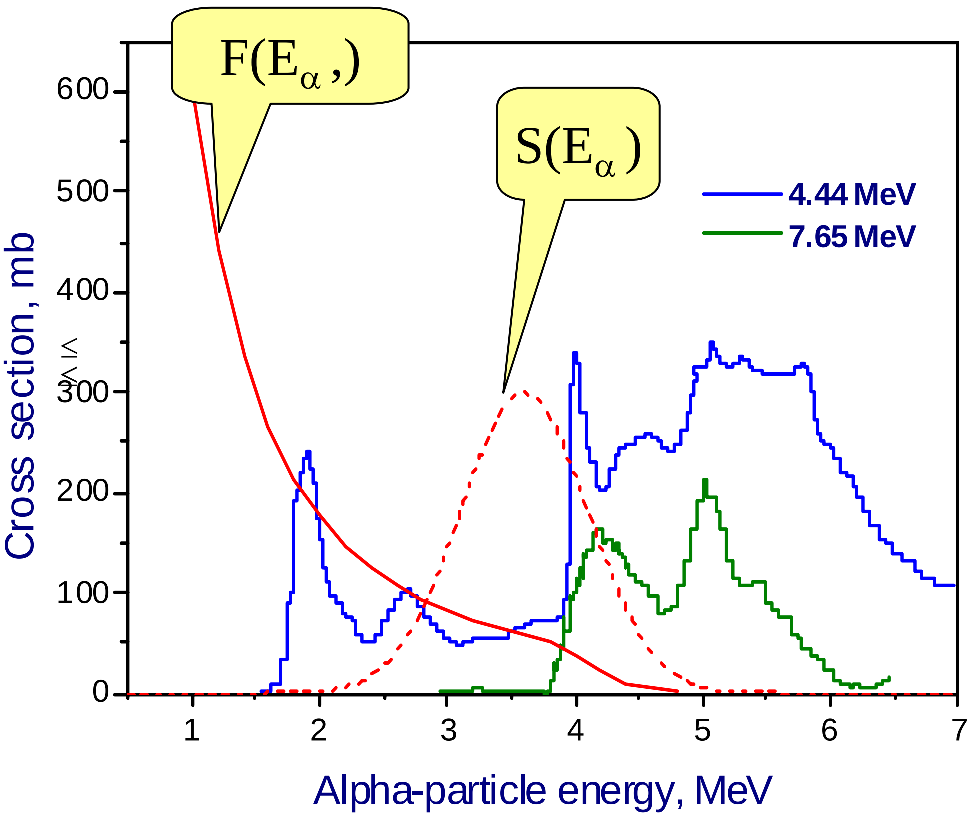

Acceleration of ^{4}He and D-ions in 3rd harmonic Ion Cyclotron RF heating experiments

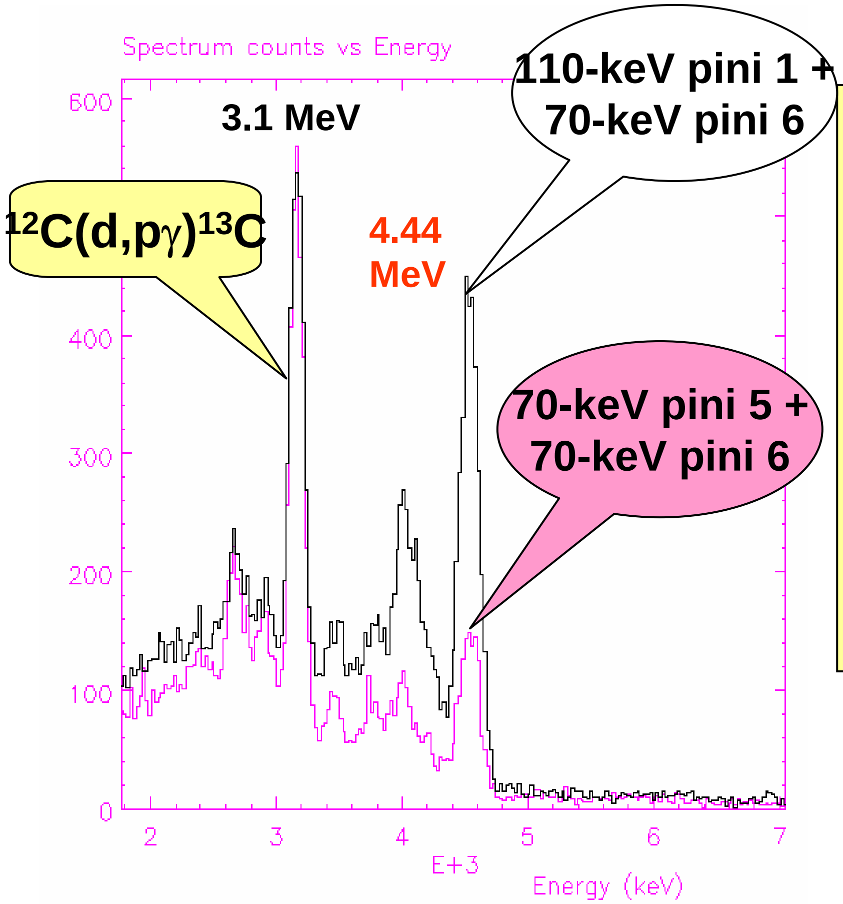

Nuclear reactions:

$^{9}Be(\alpha,n\gamma)^{12}C$ and $^{12}C(d,p\gamma)^{13}C$

γ-ray spectra are used for the ^{4}He-and D-ion tail temperature and slowing-down time assessments.

Kiptily V , Nucl. Fusion 42, 999 (2002)

The tail-like ^{4}He energy-distribution function is similar to the fusion α distribution in the TTE.

Typical tail-temperature in these experiments:
$\langle T\rangle_{He}$ ~ 300 - 700 keV

Simultaneous spectroscopic γ-ray imaging of ^{4}He and D-ions

$^{12}C(d,p\gamma)^{13}C$, 3.1 MeV and $^9Be(\alpha,n\gamma)^{12}C$, 4.44 MeV

Kiptily et al. Nuclear Fusion 45 (2005) L21-L25.

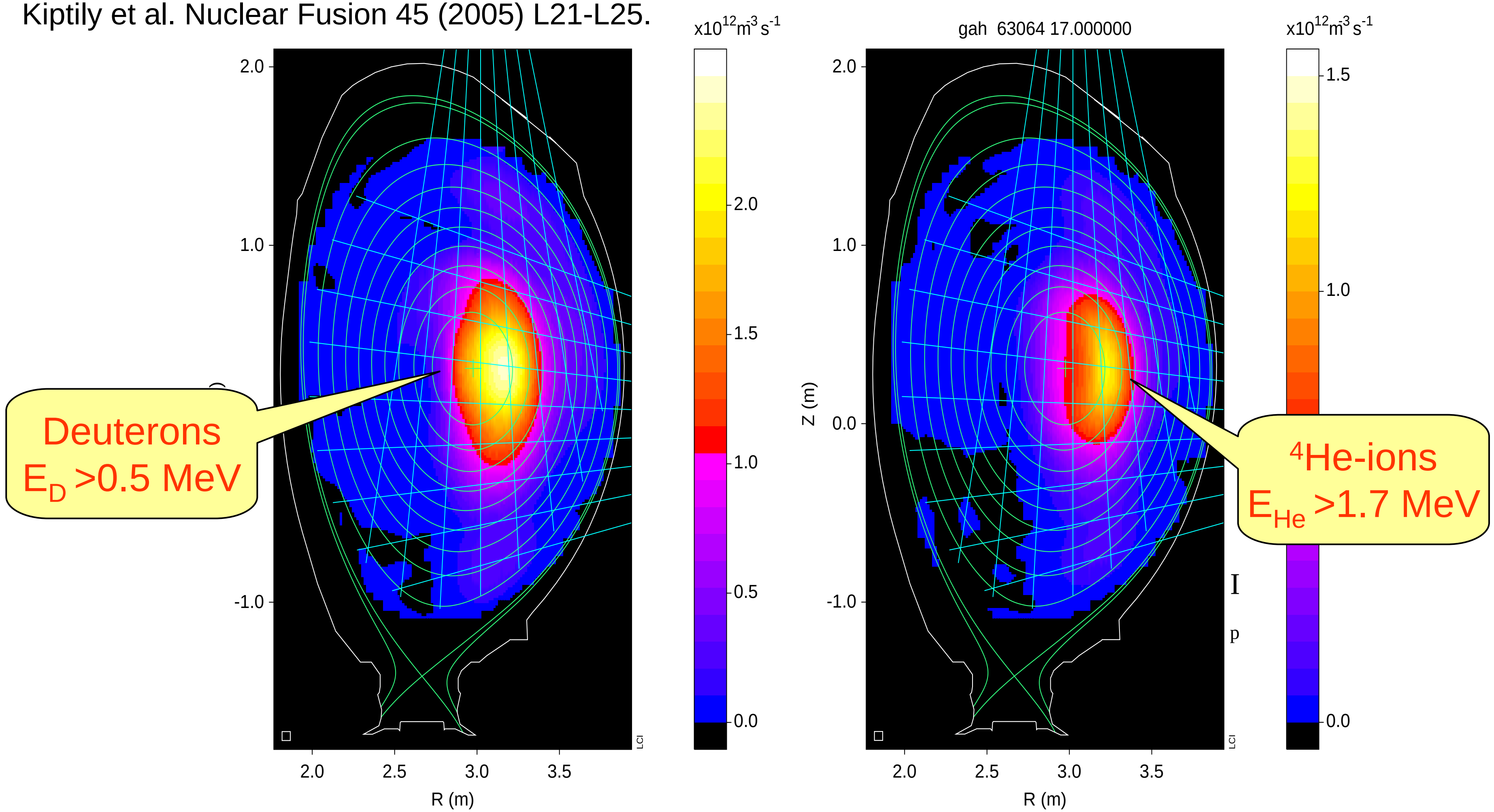

7.8 MW ICRH with co-current wave launch, 2 MW NBI, monotonic q-profile

Possible integration of γ-cameras in ITER
Shared with radial and vertical neutron cameras

Vertical Camera:

3 - 5 LoS

Radial Camera:

5 - 7 LoS

Lost alphas:

2 LoS

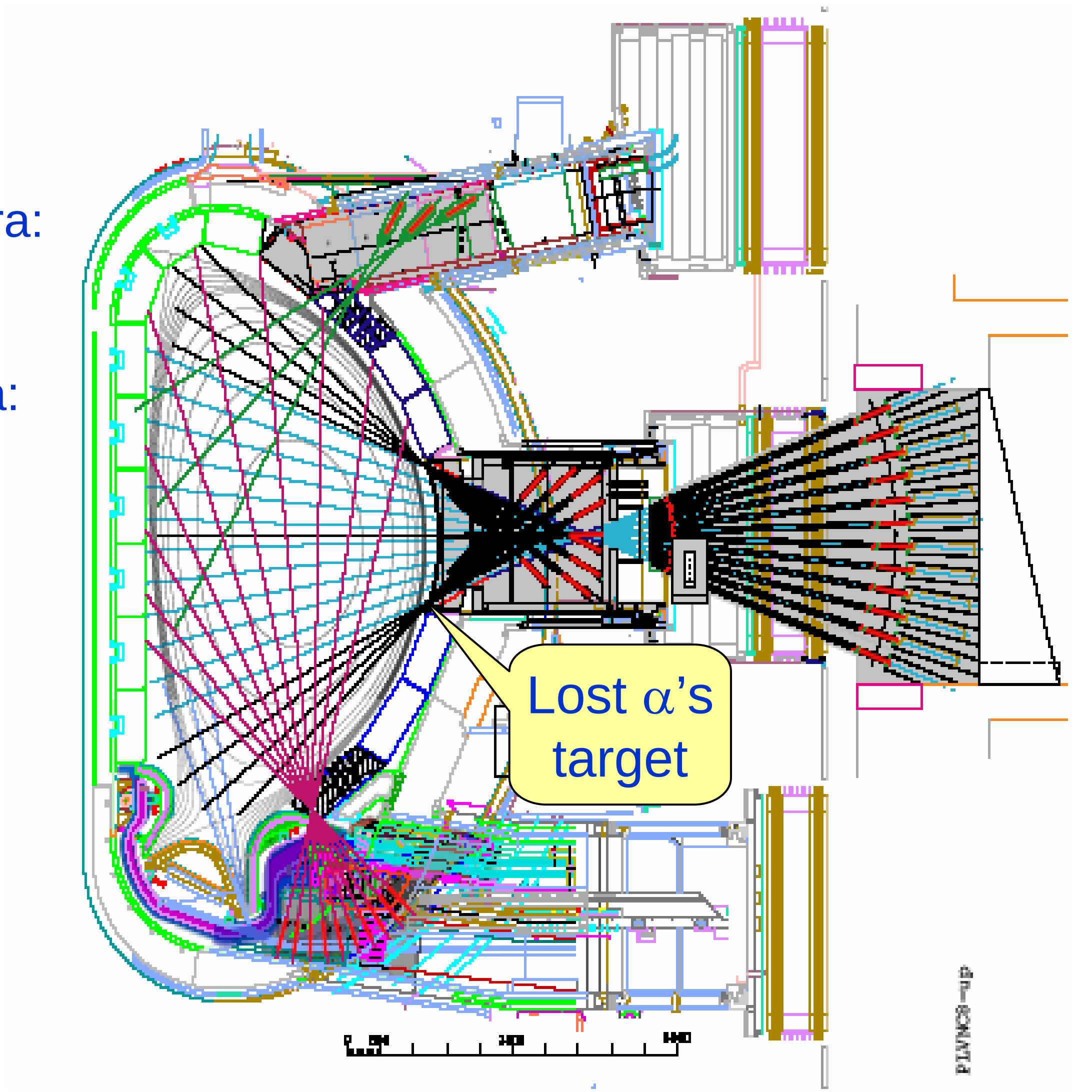

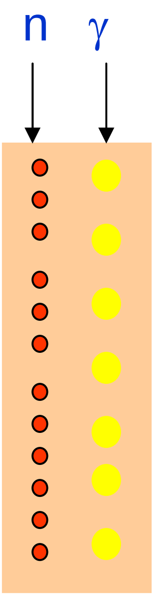

Prospects for radiation imaging detectors in fusion research

Fusion research in general

- There is a move from discrete views towards imaging instruments and detectors.

  Already in IR, Visible, x-ray

  Required for VUV

  Potential for gamma-ray?

- Existing and planned ITER prototypes could use fast 2D detectors immediately

  Imaging x-ray crystal spectrometer for MAST

  Imaging/scanning VUV spectrometer upgrade for JET

ITER diagnostics

- We need fast, 2d, radiation-hard, photon-counting detectors with background rejection.

- Reference diagnostic designs are based on current technology – often conservative.

- Improved radiation hardness and background rejection would improve performance:

  More open apertures

  Reduced labyrinths

  Detector closer to plasma

  - There is considerable flexibility for new techniques and detectors.